

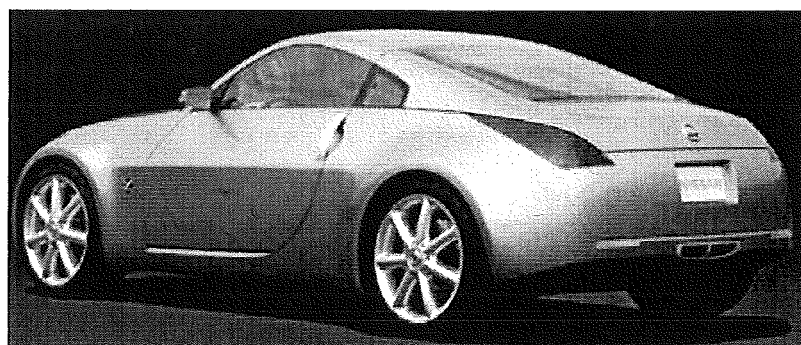
**METALLURGICAL PHENOMENA GOVERNING  
THE BAKE HARDENING RESPONSE OF BAKE  
HARDENABLE STEELS**

**JUAN JOSE MORENO EXEBIO**

**Master of Science Thesis**

**Academic Supervisor: Dr. Ir. Jilt Sietsma  
Department of Materials Engineering  
Delft University of Technology – Delft**

**Industrial Supervisor: Ir. Ronald Koenis  
Corus Research, Development & Technology  
IJmuiden Technology Centre**



**July 2002**

# Index

Index.....	1
List of figures .....	2
List of tables .....	3
Acknowledgements .....	5
List of symbols .....	6
Chapter 1: Introduction .....	8
Chapter 2: Literature review.....	10
2.1 Introduction .....	10
2.2 The standard bake hardening test.....	11
2.3 On the mechanism of bake hardening.....	13
2.3.1 Snoek effect .....	14
2.3.2 Cottrell atmosphere.....	15
2.3.3 Carbide precipitation .....	18
2.3.4 Description of the kinetics of bake hardening.....	18
2.4 Effect of carbon (C) and/or nitrogen (N) content .....	19
2.5 Effect of grain size on the bake hardening response.....	21
2.6 Effect of prestrain level, temperature and ageing time .....	22
2.7 Discussion.....	24
2.7.1 Prestrain orientation.....	24
2.7.2 Time and temperature bake hardening treatment .....	27
Chapter 3: Experimental procedure.....	30
3.1 Introduction .....	30
3.2 Material .....	30
3.3 Sample preparation and orientation .....	31
3.3.1 Tensile samples.....	31
3.3.2 Compression samples.....	32
3.4 Heat treatment.....	33
3.4.1 For tensile samples.....	33
3.4.1.1 Single bake hardening treatment .....	33
3.4.1.2 Double bake hardening treatment.....	33
3.4.2 For compression samples .....	34
3.5 Mechanical testing .....	34
3.5.1 Tensile test.....	34
3.5.1.1 Single bake hardening treatment .....	34
3.5.1.2 Double bake hardening treatment.....	35
3.5.2 Compression tests .....	36
3.6 Strain distribution .....	37
3.7 Transmission electron microscopy (TEM) .....	42
3.8 Calculation of the bake hardening response .....	42
Chapter 4: Results .....	44
4.1 Introduction .....	44
4.2 Microstructure .....	44
4.3 Tensile tests .....	45
4.3.1 X samples.....	48
4.3.1.1 Dependence on prestrain and temperature .....	48
4.3.1.2 Dependence on baking time and temperature for a prestrain level of 2%.....	49
4.3.2 Y samples.....	50
4.3.2.1 Dependence on prestrain and temperature .....	50
4.3.2.2 Dependence on baking time and temperature for a level of prestrain of 2%.....	51
4.3.3 Double bake hardening treatment .....	52
4.4 Compression tests .....	53
4.4.1 Cube-samples.....	54
4.4.1.1 Dependence on prestrain and temperature .....	54
4.5 Transmission electron microscopy (TEM) .....	55
Chapter 5: Discussion of results .....	57
5.1 Introduction .....	57
5.2 Influence of deformation type.....	57
5.3 Influence of sample orientation .....	57

5.4 Influence of prestrain .....	59
5.4.1 Precipitation .....	60
5.5 Influence of baking temperature and time .....	64
Chapter 6: conclusions & references .....	66
6.1 Conclusions .....	66
6.2 References .....	67

## List of figures

Figure 1 Applications of bake hardenable steels in cars .....	8
Figure 2 Strength and formability for mild, conventional and advanced high strength steels .....	10
Figure 3 Schematic illustration of the increase in yield stress after press-forming and after bake hardening treatment <sup>(4)</sup> .....	11
Figure 4 Schematic bake hardening procedure according to the standard test .....	12
Figure 5 Schematic presentation of the combined stress-strain curves before and after bake hardening and the microstructure change during bake hardening test <sup>(4)</sup> .....	12
Figure 6 Schematic presentation of the bake hardening effect of the three stages <sup>(4)</sup> .....	14
Figure 7 Fractional increase in yield-stress increment, $\Delta\sigma/\bar{\sigma}$ vs. $t^{2/3}$ for single-crystal specimens quenched from 700 °C <sup>(13)</sup> .....	15
Figure 8 Carbon atoms in the strain field of a positive edge dislocation and the central carbon line of Cottrell atmosphere .....	17
Figure 9 Schematic variation of yield stress with ageing time for typical age-hardening alloys with two different volume fractions of precipitate <sup>(1)</sup> .....	18
Figure 10 Increase in lower yield stress after a prestrain of 1% and ageing at 100°C for ZStE 180BH (0.03 wt% C) <sup>(4)</sup> .....	19
Figure 11 Effect of solute carbon on bake-hardenability and room temperature ageing <sup>(11)</sup> .....	20
Figure 12 Effect of grain size and solute (C+N) content on $\Delta\sigma_{BH}$ of low-C Al-killed steel after standard bake hardening treatment <sup>(1)</sup> .....	21
Figure 13 Effect of dissolved (C+N) content on $\Delta\sigma_{BH}$ for two different grain sizes of low-C Al-killed steel after standard bake hardening treatment <sup>(1)</sup> .....	22
Figure 14 Increase in lower yield stress after different prestrain levels and ageing at 150 °C for ZStE 180BH (0.03 wt% C) <sup>(4)</sup> .....	22
Figure 15 Increase in lower yield stress after different prestrain levels and ageing at 180 °C for ZStE 180BH (0.03 wt% C) <sup>(4)</sup> .....	23
Figure 16 Increase in lower yield stress after a prestrain of 2% and ageing at different temperatures for ZStE 180BH (0.03 wt% C) <sup>(4)</sup> .....	23
Figure 17 Increase in lower yield stress after a prestrain of 5% and ageing at different temperatures for ZStE 180BH (0.03 wt% C) <sup>(4)</sup> .....	24
Figure 18 Increase in lower yield stress in the first and second step of bake hardening as a function of prestrain and ageing temperature for ZStE 180BH (0.03 wt% C) <sup>(4)</sup> .....	24
Figure 19 Effect of a pre-deformation direction on bake hardening behaviour (Batch-annealed steel) <sup>(11)</sup> .....	26
Figure 20 Relationship between pre-deformation and secondary deformation direction - same direction .....	26
Figure 21 Relationship between pre-deformation and secondary deformation direction - different direction .....	27
Figure 22 Relationships between bake hardening and work hardening in Ti-added ultra-low carbon Al-killed steel <sup>(35)</sup> .....	27
Figure 23 Prestrain orientation with respect to the rolling direction .....	31
Figure 24 Orientation of machined X samples in relation to the rolling direction .....	31
Figure 25 Orientation of machined Y samples in relation to the rolling direction .....	32
Figure 26 Tensile sample dimensions .....	32
Figure 27 Schematic presentation of single bake hardening treatment and tensile testing .....	35
Figure 28 Schematic presentation of double bake hardening treatment and tensile testing .....	36
Figure 29 Biaxial stretching simulation .....	36
Figure 30 Schematic representation of grid on strip .....	37
Figure 31 2D plot of the strain distribution for strip prestrained 2% (cf. Figure 32) .....	38
Figure 32 Forming limit diagram for strip prestrained 2% .....	38
Figure 33 2D plot of the strain distribution for sample prestrained 8% (cf. Figure 34) .....	39
Figure 34 Forming limit diagram for sample prestrained 8% .....	39
Figure 35 Section plot for strip prestrained to 8% .....	40

<u>Figure 36 Uniform deformation area of strips after prestrain for X samples</u> .....	40
<u>Figure 37 Uniform deformation area of strips after prestrain for Y samples</u> .....	41
<u>Figure 38 X sample as-received condition</u> .....	44
<u>Figure 39 Y sample as-received condition</u> .....	44
<u>Figure 40 X sample (230 °C-20min-8% prestrain)</u> .....	45
<u>Figure 41 Y sample (230 °C-20min-8% prestrain)</u> .....	45
<u>Figure 42 True stress - true strain for X sample in the as-received condition</u> .....	46
<u>Figure 43 True stress - true strain for Y sample in the as-received condition</u> .....	46
<u>Figure 44 True stress - true strain for X sample after 170 °C-20 min-4% prestrain</u> .....	47
<u>Figure 45 True stress - true strain for Y sample after 170 °C-20 min-4% prestrain</u> .....	47
<u>Figure 46 Dependence of bake hardening response after various temperatures for 20 minutes and prestrain levels (X samples)</u> .....	49
<u>Figure 47 Dependence of bake hardening response at times indicated for various baking temperatures after 2% prestrain (X samples)</u> .....	50
<u>Figure 48 Dependence of bake hardening response at various temperatures for 20 minutes and prestrain levels (Y samples)</u> .....	51
<u>Figure 49 Bake hardening response as a function of baking time and temperature after 2% prestrain (Y samples)</u> .....	51
<u>Figure 50 Dependence of bake hardening response at temperatures indicated for 20 minutes according to the level of prestrain for the second bake hardening treatment only</u> .....	52
<u>Figure 51 Total bake hardening response achieved after double bake hardening treatment at the temperatures indicated for 20 minutes as a function of the level of prestrain</u> .....	53
<u>Figure 52 True stress - true strain curves for compression sample in the as-received condition</u> .....	53
<u>Figure 53 True stress - true strain curves for compression sample after 170 °C-20 min-2%prestrain</u> .....	54
<u>Figure 54 Dependence of bake hardening response at various temperatures for 20 minutes and prestrain levels</u> .....	55
<u>Figure 55 TEM-photograph of X sample after 230 °C - 20 min - 0% prestrain</u> .....	55
<u>Figure 56 TEM-photograph of X sample after 230 °C -20min - 2% prestrain</u> .....	55
<u>Figure 57 TEM-photograph of X sample after 230 °C - 20min - 0% prestrain</u> .....	56
<u>Figure 58 TEM-photograph of X sample after 230 °C - 20min - 0% prestrain</u> .....	56
<u>Figure 59 X sample after 230 °C - 20 min - 2% prestrain - diffraction pattern of epsilon-carbide precipitate</u> .....	56
<u>Figure 60 X sample after 230 °C - 20 min - 2% prestrain - diffraction pattern of epsilon-carbide precipitate</u> .....	56
<u>Figure 61 Schematic presentation of herringbone structure after temper rolling (strip width)</u> .....	58
<u>Figure 62 Through thickness microstructure of low carbon steel after 1.7% temper rolling<sup>(1)</sup></u> .....	58
<u>Figure 63 Calculated TTP-diagram for cementite precipitation in ferrite with mass content of 0,045% C; experimental points from Abe for 15% carbides precipitated in a steel with additional mass contents of 0,02% P and 0,35% Mn</u> .....	60
<u>Figure 64 Hypothetical precipitation, dislocation and soluble carbon interaction of X-samples after bake hardening at temperatures &gt;200°C</u> .....	61
<u>Figure 65 Work hardening and bake hardening for single (bar at the left) and double (bar at the right) heat treatment (140 °C – 20 minutes) at different levels of prestrain</u> .....	63
<u>Figure 66 Work hardening and bake hardening for single (bar at the left) and double (bar at the right) heat treatment (230 °C – 20 minutes) at different levels of prestrain</u> .....	63

## List of tables

<u>Table 1 Standard bake hardening tests used by the car industry</u> .....	13
<u>Table 2 Activation energies, frequency factor, diffusion coefficient and diffusion distances for diffusion of interstitial solutes in b.c.c. metals (Stephenson<sup>(1)</sup>)</u> .....	19
<u>Table 3 Determination of the ideal <math>x_c</math> level<sup>(30)</sup></u> .....	20
<u>Table 4 Chemical composition range as for H180BD (cast analysis)</u> .....	30
<u>Table 5 Required mechanical properties for H180BD in the transverse direction</u> .....	30
<u>Table 6 Dimensions (in millimetres) of test pieces (cf. Figure 27)</u> .....	32
<u>Table 7 Bake hardening treatment applied to samples with different prestrain</u> .....	33
<u>Table 8 First bake hardening treatment</u> .....	33
<u>Table 9 Second bake hardening treatment</u> .....	34
<u>Table 10 Bake hardening treatment for compression samples</u> .....	34
<u>Table 11 Major and minor strain measured in the centre of the prestrained strips</u> .....	37

<u>Table 12 Comparison of bake hardening values and standard deviations between old and new series for the various bake hardening treatments</u> .....	42
<u>Table 13 Comparison of work hardening calculations</u> .....	43
<u>Table 14 Measured-mechanical properties on H180BD</u> .....	48
<u>Table 15 Bake-hardening response after different temperatures and sample orientation for 0% prestrain</u> .....	59
<u>Table 16 Dislocation density based on tensile test curve (Figure 43) of H180BD using Bergstrom model for static strain ageing</u> .....	59

## Acknowledgements

I express my thanks to Dr. Loes Jansen (Knowledge Group Leader) and members of the automotive and packaging group of CRD&T (CORUS-IJmuiden) for their support.

I would like to express my sincere gratitude to my academic supervisor, Jilt Sietsma, who has proven to be extremely kind, tolerant and helpful.

I am deeply thankful to Ronald Koenis (Industrial supervisor) for his friendship, helpful comments, suggestions and encouragement during the preparation of this thesis.

My thanks also go to Pieter van Popta, who invested a lot of his time, knowledge and experience in materials science.

I am grateful to the members of ALM-TES and the Product Application Centre. Special thanks to Jan Brussel and to Siem Duin for their infinite assistance.

Finally, I thank my parents and brother for their patience and support.

## List of symbols

$a$	: lattice parameter in <i>b.c.c.</i>
$a_{l,c}$	: altered lattice parameters in <i>b.c.c.</i> caused by introduction of a carbon atom
$A$	: parameter measuring the interaction between the dislocation and the solute atom
$A_{80}$	: elongation
$b$	: width
<i>b.c.c.</i>	: body centre cubic
$d$	: grain diameter
$D$	: diffusion coefficient
<i>FLD</i>	: Forming Limit Diagram
$k$	: Boltzmann's constant
$K$	: strength coefficient ( $= (Q/R) \times \log e$ )
$L_0$	: original gauge length in tensile sample
$L_c$	: parallel length in tensile sample
$L$	: test piece total length in tensile sample
$n$	: work hardening rate
$n_D$	: number of atoms segregated to dislocation
$n_0$	: initial number of atoms in solid solution
$n(T,t)$	: number of solute atoms transferred to unit length of a dislocation, dependent of temperature and time
$N$	: number of solute atoms in unit volume
$q$	: ratio $n_D/n_0$
$Q_D$	: activation energy
$r$	: Lankford value or carbon atom co-ordinate relative to the dislocation
$r_a$	: atomic radius of iron
$r_0$	: minimum value for $r$
$r_{90}$	: plastic strain ratio
$R$	: gas constant or maximum value for $r$
$R_{bL1}, R_{bL2}$	: lower yield point after pre-straining and ageing
$R_{bH}$	: upper yield point after pre-straining and ageing
$R_t$	: proof stress at the pre-strain level
$R_m$	: tensile strength
$R_{p0.2}$	: 0.2%-proof strength
$t$	: time, ageing time or time of baking at artificial ageing temperature
$t_r$	: ageing time at room temperature
$T_r$	: room temperature
$T$	: artificial ageing temperature or baking temperature
<i>ULC</i>	: Ultra Low Carbon
$x_C$	: concentration of carbon in solution
$x_N$	: concentration of nitrogen in solution
$x_{C+N}$	: concentration of carbon and nitrogen in solution
$X$	: diffusion distance
$\alpha$	: angle relative to the dislocation or angle between the longest axis of the tensile sample and the rolling direction
$\varepsilon$	: general symbol for strain; true strain
$\varepsilon_t$	: pre-strain
$\lambda$	: slip distance of the dislocation

$\nu$	: Poisson's ratio
$\Theta$	: Koehler's formula for the stresses around a positive edge dislocation
$\sigma$	: normal stress; true stress
$\tau$	: temperature dependent constant
$\Delta\sigma_{WH}$	: work hardening
$\Delta\sigma_{BH}$	: increase in lower yield stress (bake hardening property)
$\Delta\sigma/\bar{\sigma}$	: fractional increase in yield stress
$\Delta\sigma_{precipitation}$	: increase in lower yield stress by precipitation
$\Delta\sigma_{Cottrell}$	: increase in lower yield stress by Cottrell atmospheres
$\Delta\sigma_{Snoek}$	: increase in lower yield stress by Snoek effect
$\Delta V$	: unit cell volume change
$\tau$	: temperature dependent constant
$2D$	: two-dimensional plot

## Chapter 1: Introduction

The metallurgical phenomena responsible for the increase in yield strength during bake hardening (bake hardening response) of bake hardenable steels are the diffusion of dissolved interstitial  $C$  atoms to dislocations and grain boundaries and/or  $\epsilon$ -carbide precipitation.

Bake hardenable steel is mainly used for the manufacture of outer doors, fenders, boot lids and bonnets of automobiles (Figure 1) <sup>(1)</sup>. With this type of steel a higher yield strength in the final product is obtained whereby a reduction in thickness of the body panel is possible. The increase in yield strength takes place after press-formed parts, pass through paint curing lines (temperatures between 150 – 200 °C). Press forming is therefore easier because the increase in strength occurs after the press forming operation.

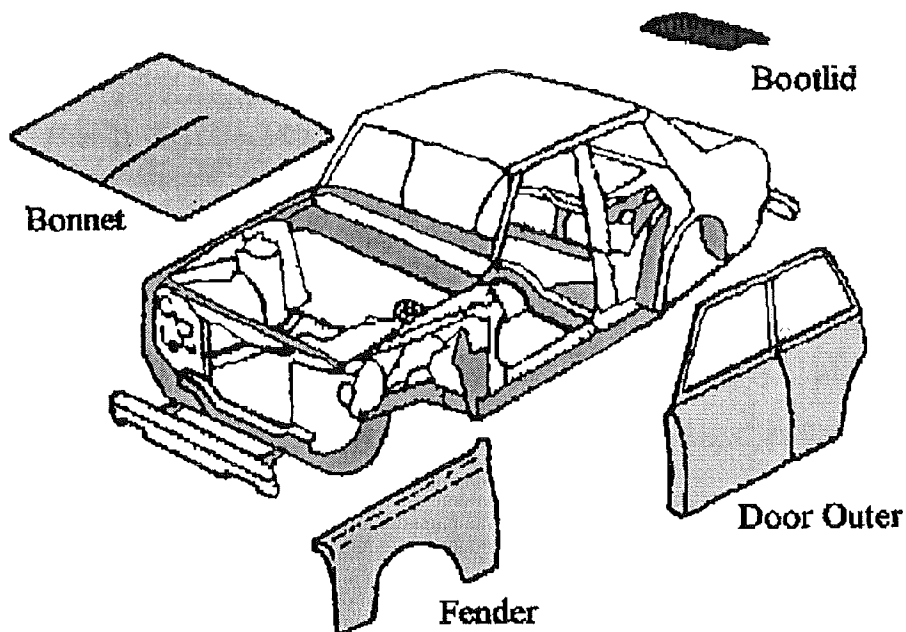


Figure 1 Applications of bake hardenable steels in cars

The steel properties leading to good formability are a relatively low yield stress, suitable texture to give an adequate  $r$ -value, no yield point elongation (or Lüders strain), and a high  $n$  value (work hardening rate as in the Hollomon equation ( $\sigma=K\epsilon^n$ )). The latter two properties are strongly influenced by temper rolling of the steel prior to delivery to the stamping plant. The yield stress after baking increases with increased solute  $C$  (dissolved  $C$ ) content in the steel; however, if the amount of  $C$  in solution is larger than 25 wt-ppm, strain ageing occurs at room temperature leading to an unacceptable yielding behaviour and poor surface quality on the stamped product. Consequently the need for room temperature stability limits the  $C$  content between 10 and 25 wt-ppm and therefore the amount of bake hardening response that may be achieved.

In the standard bake hardening test, a tensile sample is 2% uniaxially prestrained, unloaded and aged at 170 °C for 20 minutes (accelerated strain ageing) and subsequently re-strained until failure.

Although the knowledge of bake hardening is rather extensive, it is believed that the bake hardening response cannot be predicted precisely by an accelerated strain-ageing test because of:

- Sample orientation: a different bake hardening response is observed in different relative orientations for the pre-treatment deformation and the testing deformation, even though the diffusion of *C* is intrinsically similar
- Prestrain path: simple unidirectional tensile tests of bake hardenability, in which ageing is confined to a short time (20 minutes) at a temperature up to 170° C, gives a misleading bake hardening response compared to that attained in applications which involve stress systems applied in service
- Baking temperatures: temperatures in the 200 to 230 °C range renders carbide precipitation that may not thermodynamically precipitate at lower temperatures

It is thus the aim of this project to clarify how the bake hardening response in bake-hardenable steels is influenced by different sample orientations, prestrain levels, and baking temperatures and times. The observed tendencies are discussed in terms of the metallurgical processes taking place.

For this research:

- A comprehensive literature review was conducted to establish the current state of knowledge in this field of study. The results are reported in Chapter II. Special attention was given to the standard bake hardening test, theoretical background on the bake hardening mechanism and the influence of prestrain, temperature and time of baking on bake hardening.
- A detailed experimental plan was then designed and executed to investigate the bake hardening mechanism. Details are given in Chapter III. The plan included sample preparation and orientation of tests, bake hardening simulation as applied by steel producers, and tensile and compression tests to simulate the bake hardening response.
- A result section is given in Chapter IV, where the influence of parameters such as level of prestrain, temperature and time of baking on the bake hardening response for tensile and compression samples is described
- Finally, there is a discussion section in Chapter V that reviews the influence of test type, sample orientation, prestrain and baking temperature and time in detail.

This project is sponsored by CORUS-IJmuiden (The Netherlands).

## Chapter 2: Literature review

### 2.1 Introduction

Environmental pressures increasingly necessitate further reduction of a vehicle's weight in order to achieve better fuel consumption <sup>(2)</sup>. In addition to this, the improvement of safety is also an important consideration during material selection and design of new car models. These issues are addressed by using high-strength steel sheets, but the increased strength makes press forming difficult. Bake hardenable steel is one way to obtain a higher yield strength in the final product, whereby a reduction in thickness of the body panel is possible, without deterioration of the press-formability <sup>(1)</sup>. Bake hardenable steels have a relatively low initial yield strength and good formability compared with other types of steels (Figure 2), associated with an excellent bake hardening property, which provides a yield strength improvement of approximately 20% after paint baking <sup>(3, 4, 5, 6, 7)</sup>.

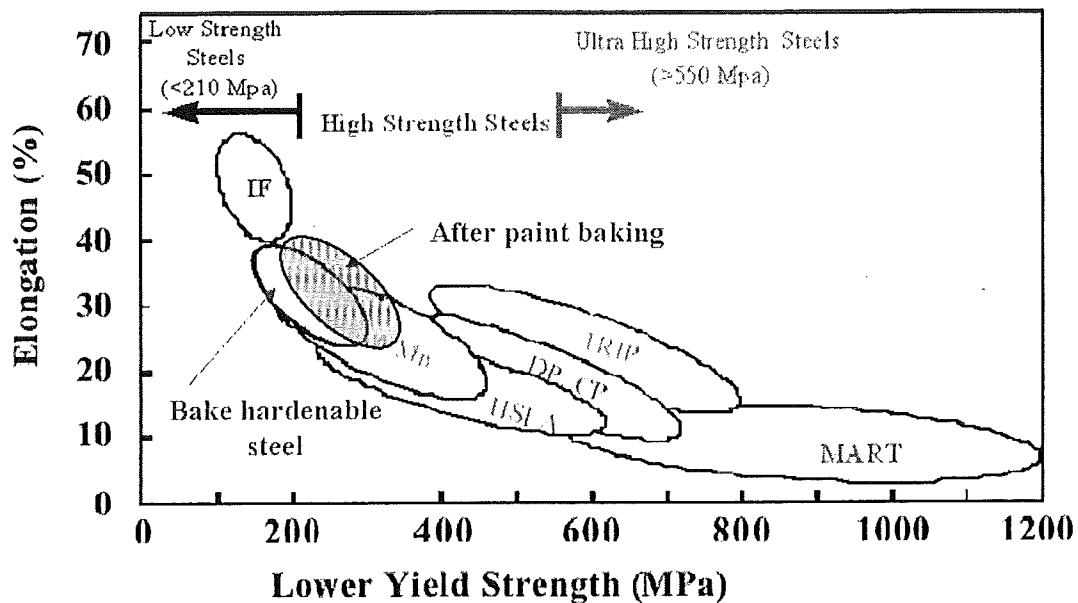


Figure 2 Strength and formability for mild, conventional and advanced high strength steels

After press forming, painted parts pass through drying furnaces at temperatures between 150 °C and 200 °C, where the different layers of primer and coating are baked for 10 to 30 min. It is during this stage that the yield strength increases. (Figure 3)

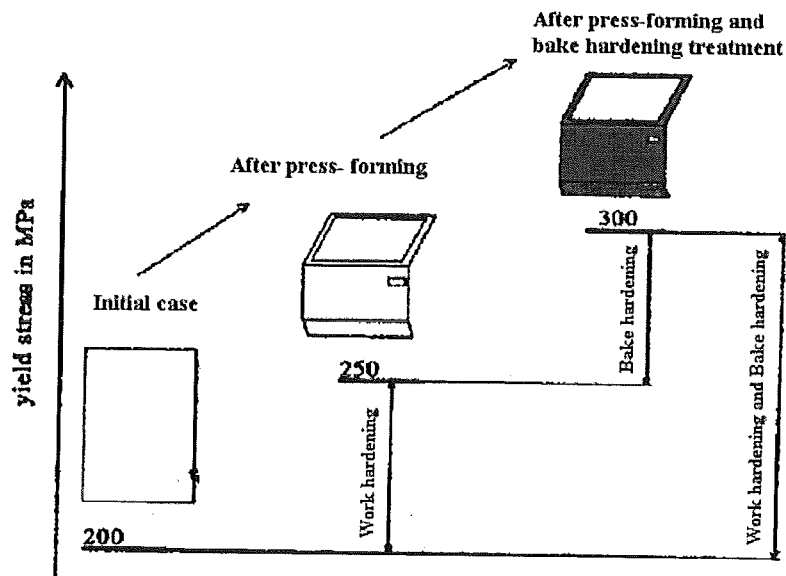


Figure 3 Schematic illustration of the increase in yield stress after press-forming and after bake hardening treatment<sup>(4)</sup>

In view of the current importance of bake hardenable steels in the automotive industry, a review of the mechanisms of bake hardening and parameters which control it, will be presented according to the following structure:

- A description of a standard test to assess the bake hardening response in §2.2
- A basic theoretical background in §2.3. Parameters (such as grain size and alloying elements) used by steel producers to promote a bake hardening response of bake hardenable steels are presented in §2.4 and §2.5
- The means that car producers have to improve a bake hardening response in bake hardenable steels (like type and amount of prestrain, temperature and time of baking) are presented in §2.6 and §2.7
- Finally, a discussion of the literature reviewed for this report in §2.8

## 2.2 The standard bake hardening test

To accurately predict the performance of bake-hardenable steels in-service, it would be necessary to form components, paint and then bake them in an automotive paint curing line, before testing the mechanical properties. Obviously, this is a time consuming and costly process, hence a simple tensile test has been developed to simulate the conditions encountered by these steels when they are used in auto-body construction. In the standard bake hardening test, a tensile sample is 2% uniaxially prestrained, unloaded and aged at 170 °C for 20 minutes and subsequently uniaxially re-strained until failure. (Figure 4)

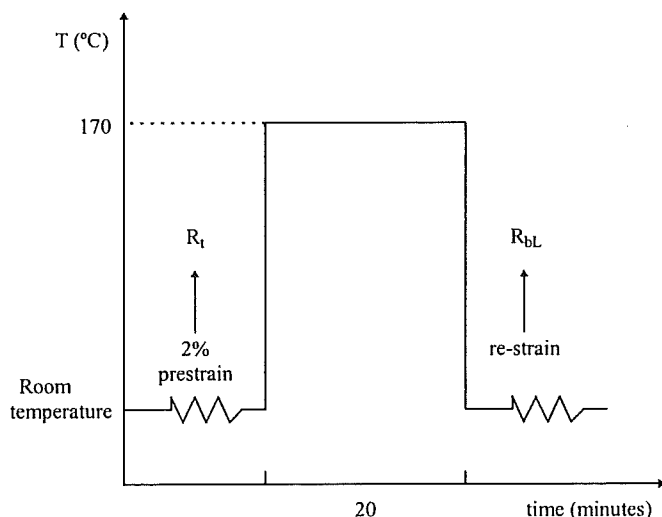


Figure 4 Schematic bake hardening procedure according to the standard test

The Bake hardening is defined as the difference between the lower yield point after pre-straining and ageing ( $R_{bL}$ ) and the proof stress at the prestrain level ( $R_t$ ) (Figure 5).

The return of the yield point is due to the diffusion of carbon atoms to the dislocations during the ageing period to form new atmospheres of interstitials anchoring the dislocations<sup>(27)</sup>. The most common measure to describe the bake hardening behaviour is the increase in lower yield stress ( $\Delta\sigma_{BH}$ ) as illustrated in Figure 5.

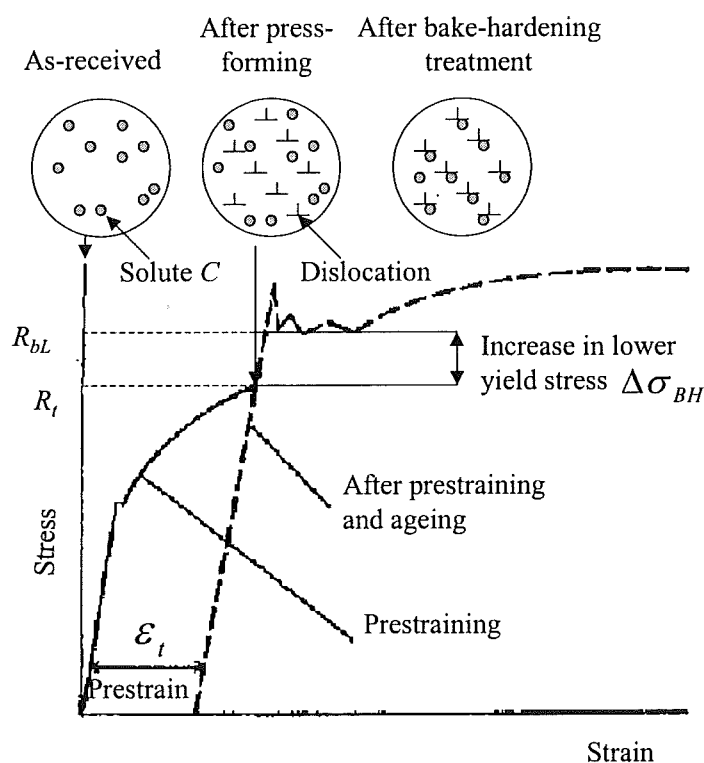


Figure 5 Schematic presentation of the combined stress-strain curves before and after bake hardening and the microstructure change during bake hardening test<sup>(4)</sup>

An indication of how the microstructure changes during the bake hardening test is also presented with a typical stress-strain measurement obtained during bake hardening testing in Figure 5. In the as-received condition carbon in solution (typical concentration 20 wt-ppm) is uniformly distributed. During prestraining, new dislocations are created and in the subsequent baking process, diffusion of interstitials to dislocations takes place.

The various standards for bake hardening testing are shown in Table 1 (the rolling direction refers to the original plate material). The differences in testing and calculation procedures could imply that material that satisfy a steelmaker's release test, may be rejected by a customer, simply because of the different test method used. Hopefully, the adoption of the European norm proposal will make bake hardening results comparable, for both, the steel makers and their customers.

Table 1 Standard bake hardening tests used by the car industry

Bake hardening test variable	JIS G3135 (Japanese std.) <sup>(8)</sup>	ISO 14590 (International std.) <sup>(9)</sup>	SEW 094 (German std.) <sup>(10)</sup>	European Proposal
Test piece	JIS No. 5	ISO 80 mm	ISO 80 mm	DIN EN10002
Orientation test sample respect to rolling direction	90°	90°	90°	90°
Prestrain	2% total elongation	2% total elongation	2% total elongation	2% plastic deformation
Baking treatment	20 min - 170 °C	20 min - 170 °C	20 min - 170 °C	20 min - 170 °C
<b>Calculation of the bake hardening response</b>				
Cross-sectional area	Original	Original	Prestrained	Prestrained
Lower yield stress ( $R_{bL}$ ) or Upper yield stress ( $R_{bH}$ )	$R_{bH}$	$R_{bH}$	$R_{bH}$	$R_{bL}$
Accuracy	10 N/mm <sup>2</sup>	10 N/mm <sup>2</sup>	Not stated	10 N/mm <sup>2</sup>

### 2.3 On the mechanism of bake hardening

It is assumed that the bake hardening process is a kind of strain ageing caused by segregation of carbon and/or nitrogen atoms to the dislocations generated during press forming<sup>(4, 11)</sup> or prestraining in the test procedure. It is generally established that strain ageing occurs in three continuous and successive stages, and that there is a gradual change from one stage to another (Figure 6).

- In the first stage there is an initial rapid increase in the upper yield point that is explained by stress induced rearrangement of the interstitial atoms in the stress field of dislocations, called the Snoek-effect.
- In the second stage a pronounced increase in yield stress is caused by medium-range diffusion of carbon and/or nitrogen to dislocations (in the standard test the diffusion distance for C and N is approximately 0.8  $\mu\text{m}$ ). These atoms gather in the stress field

of a dislocation and form the so-called Cottrell-atmosphere, which can pin the dislocations effectively and give an increase in strength. This is the most significant stage of the three that govern the return of the yield point (discontinuous yielding).

- In the third stage the  $\epsilon$ -carbides precipitate. An initial increase in strength takes place (Kelly-fine mechanism) but with increasing ageing time (Orowan mechanism) a decrease is observed due to  $\epsilon$ -carbides coarsening.

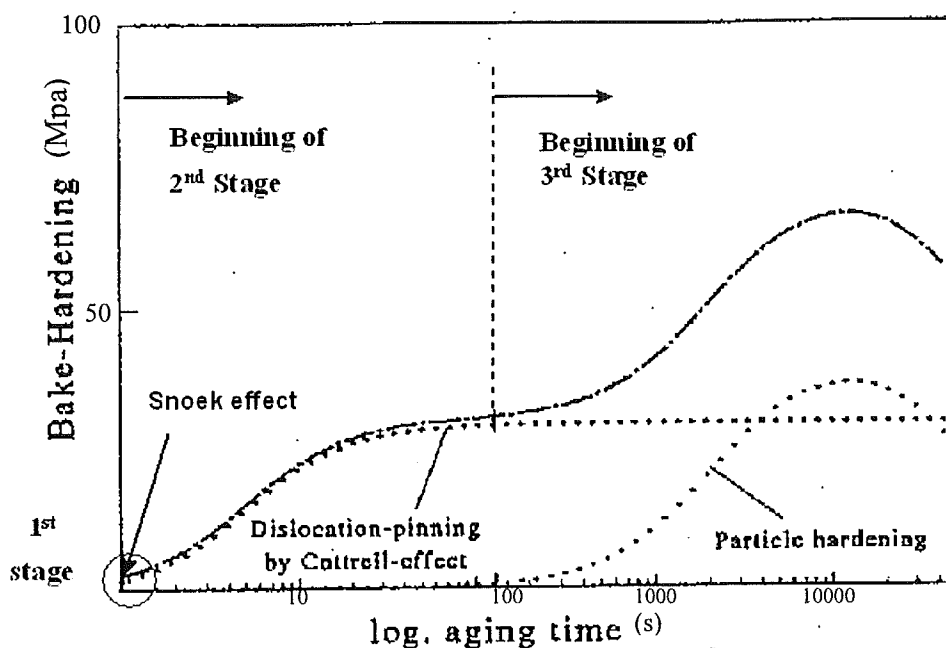


Figure 6 Schematic presentation of the bake hardening effect of the three stages <sup>(4)</sup>

### 2.3.1 Snoek effect

The Snoek effect or Snoek rearrangement is essentially associated with a single atomic jump of an interstitial atom in the dislocation stress field. Since interstitials that are initially close to the dislocations move through the distorted region near the dislocations more rapidly than distant interstitials diffuse through the bulk, the first stage of the strain process is attributed to a rearrangement of interstitials around dislocations as described by Shoenck and Seeger<sup>(12)</sup>. They consider a *b.c.c.* lattice in which the concentration of interstitial atoms is low enough to keep the interaction between interstitials small. Three types of interstitial sites - corresponding to the three directions of a cubic cell - exist. If no stress is applied, the three interstitial sites will be occupied by the same fraction of interstitial atoms. If, however, a (non-hydrostatic) stress is applied the energy of interaction between the stress and the interstitials will in general depend on the type of site occupied. Hence, at temperatures where the interstitials can diffuse, an applied stress will cause a redistribution of the population of the different lattice sites and the population of the sites with lower energy will increase, whereas that of the sites with higher energy will decrease. A similar redistribution of interstitials on different lattice sites will take place in the stress field of a dislocation. By this process the energy of the system is lowered and therefore the dislocation locked. This process is known as the Snoek effect.

The first stage of strain ageing, attributed to Snoek rearrangement of interstitials in the stress field of the dislocation, can be described as follows. Initially there is a random

distribution of interstitials in the matrix. After an applied deformation, the interstitials in the stress field of a dislocation attempt to minimise the strain energy in the region of the dislocation by moving to minimum energy site positions<sup>(13, 14, 15)</sup>.

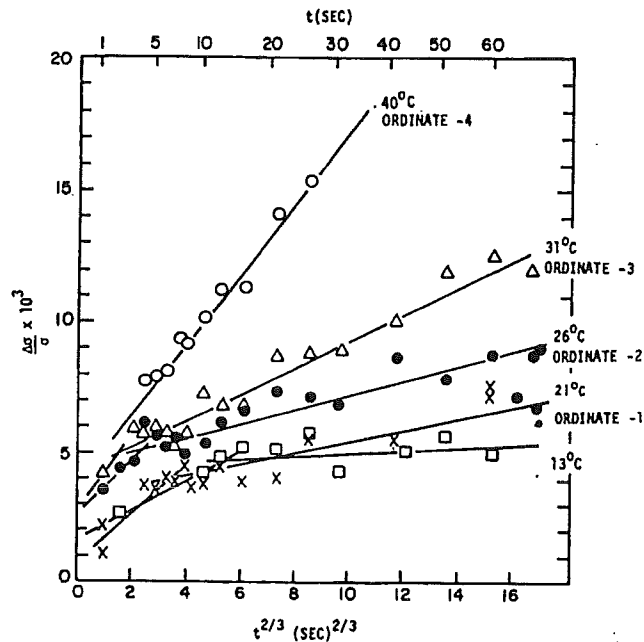


Figure 7 Fractional increase in yield-stress increment,  $\Delta\sigma/\bar{\sigma}$  vs.  $t^{2/3}$  for single-crystal specimens quenched from 700 °C<sup>(13)</sup>

Figure 7 reveals that the fractional increase in yield stress in iron single crystals occurs in two successive stages, represented by two different slopes. The first stage is considered to be due to Snoek effect and the second one due to Cottrell atmosphere (discussed more extensively in the next section). For temperatures of 40 °C or higher, the first stage cannot be seen due to its rapid completion; increasing the temperature decreases the time required for its completion (11 s at 13 °C but 2 s at 31 °C). Both stages follow a  $t^{2/3}$  law (Equation 1). Authors like Nakada and Keh<sup>(16)</sup> have pointed out that the apparent intercept of the “ $\Delta\sigma/\sigma$ ” (fractional increase in yield stress) plot at zero ageing time, from second stage, is positive if Snoek rearrangement precedes Cottrell-atmosphere formation. In this case no incubation time is required for the occurrence of Snoek rearrangement.

The initial stage has an activation energy corresponding to short-range motion of interstitials in dislocation stress fields (Snoek effect) of  $62 \pm 2$  kJ/mol, whereas the later stage corresponds to longer-range diffusion (resulting in a Cottrell atmosphere) with an activation energy of 75 to 92 kJ/mol<sup>(13)</sup>.

### 2.3.2 Cottrell atmosphere

The medium-range diffusion of carbon atoms to the stress field of the dislocations, called Cottrell-effect, is assumed to be the mechanism dominating the magnitude of the bake hardening response. Cottrell and Bilby<sup>(21)</sup> analysed the kinetics of the formation of the carbon atmosphere around dislocations produced by straining based on the assumption that the only important phenomenon would be the “drift force” pulling carbon atoms towards the dislocation core. This drift force arises from the decrease in the dilatational energy of a carbon atom in sites near the tension side of an edge

dislocation. It was indicated that a drift force of a similar magnitude should also exist near a screw dislocation.

Cottrell's model (in its original form) of atmosphere formation around dislocations, extended by Harper<sup>(17)</sup>, only describes the kinetics of the change of carbon content in solution in the bulk due to diffusion to dislocations. The general form is:

$$\frac{n_D}{n_0} = q = 1 - \exp\left(-\left[\frac{t}{\tau}\right]^{2/3}\right)$$

1

$n_D$  being the number of atoms segregated to dislocations,  $n_0$  the initial number of atoms in solution,  $t$  the ageing time and  $\tau$  a temperature dependent constant. This equation is often used to describe the change of mechanical or physical properties during ageing. This is only valid as long as the change of the properties is directly proportional to the change of the carbon content in solution. Many investigations have shown that this proportionality is valid for the beginning but not for the end of the ageing process. The increase in yield stress caused by the formation of carbon atmospheres around dislocations rises with the number of atoms that gather in an atmosphere, but the interaction and the pinning-effect decrease with increasing distance between the dislocation and the carbon atom. Cottrell also mentioned that the first atoms that arrive at a dislocation ought to be more effective in anchoring it than those that arrive later<sup>(18, 19, 20)</sup>. Thereby, it is obvious that for the later stages of ageing the direct proportionality between the numbers of carbon atoms around a dislocation and the yield stress cannot be valid.

It is possible to estimate the number of atoms required for saturation (interstitial-dislocation interaction) by equating the volume changes produced by the interstitial atoms and by the dislocation field. Assuming that each carbon alters the edges of the unit-cell in which it is from " $a, a, a$ " to " $c, a_1, a_1$ " and using the lattice parameter measurements in martensite of Lipson and Parker (1944), the unit cell volume change caused by the introduction of a carbon atom is given as  $\Delta V = 7.8 \times 10^{-30} \text{ m}^3$ <sup>(21)</sup>. Should we then take a region consisting of one atomic plane threaded by the dislocation line (Figure 8), the radius  $r = R$  ( $\sim 10 \text{ \AA}$ ) of a semi-circular annulus in which the total volume change produced by the dislocation is equal to that produced by introducing "one" carbon atom, the volume change can be determined by

$$\Delta V = \lambda \int_{r_0}^R \int_{\pi}^{2\pi} \Theta r dr d\alpha$$

2

where:

$\lambda$  = slip distance of the dislocation  $\sim 2r_a = 0.248 \times 10^{-9} \text{ m}$

$r_a$  = atomic radius of iron =  $0.124 \times 10^{-9} \text{ m}$

$r, \alpha$  = carbon atom co-ordinates relative to the dislocation

$r_0$  = minimum value for  $r \sim 2 \text{ \AA}$

$R$  = maximum value for  $r \sim 10 \text{ \AA}$

$\Theta$  = stresses caused by dislocation

and using Koehler's (1941) formula for the stresses around a positive edge dislocation

$$\Theta = -\frac{\lambda}{2\pi} \frac{1-2\nu}{1-\nu} \frac{\sin \alpha}{r}$$

3

with

$\nu$  = Poisson's ratio = 0.28

To a first approximation the stress caused by the dislocation becomes infinite at the centre of a dislocation where the elastic continuum theory from which it is calculated is not valid. In a crystal this "infinity at the centre" is limited by a "cut-off" at a certain minimum radius  $r_0$  inside which is deemed to be the "core" of the dislocation. There are two reasons for  $r_0$ : (i) the failure of Hooke's law at large strains and, (ii) the discreteness of the atomic structure, the displacements and forces between atoms in the core being finite<sup>(22)</sup>. So, assuming that the minimum value for  $r = r_0 \sim \lambda$  and using the calculated value of  $\Delta V (=7.8 \times 10^{-30} \text{ m}^3)$ ,  $R$  is about 10 Å. It is thus reasonable to assume that in the equilibrium state only "one" carbon atom per atom plane is present within 10 Å of the dislocation centre. Since the greatest tensile strain must occur immediately below the dislocation centre and in the atomic plane which constitutes the lower side of the slip plane, the most favourable position for the central carbon atom will be at  $\alpha = 3\pi/2$  and  $r \sim 2$  Å, and it seems likely that the central part of the atmosphere consists of a line of carbon atoms, parallel to the dislocation line, in this position (Figure 8).

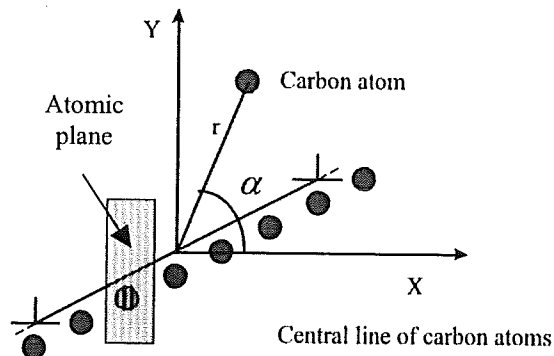


Figure 8 Carbon atoms in the strain field of a positive edge dislocation and the central carbon line of Cottrell atmosphere

In the annulus between 10-20 Å, the total volume change is again about the same as that produced by one carbon atom per atom plane, but this volume change is spread more uniformly over a much larger region of the crystal and, in this case, the carbon atoms are not linearly arranged.

It can be concluded that an extremely small amount of carbon is required to provide atmospheres for all dislocations in a crystal; although the actual value depends, of course, on the density of dislocations. Cottrell determined that for a dislocation density of  $10^{12} \text{ m}^{-2}$  the amount of C absorbed by dislocations for full yield point (under the assumption that every dislocation has one carbon atom per atom plane) was about 1 wt-ppm<sup>(21)</sup>. The amount of carbon necessarily to pin all dislocations, has been confirmed by Vandeputte and De Cooman<sup>(23)</sup>. They established that for a total dislocation density

after a tensile prestraining of 10% in an ultra low carbon bake hardening steel [ $2.8 \times 10^{13} \text{ m}^{-2}$  -  $1.3 \times 10^{14} \text{ m}^{-2}$ ], the required carbon for saturation is 0.25 - 1.2 wt-ppm.

### 2.3.3 Carbide precipitation

The last stage of the bake hardening process is the precipitation of  $\epsilon$ -carbides. It is supposed that the precipitation of carbides during ageing occurs preferentially at dislocations. As the process continues, more interstitials arrive at dislocations and denser atmospheres are formed around them. These atmospheres act as nuclei for the precipitation during the last stage, but for growth, there is – within the time of ageing – no more carbon available than that in solid solution. Therefore, the volume fraction of possible precipitation is fixed for a specific steel. However, the size of the particles is dependent on the number of nuclei per unit volume. If the dislocation density is increased by pre-deformation, the number of favourable precipitation sites increases and with that the number of particles will rise. In this case the particle size decreases because of the constant total volume fraction of carbides. The stress increase due to the cutting of coherent precipitates (Kelly-fine mechanism) is proportional to the particle size; and decreases if the particle size decreases. With increasing prestrain (and therefore decreasing particle size)  $\Delta\sigma_{\text{precipitation}}$  (the largest possible increase in the third stage of bake hardening) decreases<sup>(4, 20, 23, 24, 25, 26)</sup>. If time of ageing is long enough for particles to coarsen, then the dislocation bows around the particle (Orowan mechanism) can progress more easily by not cutting through the precipitate (Figure 9). Larger particles mean fewer particles (via coarsening) hence lower flow stresses<sup>(27)</sup>.

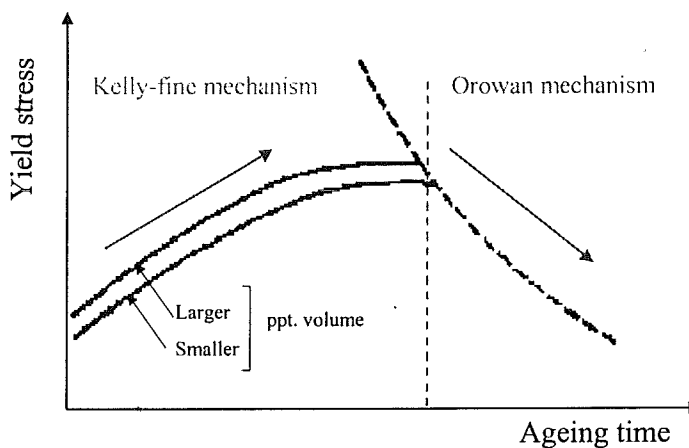


Figure 9 Schematic variation of yield stress with ageing time for typical age-hardening alloys with two different volume fractions of precipitate<sup>(28)</sup>

### 2.3.4 Description of the kinetics of bake hardening

Strengthening by the Snoek-effect, Cottrell-effect and particle hardening occur as a continuous process (Figure 10) and can be summarised as a “diffusion process”. Precipitation follows the formation of Cottrell-atmosphere and the latter occurs after the Snoek-effect. However, it is possible to simplify the process by treating the three stages as an additive process. This will allow a better understanding of the influence of each stage on the bake hardening response. The increase in yield stress during baking treatment can then be expressed by:

$$\Delta\sigma_{BH} = \Delta\sigma_{\text{Snoek}} + \Delta\sigma_{\text{Cottrell}} + \Delta\sigma_{\text{precipitation}}$$

As mentioned before, the Cottrell-effect is the most important of the three stages, followed by the precipitation process. The Snoek effect is always completed (due to its rapid mechanism) and cannot be further influenced by the bake hardening treatments applied by car manufacturers (150-200 °C). The long times (see Figure 10) and/or high temperature needed for the precipitation stage restrict its use for increasing the bake hardening response during conventional manufacturing.

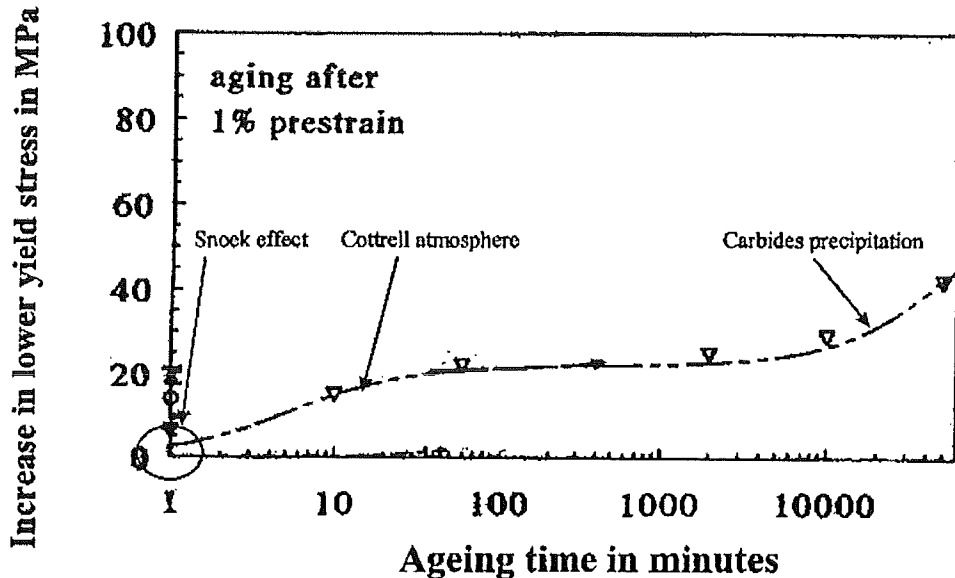


Figure 10 Increase in lower yield stress after a prestrain of 1% and ageing at 100°C for ZStE 180BH (0.03 wt% C)<sup>(9)</sup>

## 2.4 Effect of carbon (c) and/or nitrogen (n) content

If  $x_C$  (concentration of C in solution),  $x_N$  (concentration of N in solution) or the combined level of  $x_{C+N}$  is too high, then spontaneous strain ageing after temper rolling can occur during storage of the steel at ambient temperatures. For bake hardening, solute  $x_N$  can not be utilised, since  $x_N$  diffuses too fast, hence causes room temperature ageing<sup>(1, 11, 29, 30)</sup> (see Table 2).

Table 2 Activation energies, frequency factor, diffusion coefficient and diffusion distances for diffusion of interstitial solutes in b.c.c. metals (Stephenson<sup>(31)</sup>)

Parameter	Fe:C	Fe:N
Activation energy $Q_D$ (kJ/mol)	80.2 - 84.1	73.2 - 77.8
Frequency factor $D_o$ (cm <sup>2</sup> s <sup>-1</sup> )	$6.2 \times 10^{-3}$	$3.0 \times 10^{-3}$
Diffusion coefficient $D$ at 25°C (cm <sup>2</sup> s <sup>-1</sup> )	$5.9 \times 10^{-17}$	$1.4 \times 10^{-16}$
Diffusion distance $X = \sqrt{2Dt}$ (μm) at 25°C, for $t = 6$ months	0.43	0.66
Diffusion distance $X = \sqrt{2Dt}$ (μm) at 170°C, for $t = 20$ min	0.74	0.89

Generally, N is tied up by adding Al and conventionally, the solute  $x_C$  is limited to 25 wt-ppm. or less to avoid strain ageing (i.e. diffusion of C atoms to dislocations during storage or transportation of the steel). According to Atsuki Okamoto et al.<sup>(11)</sup> a bake

hardenable sheet steel with non-ageing properties at room temperature can be obtained by controlling the free nitrogen content to around 8 ppm., via open coil annealing in a controlled atmosphere of hydrogen and nitrogen. The bake hardening, as expected, increases with  $x_C$  (Figure 11).

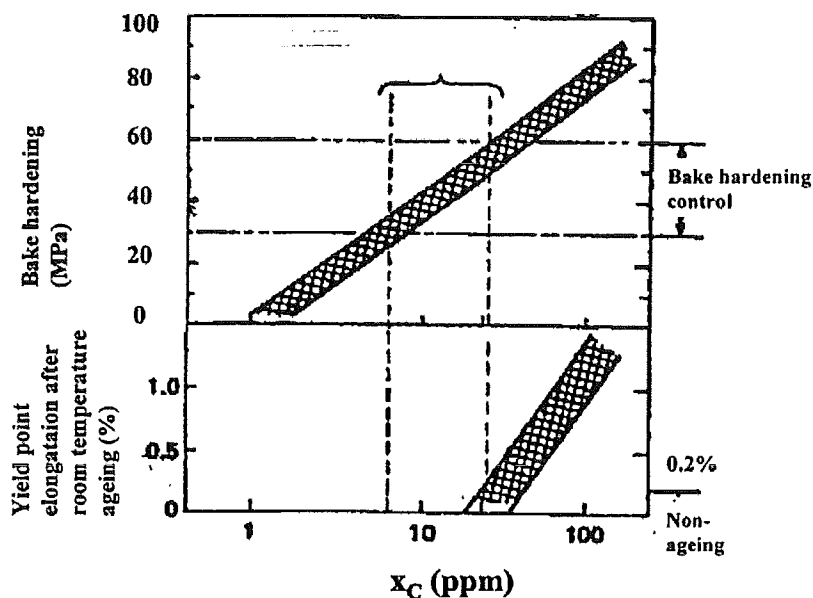


Figure 11 Effect of solute carbon on bake-hardenability and room temperature ageing<sup>(11)</sup>

For ultra low carbon titanium steels where most of the  $C$  is used to form ( $Ti_4C_2S_2$ ) precipitates, the acceptable minimum and maximum  $x_C$  levels depend on the yield strength, uniform elongation, plain strain ratio and bake hardening response required. To satisfy all these requirements, the amount of carbon in solution needs to be in the range 10 to 45 ppm. The lower limit for excess carbon is controlled by the minimum bake hardening required ( $\Delta\sigma_{BH}$ ) and the upper limit is governed by the ageing resistance and drawability requirement ( $r_{90} \geq 1.60$ )<sup>(30)</sup>(Table 3).

Table 3 Determination of the ideal  $x_C$  level<sup>(30)</sup>

Property specification	Minimum $x_C$	Maximum $x_C$
Yield strength: 180 -260 MPa	No minimum	68 ppm
%Uniform elongation: 17-25%	No minimum	2 000 ppm
$r_{90}$ : 1.6-2.5	No minimum	45 ppm
$\Delta\sigma_{BH}$ : 25-55 MPa	10 ppm	45 ppm

Mitsui et al.<sup>(32)</sup> reported that  $\Delta\sigma_{BH}$  should be kept below 60 MPa to ensure that the yield point elongation is less than 0.2% after ageing to avoid stretcher strain problems. Consequently, the need for room temperature stability limits the amount of  $C$  in solution and the amount of bake hardening that may be achieved<sup>(32)</sup>. Reducing the diffusivity of  $C$  is one possibility to combine high ageing resistance and good bake hardenability. This can be achieved by complexing. If the solute atom has a smaller size than that of *b.c.c.*  $Fe$ , there will be an interaction between the small interstitial atoms and the solute atoms, thereby reducing the lattice strain energy and reducing the diffusivity. Such complexing is known to occur between  $C$  and  $Mn$ <sup>(33)</sup>.

## 2.5 Effect of grain size on the bake hardening response

The stable processing of bake hardening steels requires proper grain size control as grain boundaries provide low energy sites for interstitial carbon atoms. A variation of the grain size influences the distribution of carbon between the grain interior and the grain boundary by changing the number of segregation sites at the grain boundary. With an increase in grain size the grain boundary area decreases and the total amount of carbon that can be stored in the grain boundary decreases compared to that in a fine grained structure (2, 5, 7, 11, 33). It was suggested that at room temperature the carbon situated at grain boundaries would not contribute to room temperature ageing as it would already occupy the lowest energy position. It was postulated however, that at the elevated temperatures used during paint curing operations (170 °C), it would be possible for this carbon to diffuse from grain boundaries and contribute to bake hardening. As a fine grain size offers more grain boundary sites for the diffusion of carbon, it was suggested that it was this mechanism that was responsible for the observed increases in bake hardening with decreasing grain size.

Figure 12 shows the relationship between the grain size  $d$  and  $x_{C+N}$  (concentration of C+N in solution), based on the measurement of  $\Delta\sigma_{BH}$ . The solid lines give combinations of  $x_{C+N}$  and  $d$  which will result in a certain value for  $\Delta\sigma_{BH}$  after standard bake hardening treatment (2% prestrain, 170°C for 20 minutes).

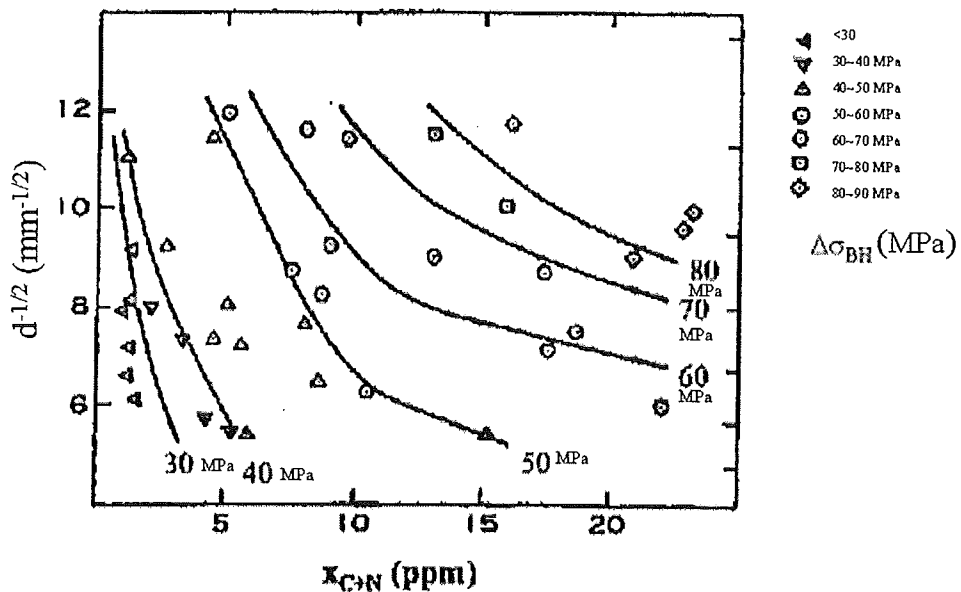


Figure 12 Effect of grain size and solute (C+N) content on  $\Delta\sigma_{BH}$  of low-C Al-killed steel after standard bake hardening treatment<sup>(1)</sup>

Figure 13 shows the relation of  $\Delta\sigma_{BH}$  and  $x_{C+N}$  for two grain sizes, for which the reciprocals of the square root is  $6 \text{ mm}^{-1/2}$  and  $11 \text{ mm}^{-1/2}$ .  $\Delta\sigma_{BH}$  increases in proportion to  $x_{C+N}$  when  $x_{C+N}$  is small, but becomes constant beyond a certain level of  $x_{C+N}$ . What is remarkable is that the onset of saturation varies with the grain size. The smaller the grain size, the larger the saturated value of  $\Delta\sigma_{BH}$ . Thus  $R_{BL}$  is a function of  $x_{C+N}$ , which in turn governs the intensity of the grain size effect on the bake hardening response.<sup>(1, 34)</sup>

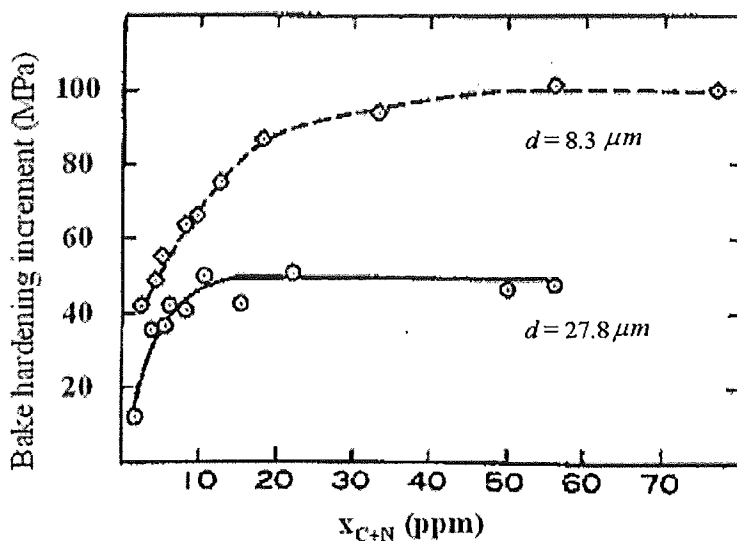


Figure 13 Effect of dissolved (C+N) content on  $\Delta\sigma_{BH}$  for two different grain sizes of low-C Al-killed steel after standard bake hardening treatment <sup>(1)</sup>

## 2.6 Effect of prestrain level, temperature and ageing time

The increase in lower yield stress,  $\Delta\sigma_{BH}$ , after a prestrain level of respectively, 1, 2 and 5%, and ageing at 150 °C is shown in Figure 14. It can be clearly seen that the yield stress rises in two steps<sup>(25, 26)</sup>. A yield strength increase of 20 MPa is reached after a short time of ageing (this level is characterised as  $(\Delta\sigma_{Snoek} + \Delta\sigma_{Cottrell})$ ). This increase can be attributed to the Snoek effect and Cottrell atmosphere formation, but it is not possible to define what the contribution of each is. In the last step (precipitation) there is an additional increase of the yield stress. With increasing prestrain the maximum strength increase in the last step ( $\Delta\sigma_{Precipitation}$ ) decreases. Both the first and the second step of the increase in  $\Delta\sigma_{BH}$  are shifted to shorter times if the ageing temperature is increased. This effect is proven by comparing Figure 15 (giving the results of ageing at 180 °C) to Figure 14 (giving the results of ageing at 150 °C) where the onset of the second step starts 20 times earlier.

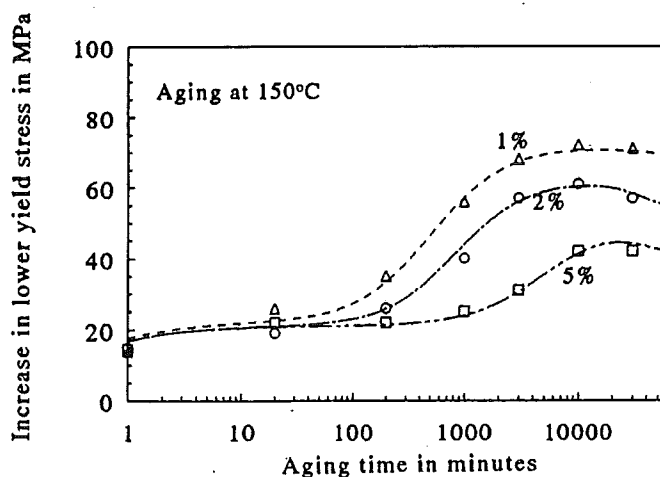


Figure 14 Increase in lower yield stress after different prestrain levels and ageing at 150 °C for ZStE 180BH (0.03 wt% C) <sup>(4)</sup>

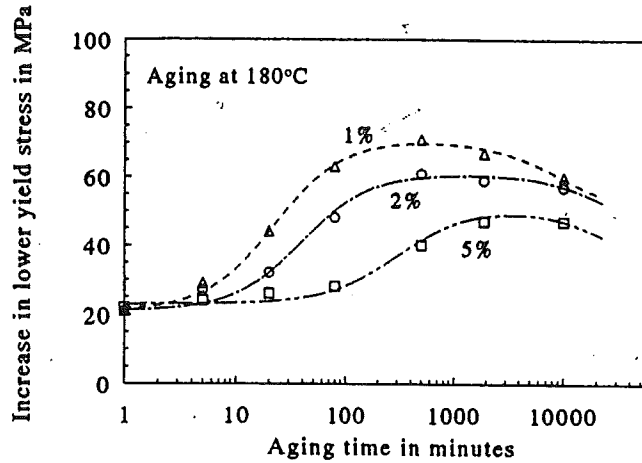


Figure 15 Increase in lower yield stress after different prestrain levels and ageing at 180 °C for ZStE 180BH (0.03 wt% C) <sup>(4)</sup>

Figure 16 to Figure 17 summarise the results of ageing experiments at different ageing temperatures (50-180 °C) after a prestrain of 2 and 5%. At low temperatures, i.e. 50 to 120 °C, the first step of the increase in yield stress depends on time. At temperatures above 120 °C the first step is already finished within the first minutes of ageing. From Figures 16 to 17 it can be seen that for a constant prestrain the maximum increase in  $\Delta \sigma_{BH}$  in the last step is independent of the ageing temperature for ageing temperatures greater than 120 °C. The same level of  $\Delta \sigma_{Precipitation}$  is always reached, if the ageing time is sufficiently long. The ageing temperature has a strong influence on the rate at which the yield point increases. To realise an increase in  $\Delta \sigma_{BH}$  of 40 MPa after a prestrain of 2% an ageing time of  $\sim 100$  min at 170 °C is necessary. The time has to be increased by a factor of 100 to get the same value of  $\Delta \sigma_{BH}$  by ageing at 120 °C.

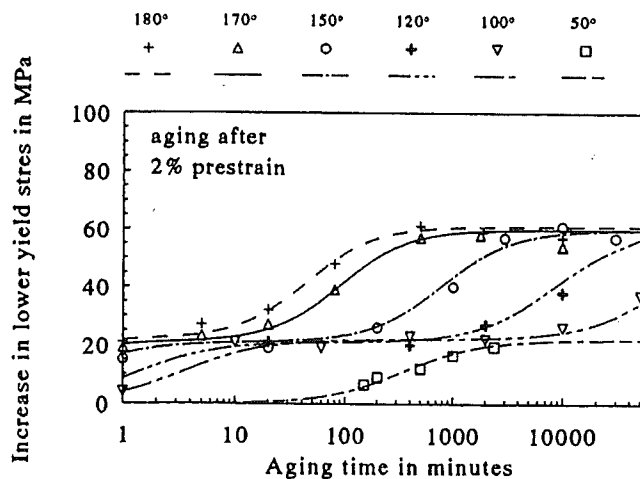


Figure 16 Increase in lower yield stress after a prestrain of 2% and ageing at different temperatures for ZStE 180BH (0.03 wt% C) <sup>(4)</sup>

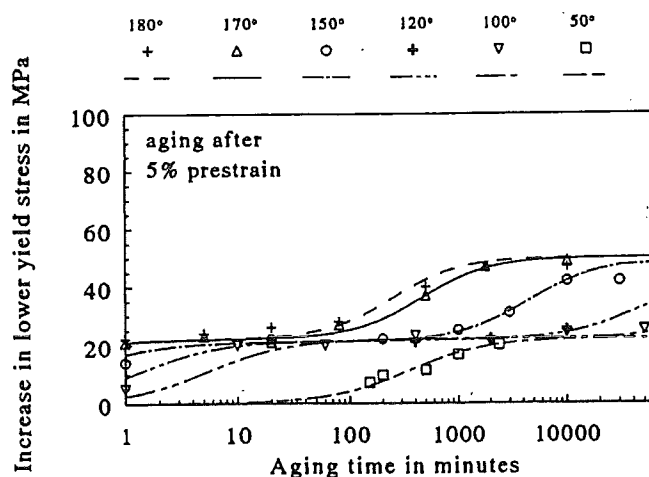


Figure 17 Increase in lower yield stress after a prestrain of 5% and ageing at different temperatures for ZStE 180BH (0.03 wt% C)<sup>(4)</sup>

A quantitative evaluation of the maximum increase in yield stress in the first and second step as a function of prestrain and ageing temperature is shown in Figure 18. The open symbols indicate the maximum increase in yield stress in the first step, the filled symbols represent the additional increase in the second step. The evaluation was carried out for four ageing temperatures. Within the investigated temperature and prestrain range it is evident that the first rise is independent of ageing temperature and prestrain level. There is a constant or maximum level for the first step. The maximum increase in the second step is only a function of prestrain and independent of the ageing temperature provided sufficient time is allowed. With increasing prestrain level the strengthening in the second step decreases. This is in agreement with a carbide precipitation mechanism (see §2.3).

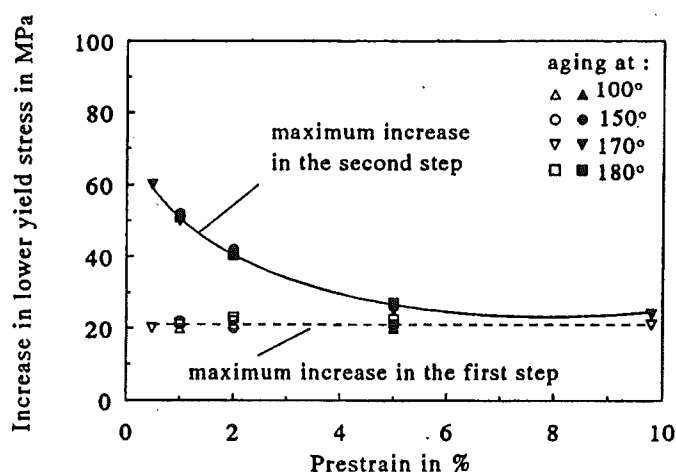


Figure 18 Increase in lower yield stress in the first and second step of bake hardening as a function of prestrain and ageing temperature for ZStE 180BH (0.03 wt% C)<sup>(4)</sup>

## 2.7 Discussion

### 2.7.1 Prestrain orientation

The bake hardening test is conventionally a simulation of the stamping and paint baking process by an “accelerated” strain-ageing test. However, many authors<sup>(35, 36, 37)</sup> consider that the bake hardening response cannot be predicted precisely by an

accelerated strain-ageing test, because the bake hardening process depends on the type (and level) of prestrain and temperature.

The temper rolling deformation is “to some extent” analogous to the deformation introduced by a tensile pre-straining in an interrupted tensile test. In both cases, the cold working introduces new dislocations. These dislocations attract dissolved interstitial atoms by the general mechanism of strain ageing. Although the diffusion processes and solute-dislocation binding force are intrinsically similar in both cases, the yield point returns faster in the interrupted tensile test. In addition, the shape of the stress - strain curve is different, such that the work hardening rate of sample prestrained by tension<sup>(33)</sup> is higher.

In the interrupted tensile test, the prestrain, and the subsequent deformation are along the same strain path. In contrast, samples removed from temper rolled sheet experienced rolling (plane strain) and tensile deformation. As the diffusion of  $x_C$  is intrinsically similar in both cases, the difference in ageing response and yielding behaviour is indicative of the influence of the different dislocation distributions introduced by the type of prestrain<sup>(33)</sup>.

This behaviour can be explained by the Bauschinger effect that aids activation of dislocation sources when the direction of straining is different from the direction of prestrain. The mechanism of the Bauschinger effect lies in the structure of the cold-worked state. Orowan<sup>(38)</sup> has pointed out that during plastic deformation dislocations will accumulate at barriers in tangles, and eventually form cells. Now, when the load is removed, the dislocation lines will not move because the structure is mechanically stable. However, when the direction of loading is reversed, some dislocation lines can move an appreciable distance at a low shear stress because the barriers to the rear of the dislocations are not likely to be so strong and closely spaced as those immediately in front. This gives rise to initial yielding at a lower stress level when the loading direction is reversed<sup>(6, 11, 27, 39)</sup>.

Figure 19 shows tensile load-elongation curves of specimens cut out in two directions from a stamped panel uniaxially deformed by 4% strain. In the one case the tensile tests were conducted on the as machined sample and on the second after a heat treatment. When pre-deformation and secondary deformation are in the same direction, an upper yield point and yield point elongation is evident. However, when the directions are perpendicular to each other (even when a heat treatment is applied) the yield strength is low (absent of yield point)<sup>(11)</sup>. The differences of the stress-strain curves “just after pre-straining” could be due to the fact that the work hardening during pre-straining is also directional. It is observed that there is almost no increase in the yield strength after baking when re-straining occurs perpendicular to the original pre-straining direction.

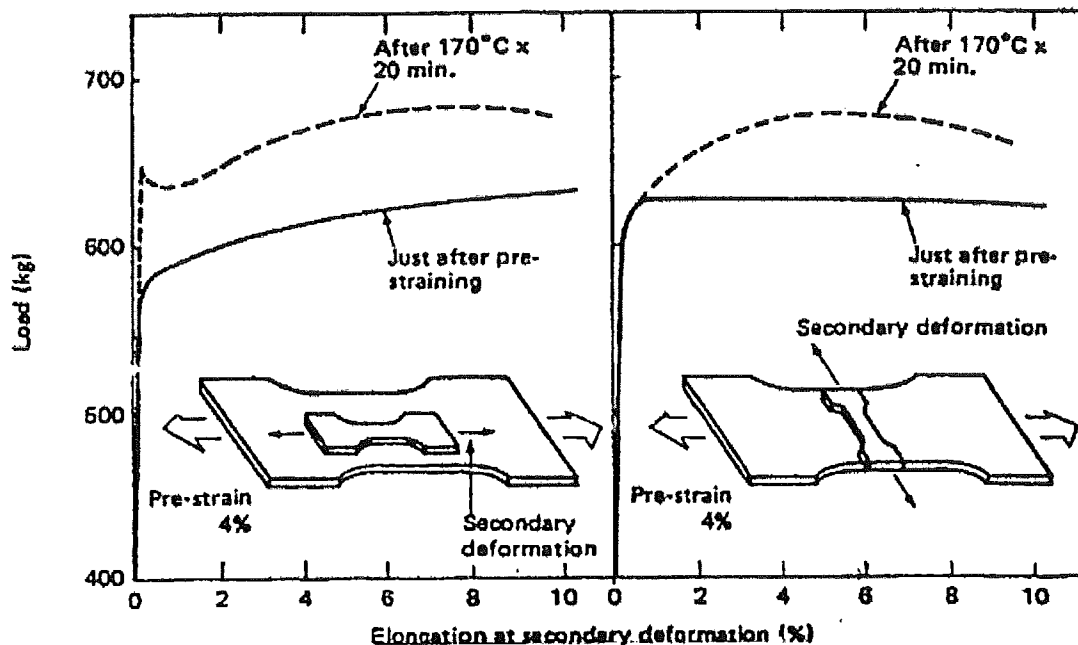


Figure 19 Effect of a pre-deformation direction on bake hardening behaviour (Batch-annealed steel)<sup>(11)</sup>

This phenomenon is metallographically explained in Figure 20 and Figure 21. That is, if the stress direction of pre-deformation and subsequent deformation is the same, the active slip systems will be similar. The dislocations locked by  $C$  and  $N$  during pre-straining will become a significant barrier to subsequent deformation thereby raising the yield strength. However if the stress direction of the secondary deformation is different from that of the pre-deformation, another slip system will come into play, which does not have as many dislocations locked by  $C/N$  due to the initial lower concentration of that orientation. The yield strength, as a result, does not increase as much. This suggests that the bake hardening response is more related to locking of mobile dislocations than to matrix strengthening via precipitation.

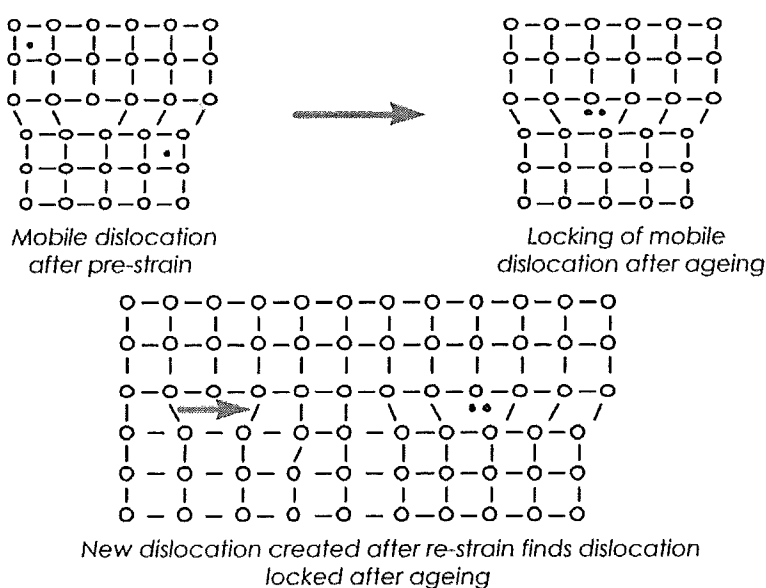


Figure 20 Relationship between pre-deformation and secondary deformation direction - same direction

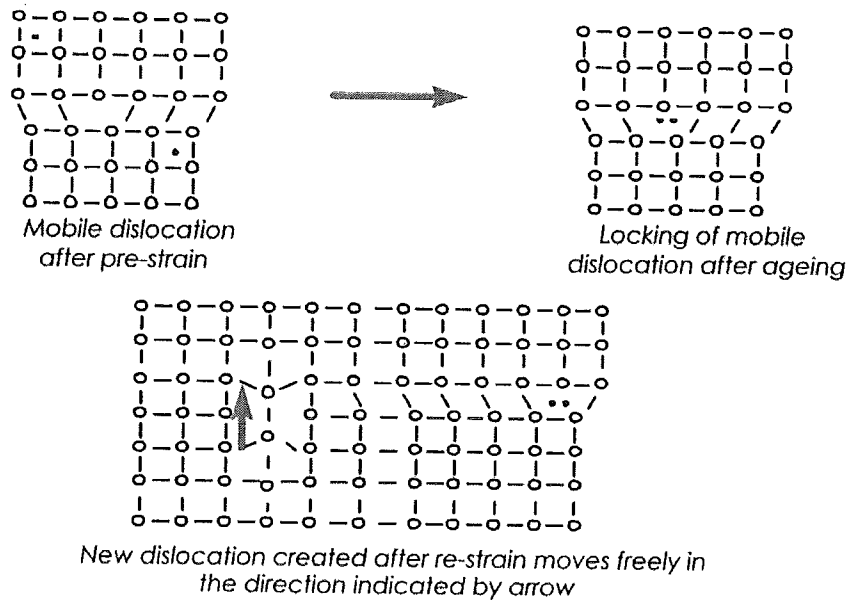


Figure 21 Relationship between pre-deformation and secondary deformation direction - different direction

The influence of the amount of prestrain on the bake hardening response was given in Figure 18. It was concluded that the maximum bake hardening response decreases with increasing pre-strain. However, Jeong<sup>(35)</sup> found that for samples prestrained and baked at 170 °C (0-0° test), an optimum level of work hardening (level of deformation) exists that renders a maximum bake hardening response. From Figure 22 it is apparent that the highest level of yield strength increase after baking is obtained by a work hardening degree of 17 MPa. A clear explanation is not given and this needs further research.

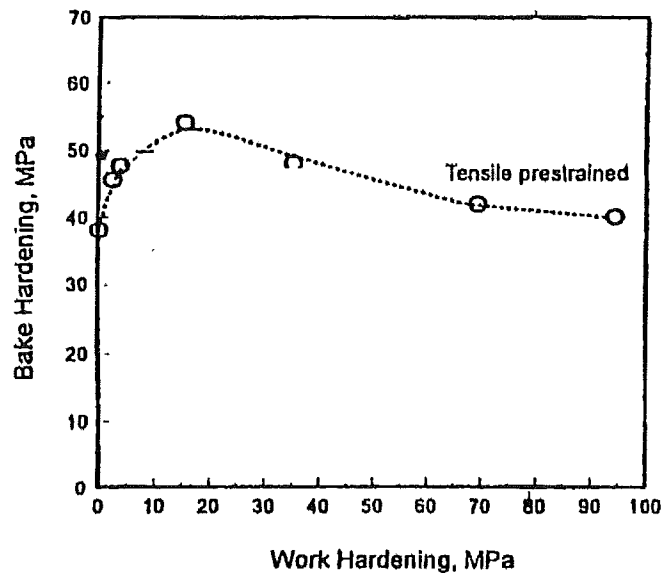


Figure 22 Relationships between bake hardening and work hardening in Ti-added ultra-low carbon Al-killed steel<sup>(35)</sup>

### 2.7.2 Time and temperature bake hardening treatment

To determine temperature and time equivalents, that would result in similar bake hardening responses it is common practice to use Hundy's<sup>(40)</sup> equation as a first approximation. This equation assumes that the bake hardening process is a kind of

strain ageing and is based on the equation by Cottrell and Bilby,<sup>(21)</sup> which gives the number of solute atoms arriving at a unit length of edge dislocations. The Hundy derivative relates the time of strain ageing at room temperature to that at a different temperature.

Cottrell and Bilby have shown theoretically, and Harper<sup>(17)</sup> has confirmed this experimentally, that strain ageing is governed by the equation

$$n(T, t) = \alpha N \left( A \frac{Dt}{kT} \right)^{2/3}$$

5

where

$n(T, t)$  = number of solute atoms transferred to unit length of a dislocation in a time  $t$   
(this is a measure of the degree of ageing)

$\alpha$  = a number equal to 3

$N$  = number of solute atoms in unit volume

$A$  = parameter measuring the interaction between the dislocation and the solute atom

$D$  = diffusion coefficient of the solute in  $\alpha$ -iron

$k$  = Boltzmann's constant

$T$  = temperature

For equal degrees of strain ageing at different temperatures, assuming  $\alpha$ ,  $N$ ,  $A$  to be temperature-independent, the Hundy's equation results from the assumption that  $n(T, t) = N(T_r, t_r)$  (e.g., at room temperature  $T_r$  and some other temperature  $T$ ), which would render;

$$\log \frac{t_r}{t} = \frac{Q}{R} \times \log e \times \left( \frac{1}{T_r} - \frac{1}{T} \right) - \log \left( \frac{T}{T_r} \right)$$

6

Therefore,

$$\log \left( \frac{t_r}{t} \right) = K \left( \frac{1}{T_r} - \frac{1}{T} \right) - \log \left( \frac{T}{T_r} \right)$$

7

where

$Q_D$  is the activation energy

$R$  is the gas constant

$K$  is  $(Q/R) \times \log e$  (for  $C$ ,  $K=4400K$ ; for  $N$ ,  $K=4000K$ ) and

$t_r$  is the ageing time at room temperature  $T_r$ .

Equation 7 enables one to convert a known ageing time and temperature to an equivalent ageing time, that will render a similar degree of ageing, at another temperature. However, it was pointed out by many authors<sup>(35, 40)</sup> that Hundy's equation is only valid below 100 °C and the discrepancy, 2 to 3 orders of magnitude, between the calculated equivalent ageing times and those determined by experiments for temperatures higher than 100 °C is due to the incorrect assumption that the amount of solute atoms is independent of temperature.

Simple unidirectional tensile tests of bake-hardenability, in which ageing is confined to a short time at a temperature up to 170 °C, can give a misleading bake hardening response compared to that attained in applications which involve stress systems applied in service. The reason for the direction dependence, is primarily due to the work-hardened structure, but this is enhanced by strain-ageing.

For some applications, it would be advantageous to separate the strain ageing process from the paint baking process, particularly in view of the tendency to reduce paint baking temperatures. There are also potential benefits of baking in the 200 °C to 230 °C range to obtain an even greater bake hardening response without deteriorating formability in the case of dispersion-hardened and dual-phase steels.

## Chapter 3: Experimental procedure

### 3.1 Introduction

The experiments carried out as part of this research are presented according to the following structure:

- An outline of the material in §3.2
- Sample preparation and orientation for tests in §3.3
- The bake hardening simulation as applied by steel's producers in §3.4
- Tensile and compression tests used to simulate the bake hardening response in §3.5
- Determination of strain distribution after predeformation in §3.6
- Transmission electron microscopy (*TEM*) for analysing the microstructure in §3.7 and,
- A review on the calculation of the bake hardening response in §3.8

### 3.2 Material

The material used in this investigation was an *ULC* based *H180BD* grade. The *H* denotes cold rolled flat products of high strength for cold forming, *180* the minimum proof strength ( $R_{p0.2}$ ) in  $\text{N/mm}^2$ , *B* bake-hardened and *D* that the material has been hot-dip galvanised. The chemical composition and the transverse mechanical properties according to *EN10292* for *H180BD* are specified in Table 4 and Table 5.

Table 4 Chemical composition range as for *H180BD* (cast analysis)

	<i>C</i> max.	<i>Si</i> max.	<i>Mn</i> max.	<i>P</i> max.	<i>S</i> max.	<i>Al</i> min.	<i>Ti</i> <sup>(*)</sup> max.	<i>Nb</i> <sup>(*)</sup> max.
Weight %	0.04	0.50	0.70	0.06	0.025	0.02	---	---

<sup>(\*)</sup> These additional elements may be used individually or in combination. Vanadium and boron may also be added. The sum of these 4 elements should not exceed 0.22%.

Table 5 Required mechanical properties for *H180BD* in the transverse direction

0.2%-proof strength <sup>(1)</sup> $R_{p0.2}$ $\text{N/mm}^2$	Increase in proof strength after heating $\Delta\sigma_{BH}$ $\text{N/mm}^2$	Tensile strength $R_m$ $\text{N/mm}^2$	Elongation $A_{80}$ mm	Plastic strain ratio $r_{90}$ min.	Strain hardening exponent $n$ min.
180 to 240	35	300 to 400	34	1.6	0.16

<sup>(1)</sup> If the discontinuous yielding is pronounced, the values apply to the lower yield point ( $R_{bL}$ )

The material in the as-received condition were sheets of 1000 mm x 1411 mm x 0.685 mm respectively, length, width and thickness. The sheets were cut into 4 strips of 1000 mm x 300 mm (length x width) and stored at -12 °C to prevent the material from ageing.

Subsequently, the strips were cut to smaller dimensions, 120 mm x 300 mm (width x length) and were deformed in tension perpendicular to the rolling direction at prestrain levels of  $\varepsilon_t = 0\%$ , 2%, 4%, 6% and 8% total elongation. (See Figure 23)

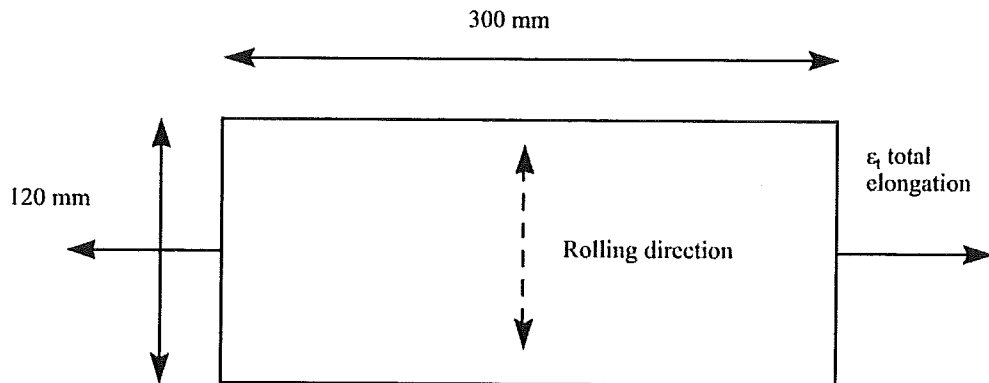


Figure 23 Prestrain orientation with respect to the rolling direction

### 3.3 Sample preparation and orientation

#### 3.3.1 Tensile samples

From the prestrained strips, tensile samples were machined. Two different orientations for the tensile samples were used, one with an angle ( $\alpha$ ) of  $90^\circ$  and another with an angle of  $0^\circ$  between the longest axis of the sample and the rolling direction, named *X* and *Y* respectively. (See Figure 24 and Figure 25)

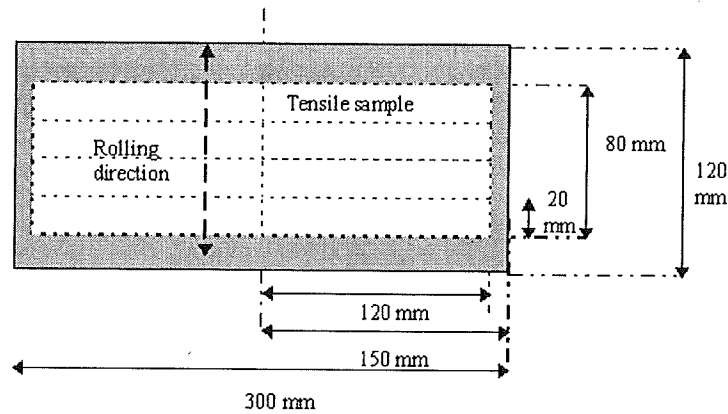


Figure 24 Orientation of machined X samples in relation to the rolling direction

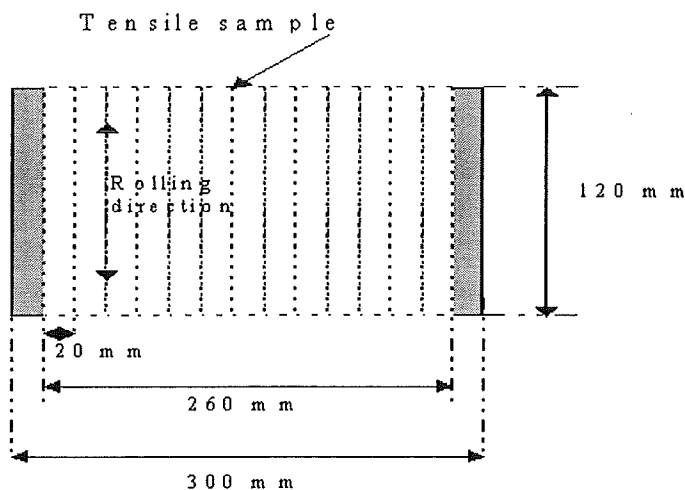


Figure 25 Orientation of machined Y samples in relation to the rolling direction

The dimensions of tensile samples are specified in Table 6 and Figure 26.

Table 6 Dimensions (in millimetres) of test pieces (cf. Figure 26)

Test piece type	Width $b$	Original gauge length $L_0$	Parallel length $L_c$	Test piece total length $L$
RJC <sup>(*)</sup>	$12.5 \pm 1$	50	60	120

(\*) Type used for tests due to sheet width limitations (max.  $L = 120$  mm)

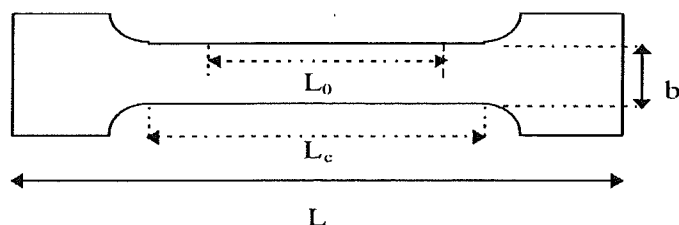


Figure 26 Tensile sample dimensions

In order to determine the as-received mechanical properties (the proof strength  $R_{p0.2}$  and the ultimate tensile strength  $R_m$ ) of the machined samples three X and Y samples (from non prestrained strips) were subjected to tension until failure.

### 3.3.2 Compression samples

For the compression samples, cubes were manufactured by stacking specimens (14) of 10 mm x 10 mm x 0.7 mm. To minimise the effects of ambient temperature ageing on the properties of the steel, all samples were stored in the freezer ( $T = -12$  °C) until required for testing.

The cubes were deformed with prestrain levels of  $\varepsilon_t = 2\%$ , 4%, 6% and 8% total elongation.

### 3.4 Heat treatment

#### 3.4.1 For tensile samples

##### 3.4.1.1 Single bake hardening treatment

To determine the bake hardening response,  $\Delta\sigma_{BH}$ , samples were subjected to a heat treatment at different temperatures and times, before testing until failure. Heat treatments were carried out using the Tamson T2500 silicon-based oil bath, with a maximum temperature of 250 °C and a tolerance of  $\pm 1$  °C. Triplicate samples were prepared for each bake hardening condition (temperature, time) in order to determine standard deviation and to estimate the test reproducibility. See Table 7 for the various conditions (temperatures and times) used during bake hardening.

Table 7 Bake hardening treatment applied to samples with different prestrain

Temperature (°C)	Time (min.)	$\epsilon_t$				
		0%	2%	4%	6%	8%
140	10		x			
	15		x			
	20	x	x	x	x	x
	25	x	x			
150	15	x	x			
	25	x	x			
170	10		x			
	15	x	x			
	20	x	x	x	x	x
	25		x			
200	10		x			
	15		x			
	20	x	x	x	x	x
	25		x			
230	10		x			
	15		x			
	20	x	x	x	x	x
	25		x			

##### 3.4.1.2 Double bake hardening treatment

In order to try to separate the contributions of the Cottrell mechanism and precipitation a double bake hardening treatment was devised. An initial thermal treatment was applied to machined samples ( $\alpha = 90^\circ$  between the longest axis of the sample and the rolling direction) with a 50 mm gauge length. See Table 8 for temperatures and time used.

Table 8 First bake hardening treatment

Temperature (°C)	Time (min.)
140	20
230	20

The baked samples were then deformed at prestrain levels of  $\varepsilon_l = 2\%$ ,  $4\%$ ,  $6\%$  and  $8\%$ . After prestraining samples were subjected to a second bake hardening treatment, with the same temperature and time as for the initial thermal treatment, before testing until failure (Table 9).

Table 9 Second bake hardening treatment

Temperature (°C)	Time (min.)	$\varepsilon_l$			
		2%	4%	6%	8%
140	20	x	x	x	x
230	20	x	x	x	x

### 3.4.2 For compression samples

To determine the bake hardening response,  $\Delta\sigma_{BH}$ , prestrained samples were subjected to a heat treatment at different temperatures for 20 minutes, before testing until failure. Triplicate samples were prepared for each bake hardening treatment (temperature, time) in order to determine a standard deviation and to verify test reproducibility. For the various paint baking conditions the reader is referred to Table 10.

Table 10 Bake hardening treatment for compression samples

Temperature (°C)	Time (min.)	$\varepsilon_l$			
		2%	4%	6%	8%
140	20	x	x	x	x
170	20	x	x	x	x
230	20	x	x	x	x

## 3.5 Mechanical testing

### 3.5.1 Tensile test

#### 3.5.1.1 Single bake hardening treatment

For the tensile tests, machined samples with a 50 mm gauge length were used. Except where stated, all samples were taken transverse to the rolling direction from the original plate. To minimise the effects of ambient ageing on the properties of the steel, all samples were stored in the freezer ( $T = -12\text{ °C}$ ) until required for testing.

Mechanical testing was performed on a Schenck tensile testing machine with a 100 kN maximum load capacity, according to the *NEN-EN 10002-2*, *ISO 7500/1* and *DIN 51302* standards at a nominal strain rate of  $1.7 \times 10^{-4} \text{ s}^{-1}$ .

The work hardening increase of the material after prestrain was calculated from

$$\Delta\sigma_{WH} = R_t - R_{p0.2}$$

8

where  $R_t$  is the flow stress in the strip after the prestrain  $\varepsilon_l$  and  $R_{p0.2}$  is the 0.2% proof-strength before prestrain.

The properties after bake hardening were then compared to the results obtained after prestraining the samples and the bake hardening response was calculated by:

$$\Delta\sigma_{BH} = R_{bL1} - R_t$$

9

where  $R_{bL1}$  constitutes the lower yield point (ignoring any initial transient effect) of the bake hardened sample and  $R_t$  represents the flow stress in the strip after a prestrain  $\varepsilon_t$ . (See Figure 27)

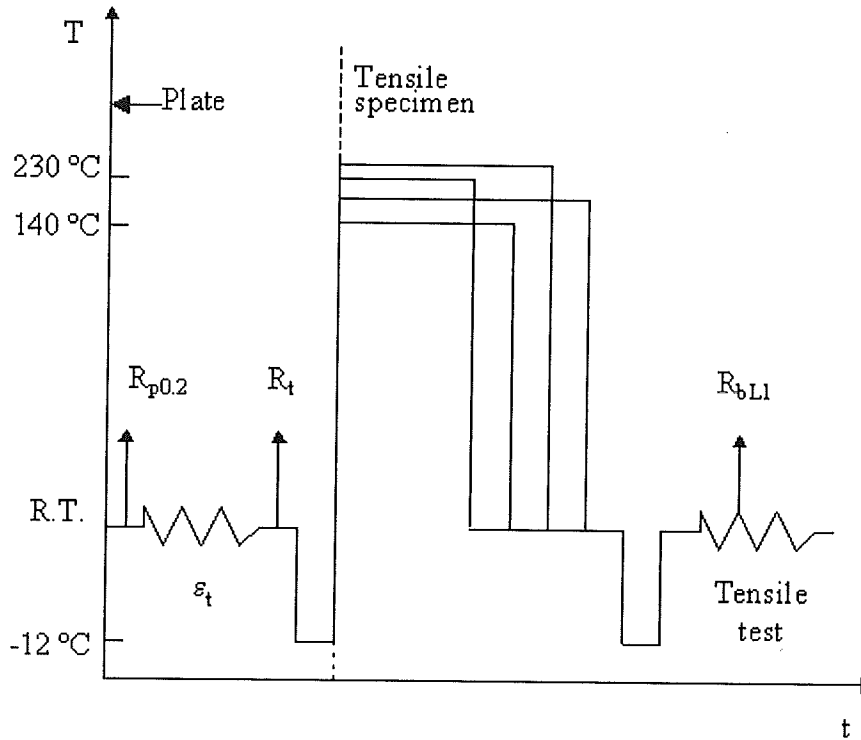


Figure 27 Schematic presentation of single bake hardening treatment and tensile testing

### 3.5.1.2 Double bake hardening treatment

The first bake hardening response was calculated from

$$\Delta\sigma_{BH1} = R_{bL1} - R_{p0.2}$$

10

where  $R_{bL1}$  is the lower yield point after the first bake hardening treatment and  $R_{p0.2}$  as defined before.

The work-hardening increase of the material after prestraining was calculated from

$$\Delta\sigma_{WH} = R_t - R_{bL1}$$

11

with  $R_t$  the flow stress in tensile sample after a prestrain  $\varepsilon_t$  and  $R_{bL1}$  as defined previously. The second bake hardening response was calculated from

$$\Delta\sigma_{BH2} = R_{bL2} - R_t$$

12

with  $R_{bL2}$  the lower yield point after the second bake hardening treatment and  $R_t$  as defined before. (See Figure 28)

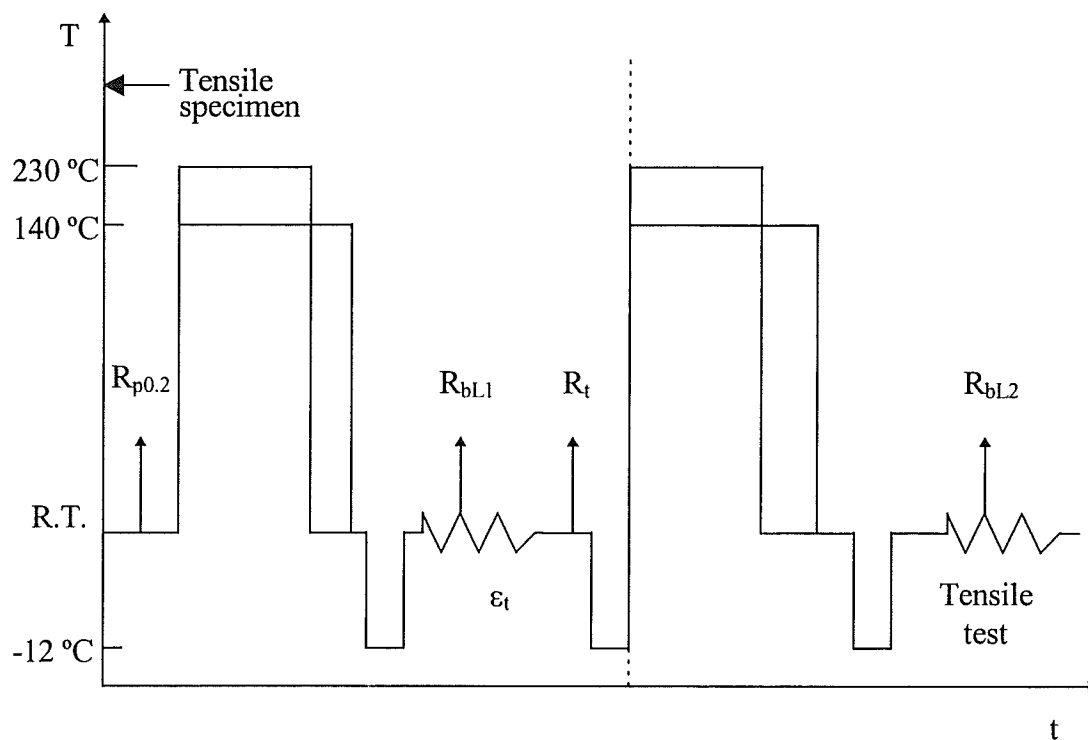
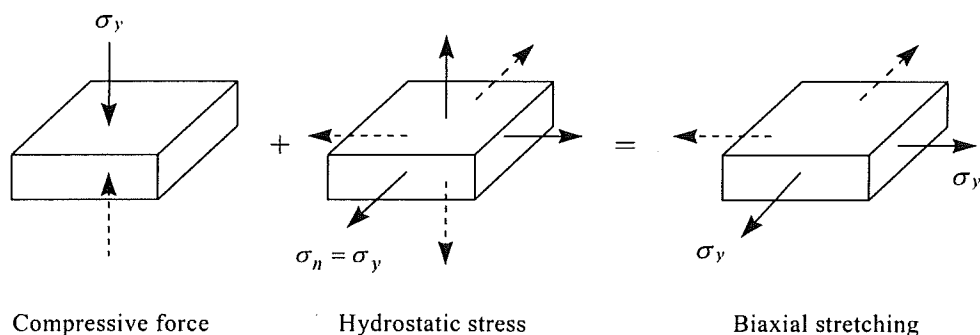


Figure 28 Schematic presentation of double bake hardening treatment and tensile testing



### 3.5.2 Compression tests

The compression tests were carried out with a Gleeble-3500 - with a 100 kN maximum load (with a force accuracy of  $\pm 1\%$ ) - at a nominal strain rate of  $1.7 \times 10^{-3} \text{ s}^{-1}$ . Teflon (PTFE) film was used as a lubricant during compression testing.

The net strain state of a compressed stacked specimen is equivalent to equi-biaxial stretching as illustrated in Figure 29.

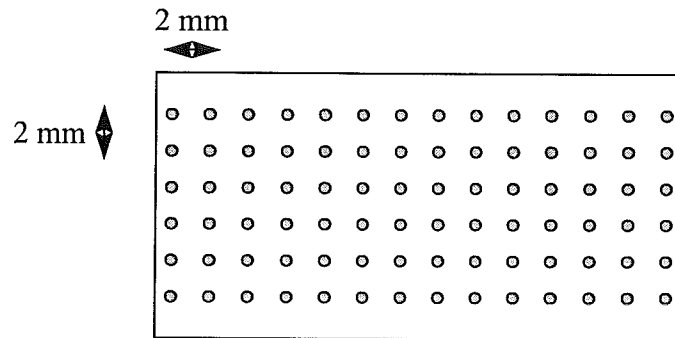
Figure 29 Biaxial stretching simulation

The equi-biaxial stretching or stretch forming is a forming process in which the material is stretched over a tool (die) under the following conditions:

$$\varepsilon_1 = \varepsilon_2 = \varepsilon, \varepsilon_3 = -2\varepsilon$$

where  $\varepsilon_1$ ,  $\varepsilon_2$  and  $\varepsilon_3$  are the principle strains.

The work hardening and bake hardening properties were determined as for tensile samples, single bake hardening treatment.



### 3.6 Strain distribution

In order to determine the real strain state after prestrain, an electro-chemically applied grid (consisting of dots of 1 mm - diameter, as shown in Figure 30) was applied on a strip before prestraining (Figure 30). After deformation at  $\varepsilon_t = 2\%$ ,  $4\%$ ,  $6\%$  and  $8\%$  with a tensile machine, the grid was re-measured with the help of Phast (software program). The eleven pictures that were taken of the grid at different angles were used as input to calculate the strain in the material. The results <sup>(41)</sup> will be presented in a two-dimensional (2D) plot and Forming Limit Diagram (FLD).

Figure 30 Schematic representation of grid on strip

Figure 31 and Figure 32 present the Two-dimensional plot (2D) and Forming Limit Diagram (FLD) for a strip deformed to 2%, whereas Figure 33 and Figure 34 present the 2D and FLD for a strip deformed to 8%. For the Forming diagrams two axes are defined: horizontal axis, the minor strain with a scale from 0 to -0.10 and a vertical axis, the major strain with a scale from 0 to +0.10. All results presented in Table 11 are the true strains.

Table 11 Major and minor strain measured in the centre of the prestrained strips

Prestrain $\varepsilon_t$ (%)	Major strain in the centre	Minor strain in the centre
2	$0.01 \pm 0.01$	$-0.02 \pm 0.01$
4	$0.03 \pm 0.01$	$-0.04 \pm 0.01$
6	$0.05 \pm 0.01$	$-0.05 \pm 0.01$
8	$0.07 \pm 0.01$	$-0.06 \pm 0.01$

From the figures it is evident that an ellipsoidal-yellow-red region (200 x 100 mm) with a rather uniform strain level exists for every strip.

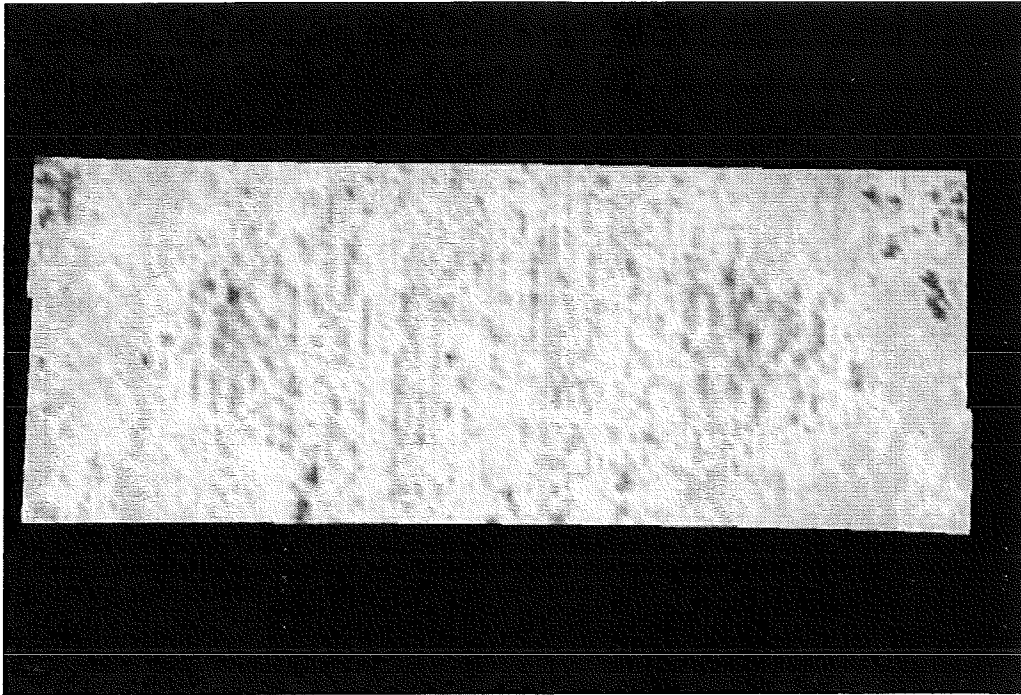


Figure 31 2D plot of the strain distribution for strip prestrained 2% (cf. Figure 32)

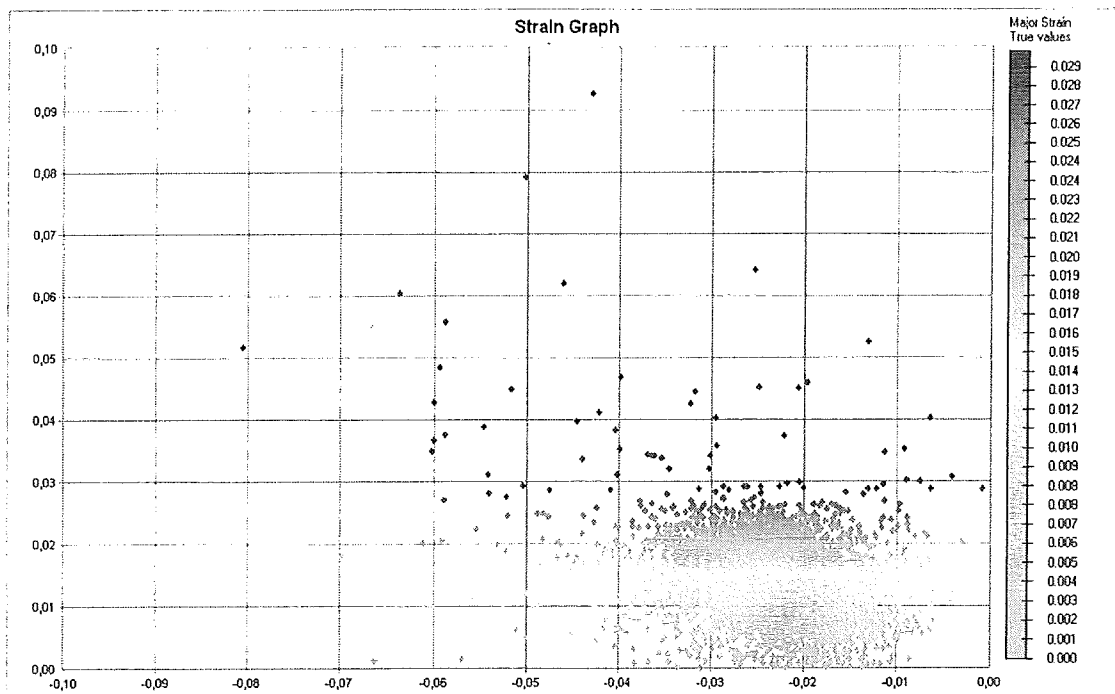


Figure 32 Forming limit diagram for strip prestrained 2%

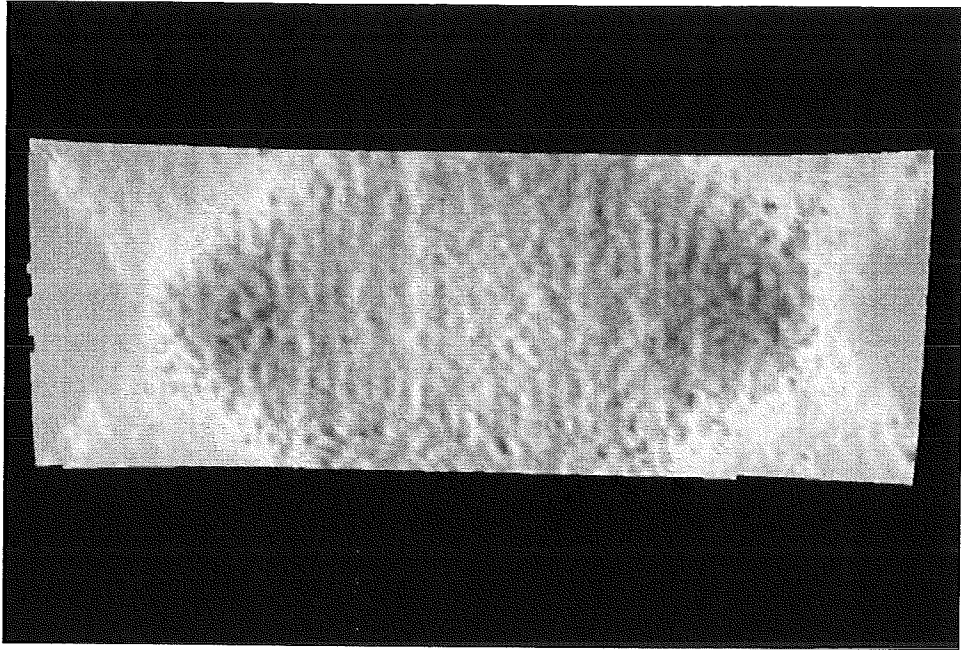


Figure 33 2D plot of the strain distribution for sample prestrained 8% (cf. Figure 34)

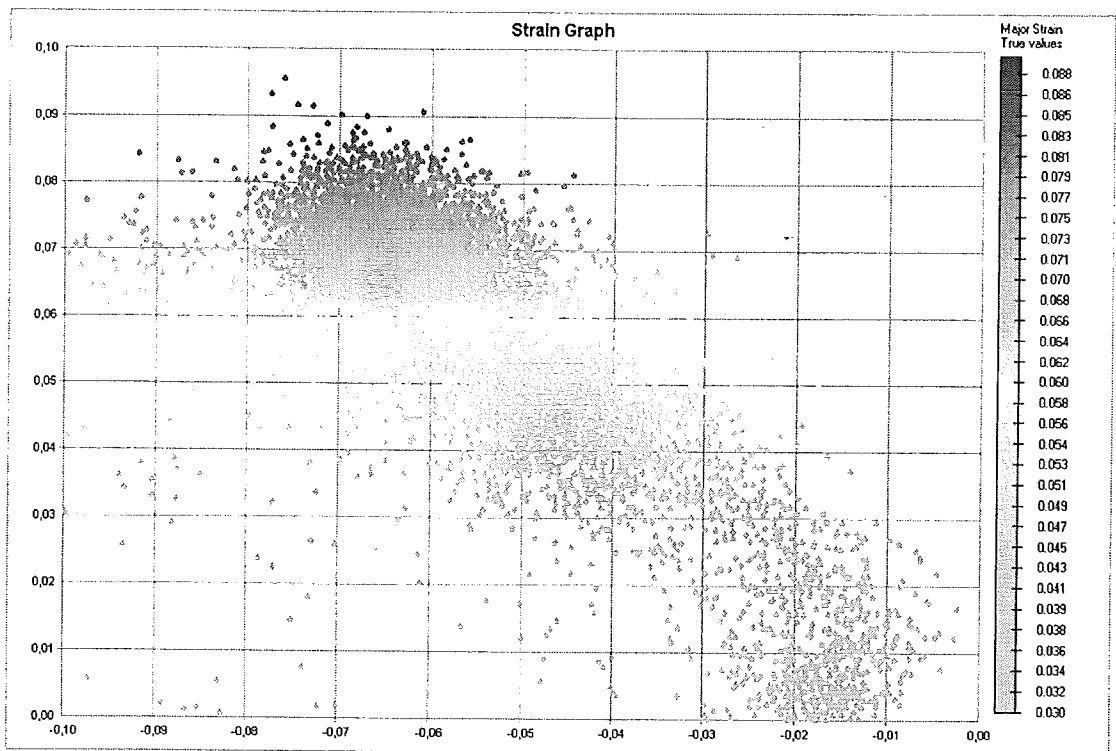


Figure 34 Forming limit diagram for sample prestrained 8%

Figure 35 shows the strain profile along the strip length of major strain for the strip prestrained to 8%. From the strain profiles it is clear that the blue line that represents the strain in the centre of sample (*maj-c*) has a uniform deformation of 8% from 50 to 270 mm along the strip length. The other two lines that represent the strain at approximately 50 mm distance from either side of the centre (*maj-b* and *maj-o*) have a uniform deformation of 8% from 90 to 210 mm along the strip length.

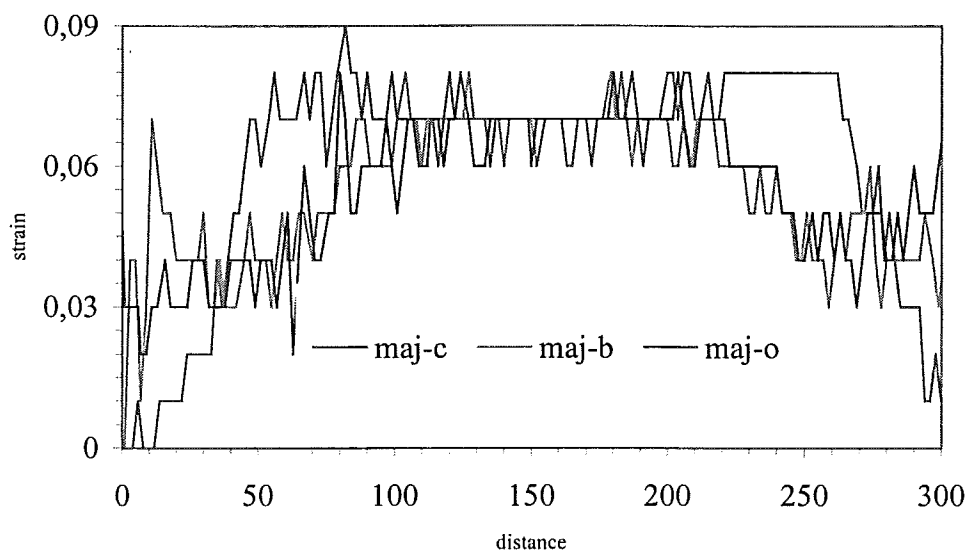


Figure 35 Section plot for strip prestrained to 8%

It could thus be concluded that for the prestrained strips, a uniform deformation is expected in the centre region for about 100 mm x 100 mm. Unfortunately, the tensile specimens (50 mm gauge length) were taken from almost the whole strip. As can be seen in Figure 36 and Figure 37, half of the samples labelled *X* and 5 of the 13 samples labelled *Y* were taken from the uniform deformation area of the strips. The bake hardening response of the *X* samples showed less scattering compared to the *Y* samples (see Chapter 4, item 4.3.1.1 and 4.3.2.1), because at least 50% of the *X* samples were taken from the uniform deformation area compared to only 38% of the *Y* samples. That would also explain the high standard deviations obtained for the results in this investigation, especially for the *Y* samples.

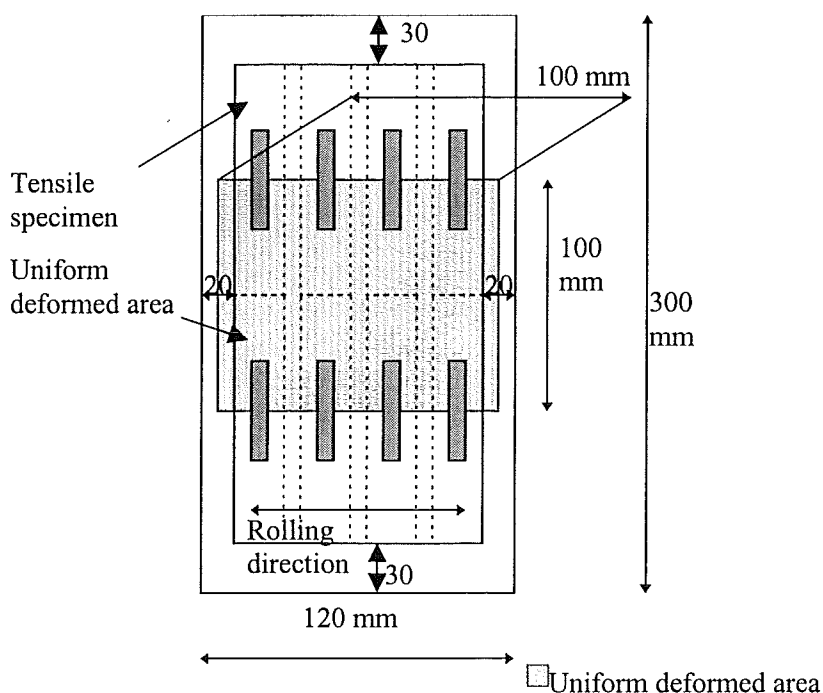


Figure 36 Uniform deformation area of strips after prestrain for *X* samples

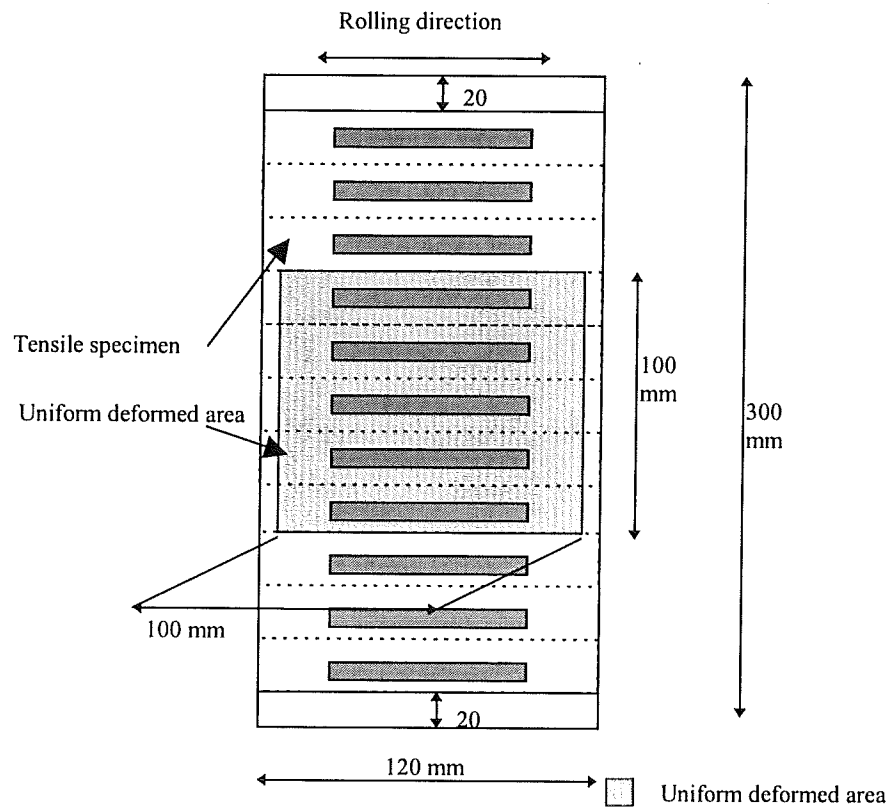


Figure 37 Uniform deformation area of strips after prestrain for Y samples

In order to confirm the aforementioned presumption a new series of tensile samples was prepared. On this occasion, tensile samples were first machined from strips (Figure 26) and then deformed perpendicular to the rolling direction at prestrain levels of  $\varepsilon_t = 2\%$ , 4%, 6% and 8% total elongation. In this case prestraining was performed on the tensile sample instead of the strips. To determine the bake hardening response  $\Delta\sigma_{BH}$ , samples were subjected to a heat treatment at 140 °C and 230 °C for 20 minutes, before testing until failure. Triplicate samples were prepared for each bake hardening condition (temperature, time) in order to determine the standard deviation. The results of this new series was compared with that obtained previously from tensile samples machined from the prestrained strips (old series). It is clearly seen (Table 12) that the bake hardening values of the new series is slightly higher and in general, the standard deviation much less than for the old series. However, the trends observed for the various temperatures and for different levels of prestrain are similar.

Table 12 Comparison of bake hardening values and standard deviations between old and new series for the various bake hardening treatments

140 °C - 20 min					
Prestrain $\varepsilon_t$ (%)		2	4	6	8
Bake hardening values (MPa)	Old series	31.9	41.0	40.7	44.1
	New series	40.6	42.1	44.8	46.2
Standard deviation (MPa)	Old series	2.5	1.5	2.3	5.1
	New series	2.6	0.6	2.4	2.6
230 °C - 20 min					
Bake hardening values (MPa)	Old series	49.5	45.5	44.1	50.0
	New series	54.3	53.8	52.0	53.3
Standard deviation (MPa)	Old series	3.0	2.3	3.1	2.0
	New series	3.1	2.3	1.8	4.0
Prestrain $\varepsilon_t$ (%)		2	4	6	8

It can thus be concluded that there is a significant influence of prestrain method on the results. If the tensile samples are machined from strips that have been prestrained, care should be taken to ensure that the samples are removed from the uniform deformed region (100 mm x 100 mm in the centre) of the strips.

### 3.7 Transmission electron microscopy (TEM)

In order to assess whether precipitates are present in this steel after bake hardening and/or to show any precipitation differences that might be induced by the level of prestrain, two bake-hardened tensile samples (230 °C and 20 minutes) after 0% and 2% prestrain were examined by transmission electron microscopy (TEM). Since it is anticipated that most of the precipitates in this steel are less than 1 micron in size, and therefore below the resolution of light microscopy, the TEM is ideal for gaining insight into the distribution, size and morphology of precipitates. A Philips CM30T, TEM operating at 300 kV was used in this investigation. Samples were electro-polished in 5% solution of  $HClO_4$  dissolved in methanol at 10 °C in a TENUPO-4 device.

### 3.8 Calculation of the bake hardening response

In general, the bake hardening response is defined as the difference of the lower yield strength after baking and the flow strength before baking. The definition of the flow strength before baking is standardised throughout the industry and is defined as the flow stress after 2% prestrain for conventional bake hardening tests, or the 0.2% proof stress in the case of a bake hardening test where no prestrain was applied. The definition of the strength after baking is nevertheless more complicated. Generally, after the material has been bake hardened, there will be discontinuous yielding with associated upper and lower yield points. The upper yield point ( $R_{bH}$ ) defines the stress that must be applied to the steel before mobile dislocations can move and new ones can be generated which would mark the onset of plastic deformation. Since the lower yield point is measured in the plastic region it can be argued that the upper yield point more accurately reflects the true yield stress of the material. However, it has been reported that the  $R_{bH}$  is highly sensitive to factors such as strain rate, test-piece preparation and specimen alignment and is therefore not very practical. In this investigation however, it only showed a small variation. The  $R_{bL}$  values have shown to be consistent for the

triplicate measurements, suggesting that a reproducible bake hardening response could be obtained by using this measurement.

The precise value of  $R_{bL}$  is dependent on the defined cross section area. As the stress is defined by the force divided with the cross sectional area, it is necessary to input the sample dimensions before testing. The use of the sample dimensions after prestraining will render an accurate reflection of the strength of the material after baking, however, when comparing this to the unbaked properties, it is possible to record a strength increase (thus a bake hardening response) for a material without any bake hardening characteristics just because of the reduction in cross-sectional area.

The level of prestrain (work hardening) could also be responsible for an artificial increase of the bake hardening response. In Equation 8, the work hardening is defined as the difference between the flow stress after  $\varepsilon_i$  prestrain and the 0.2%-proof strength in the as-received condition of the material. If  $\sigma_f$  is recalculated by not using the original cross-sectional area (initial thickness) but the instantaneous area (true stress-true strain curve) after  $\varepsilon_i$  prestrain instead, the work hardening increases dramatically for prestrain levels higher than 4% as is shown in Table 13.

Table 13 Comparison of work hardening calculations

$\varepsilon_i$ prestrain (X sample)	Work hardening using the $\sigma_f$ stresses calculated using the original cross-sectional area $A_0$	Work hardening using the $\sigma_f$ stresses calculated using the instantaneous area after $\varepsilon_i$ prestrain
2	32	36
4	54	63
6	65	80
8	74	94

This higher work hardening could imply lower bake hardening values especially at higher levels of prestrain. It is envisaged that the use of the instantaneous area for stress calculation (true stress - true strain curve) is more suitable as it allows a fair comparison of the strength before and after baking.

The calculated bake hardening values do not differ much up to a prestrain level of 2% but generally, bake hardening values are lower when using the instantaneous area. Small deviations in the test procedure can lead to significant differences in the measured bake hardening response. This sensitivity could explain the statement in the test standards<sup>(8,9,10)</sup> that the bake hardening values should be rounded to the nearest 10 N/mm<sup>2</sup>.

Finally, the test standard allows that the bake hardening response can be determined by using either the lower or upper yield point or yield point elongation. For the present investigation all values for bake hardening response are determined by using the lower yield stress  $R_{bL}$ . For the cases where a clear lower yield stress was not apparent, the 0.2% proof stress after bake hardening was used. All stresses supplied from this point on, are true stresses.

## Chapter 4: Results

### 4.1 Introduction

The results of the various tensile, compression tests and bake hardening treatments, given in this chapter are divided according to the following structure:

- Microstructure (assessed via optical microscopy) of material in the as-received and prestrained and paint-baked condition in §4.2
- The influence of parameters such as level of prestrain, temperature and time of baking on the bake hardening response for tensile and compression samples in §4.3 and §4.4 respectively
- Precipitates and dislocation structure revealed by transmission electron microscopy in §4.5

### 4.2 Microstructure

The microstructure of the samples was observed and photographed with an optical microscope at a magnification of 500. The micrographs of *X* and *Y* - samples in the as-received condition and in the prestrained and paint baked condition are shown in Figure 38 to Figure 41.

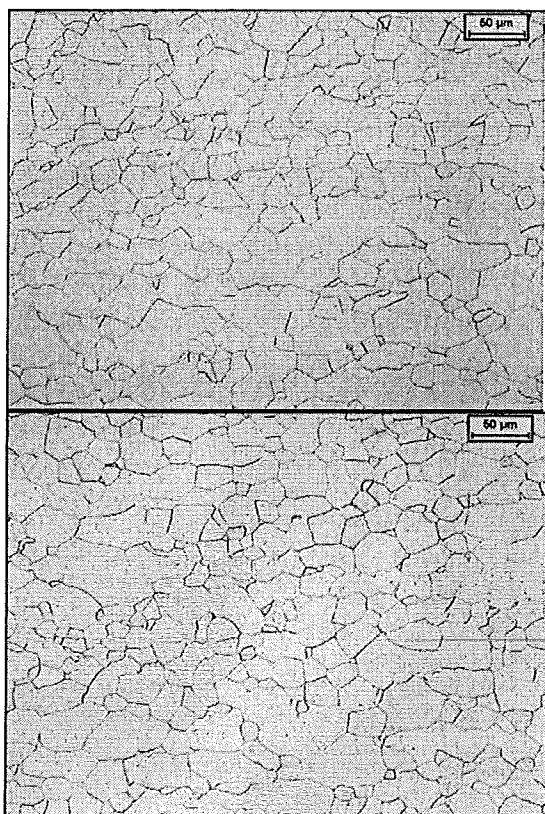


*Figure 38 X sample as-received condition*

*Figure 39 Y sample as-received condition*

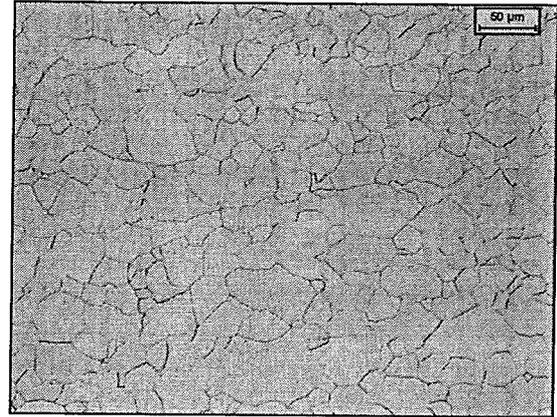
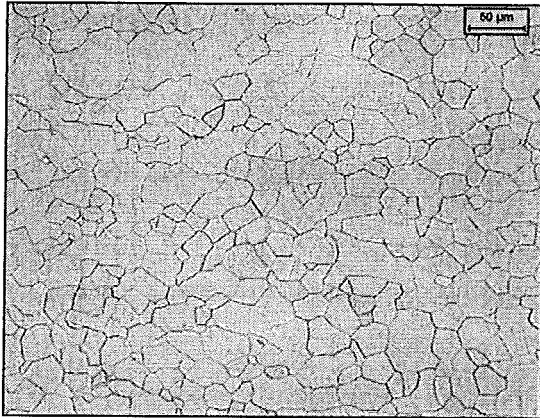


Figure 40 X sample (230 °C-20min-8% prestrain)      Figure 41 Y sample (230 °C-20min-8% prestrain)

In order to reveal the cementite structure, a 4% Picral etchant applied for a minimum of 40 s was used and for grain structure, a 5%  $NH_3$  etchant applied for a minimum of 8 s was used. The micrographs reveal a microstructure that consists mainly of a ferrite matrix with equiaxial grains (an 8.5 *ASTM* grain-size number was measured, which is equivalent to an average grain diameter of  $18 \mu m^{(27)}$ ) and no cementite could be revealed. It can be concluded from Figure 38 to Figure 41 that there is no significant microstructural difference between samples in the as-received condition and samples after bake hardening treatment (230 °C - 20 minutes - 8% prestrain).

### 4.3 Tensile tests

As mentioned before, the bake hardening response for prestrained samples was calculated by using equation 8. It should be noted that the *Y* samples were at an angle  $\alpha = 0^\circ$  with respect to the rolling direction and that the *X* samples were at an angle  $\alpha = 90^\circ$  with respect to the rolling direction. Both sets of samples were subjected to the same levels of prestrain and paint baking processes in order to determine the influence of the sample orientation. As an example a typical true stress - true strain tensile curve for the as-received condition and after bake hardening treatment for both orientations is given in Figure 42 to Figure 45.

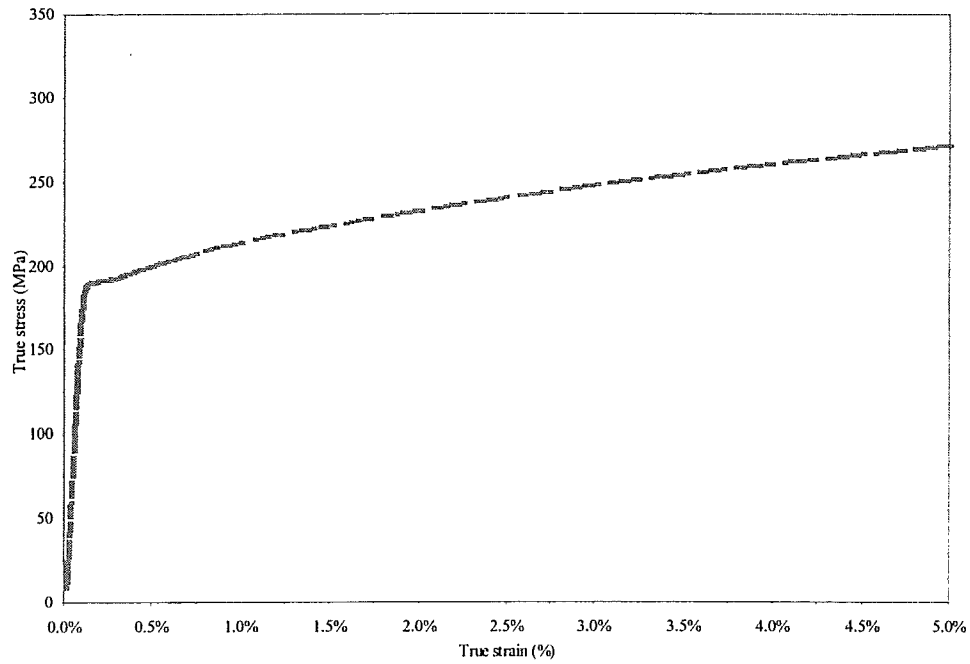


Figure 42 True stress - true strain for X sample in the as-received condition

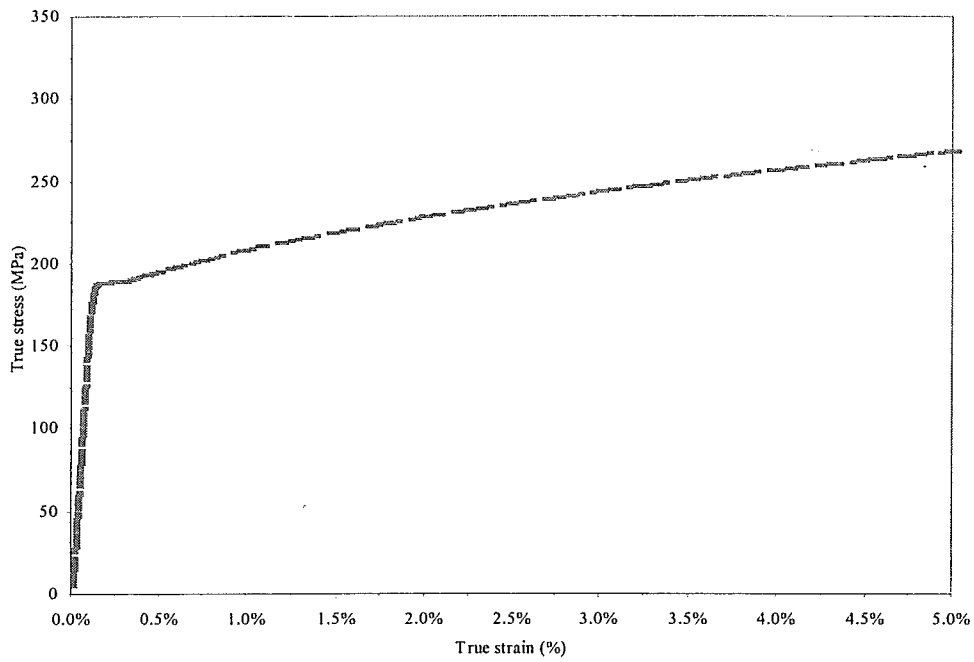


Figure 43 True stress - true strain for Y sample in the as-received condition

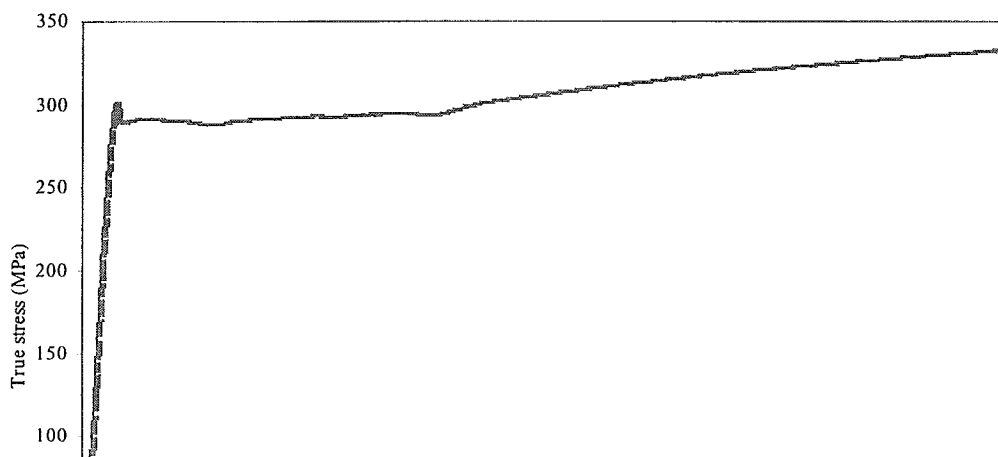


Figure 44 True stress - true strain for X sample after 170 °C-20 min-4% prestrain

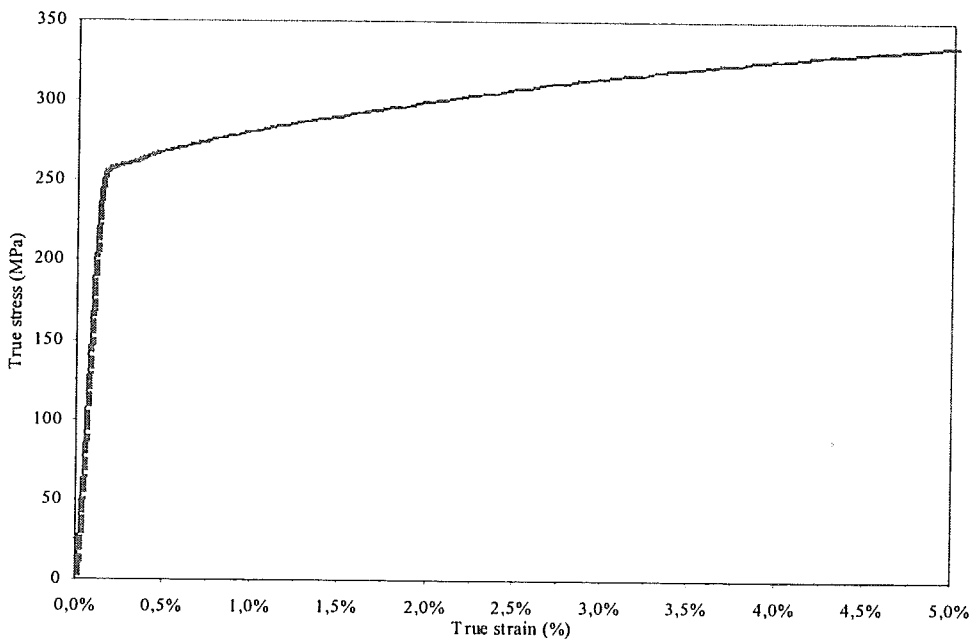


Figure 45 True stress - true strain for Y sample after 170 °C-20 min-4% prestrain

As can be seen from Figure 42 and Figure 43, the continuous yielding of the H180BD material in the as-received condition suggests that there has been no natural strain ageing (Lüders bands formation) as would be expected from material that complies to the EN10292 Standard. The as-received mechanical properties were consistent with the values expected for steels that were designed to conform the H180BD specification. (See Table 14)

Table 14 Measured-mechanical properties on H180BD

Mechanical Properties	0.2%-proof strength $R_{p0.2}$ N/mm <sup>2</sup>	Tensile strength $R_m$ N/mm <sup>2</sup>	Elongation $A_{80}$ %	Plastic strain ratio $r_{90}$	Strain hardening exponent $n$
Average	186	305	42	2.2	0.2

After bake hardening treatment (of 4% prestrained samples), at 170 °C and 20 minutes, a clear lower yield stress ( $R_{bL}$ ) is seen for the *X* sample (Figure 44) but not for the *Y* sample (Figure 45). In the latter case, the 0.2%-proof strength after bake hardening was taken as the yield stress.

From this point on the discussion and results of the research will be explained separately for the *X* and *Y* samples.

#### 4.3.1 *X* samples

These samples recorded the highest bake hardening values and have an orientation ( $\alpha = 90^\circ$ ) perpendicular to the rolling direction, similar to the proposed European standard for bake hardening tests.

##### 4.3.1.1 Dependence on prestrain and temperature

Figure 46 presents the values of bake hardening obtained after a bake hardening treatment of 20 minutes at different temperatures and at different levels of prestrain. It is immediately evident that the bake hardening response is strongly influenced by the level of prestrain for the baking temperature of 140 °C. Increasing the level of prestrain from 0% to 4%, increases the bake hardening value from 20 MPa to 40 MPa (about 5.0 MPa/% prestrain). For even higher levels of prestrain, there is no significant increase and a maximum bake hardening value of 44 MPa is achieved at 8% prestrain. The trend, however, is not the same for the other temperatures. At 170 °C, the bake hardening is 45 MPa at 0% prestrain and initially decreases (at a prestrain of 2%), but increases for prestrain levels larger than 2%. This increase abates after prestrain levels larger than 4%. The substantial difference in bake hardening response at 0% prestrain between 140 °C and 170 °C is not surprising since bake hardening is a thermally activated process. The same effect is observed when increasing the temperature even further (from 170 °C to 200 °C and 230 °C). For temperatures higher than 170 °C, the bake hardening response is dependent on the level of prestrain. There is a continuous decrease in the bake hardening response for temperatures greater than 200 °C up to 4% prestrain followed by a slight increase in the bake hardening response as more prestrain is performed. However, this is not in agreement with literature, where a continuous decrease in bake hardening response is observed with increasing prestrain.

For samples with a 0% level of prestrain the bake hardening response increases dramatically as the temperature increases, from 22 MPa to 60 MPa for 140 °C and 230 °C respectively. There is an increase of about 200% in bake hardening response between the highest and lowest temperature. At 2% prestrain the bake hardening response difference only amounts to 64%, being 32 MPa and 50 MPa for the lowest and highest temperature respectively. For  $\epsilon_i > 4\%$  there is an insignificant increase of the bake hardening response with temperature.

In Chapter 2 it was mentioned that there is an optimum level of prestrain (work hardening), for which the bake hardening response is at a maximum. For the  $X$  samples it was not possible to see such a local maximum in the bake hardening response for a certain level of prestrain.

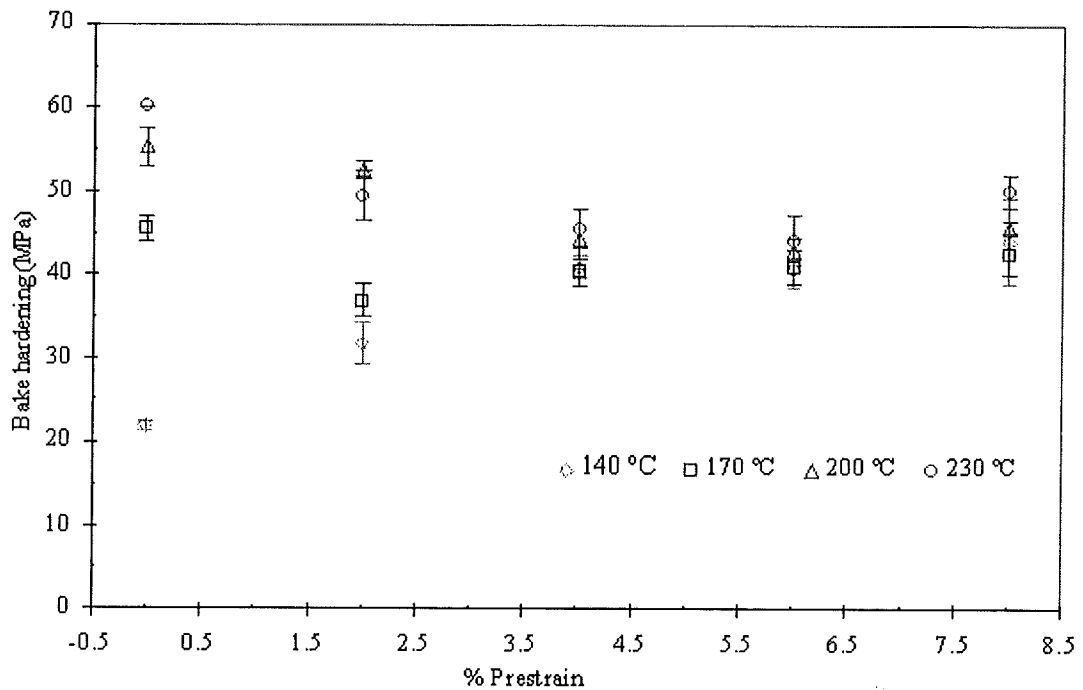


Figure 46 Dependence of bake hardening response after various temperatures for 20 minutes and prestrain levels ( $X$  samples)

#### 4.3.1.2 Dependence on baking time and temperature for a prestrain level of 2%

The time dependence of the material's bake hardening response was investigated at 4 different times, namely 25, 20, 15 and 10 minutes, at 4 different temperatures, respectively 140 °C, 170 °C, 200 °C and 230 °C. As Figure 47 shows, there is no significant influence of time on the bake hardening response, at least not for the range investigated. However, the bake hardening response is notably sensitive to the temperature. There is an improvement of approximately 15 MPa in bake hardening when the temperature increases from 170°C to 200°C independent of baking time. Most researchers try to relate the time and temperature dependence of the bake hardening response by using Hundy's equation (Chapter 2). From the data presented here it can be deduced that Hundy's equation is not valid for the time and temperature range used in this research. Further research is necessary to establish whether a time dependence for the bake hardening response exists for times shorter than 10 minutes.

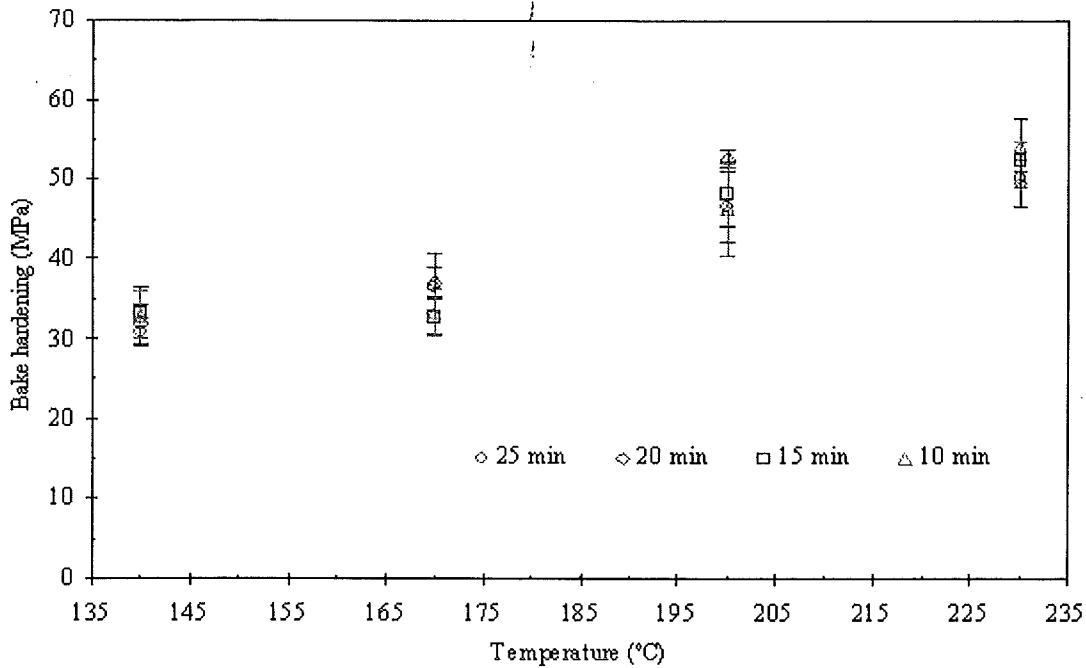


Figure 47 Dependence of bake hardening response at times indicated for various baking temperatures after 2% prestrain (*X* samples)

#### 4.3.2 *Y* samples

The *Y* samples are tensile specimens machined with the longest axis in the rolling direction ( $\alpha = 0^\circ$ ). Similarly to the *X* samples, the results are sub-divided into dependence of the bake hardening response on temperature, dependence on prestrain and dependence on time for a level of prestrain of 2%.

##### 4.3.2.1 Dependence on prestrain and temperature

The bake hardening response is lower than that for *X* samples for all conditions, especially at higher prestrains. From Figure 48 it is observed that for a temperature of 140 °C, the bake hardening response increases as the prestrain increases (i.e. 8 MPa at 0% prestrain to 23 MPa at 8% prestrain). This is a similar trend as was observed from the *X* samples at the same temperature. At a temperature of 170 °C, the bake hardening response is reduced, from 32 MPa at 0% prestrain to 14 MPa at 4% prestrain. At temperatures of 200 °C and 230 °C, there is an increase in bake hardening from 0% to 2% prestrain, 45 MPa to 47 MPa and 49 MPa to 55 MPa respectively, followed by a rapid decrease until 6% at a rate of 5.5 MPa/% prestrain. For prestrain levels larger than 6%, there is still a decrease in bake hardening response, but at a lower rate.

The effect of temperature on bake hardening was ascertained for the prestrain levels of 0% and 2% to be 4 MPa and 12 MPa at 140°C and 44 MPa to 53 MPa at 230 °C, respectively as shown in Figure 48. For prestrain values of 6% and 8%, the measured bake hardening is almost constant for any paint baking temperature. The bake hardening values for all temperatures coincide at 8% prestrain while for *X* samples this point is at 4% prestrain.

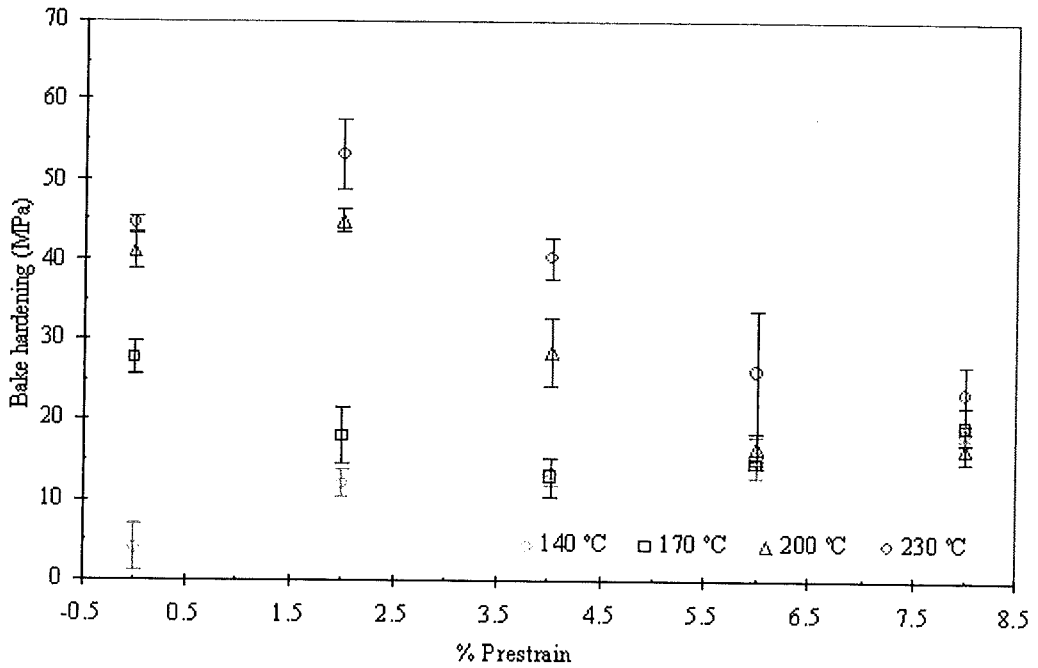


Figure 48 Dependence of bake hardening response at various temperatures for 20 minutes and prestrain levels (Y samples)

#### 4.3.2.2 Dependence on baking time and temperature for a level of prestrain of 2%

Figure 49 reveals that there is no significant difference of the bake hardening response for the times investigated. The times that were used were between 10 and 25 minutes. However, this does not allow one to preclude that there would be no influence on bake hardening response after baking for 5 minutes. Generally the bake hardening response ranges from 13 MPa at 140 °C to 55 MPa at 230 °C. The average bake hardening response for the X samples is 32 MPa compared to 11 MPa for the Y samples at 140 °C, but increases to the same bake hardening response of 55 MPa at 230 °C. For both types of samples, the bake hardening response is particularly sensitive to the temperature.

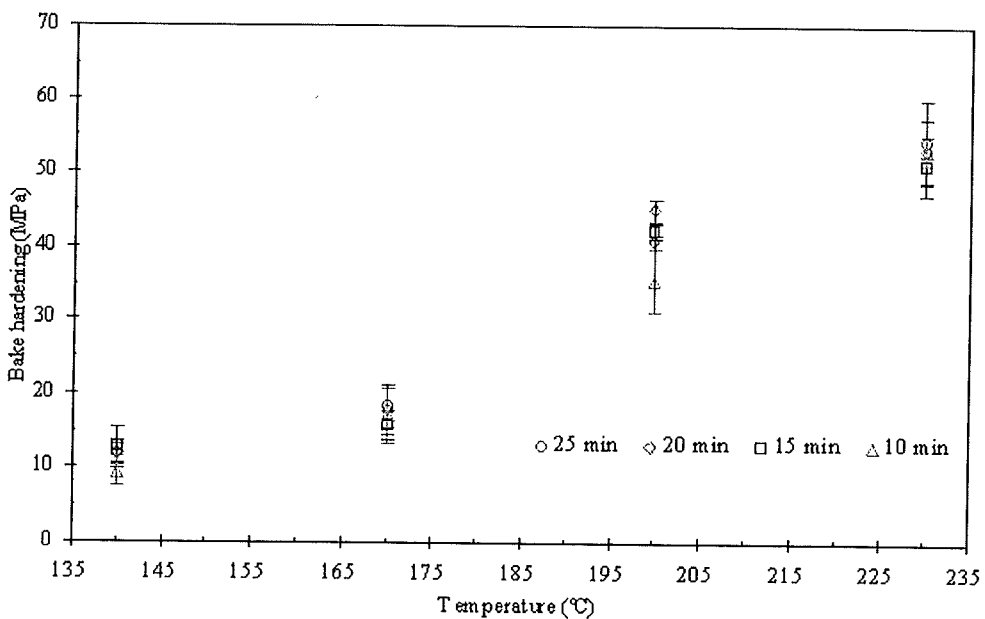


Figure 49 Bake hardening response as a function of baking time and temperature after 2% prestrain (Y samples)

### 4.3.3 Double bake hardening treatment

The purpose of these experiments was to try to separate the contributions of the Cottrell mechanism and precipitation strengthening to the overall bake hardening response. By pre-baking the specimens (prior to prestraining and re-baking) it was hoped that the effect of precipitation strengthening would be exhausted so that the total bake hardening response occurring during the second baking treatment could be attributed to the Cottrell mechanism only.

After an initial thermal treatment on machined tensile samples ( $X$  sample,  $\alpha = 90^\circ$  with respect to the rolling direction) without prestrain, a first bake hardening response of approximately 15 MPa at 140 °C and 49 MPa at 230 °C for 20 minutes was reached. Figure 50 gives the bake hardening response obtained after a second bake hardening treatment of 20 minutes at 140 °C and 230 °C. For both temperatures, the bake hardening response increases as the prestrain increases. At the lowest temperature, 140 °C, an increase in the levels of prestrain from 2% to 4% increases the bake hardening value from 35 MPa to 41 MPa. For  $\epsilon_i > 4\%$ , the bake hardening value is 43 MPa at 6% prestrain and 40 MPa at 8% prestrain. At the highest temperature, 230 °C, the bake hardening value increases from 22 MPa to a plateau level of about 46 MPa from a prestrain level equal or greater than 4%.

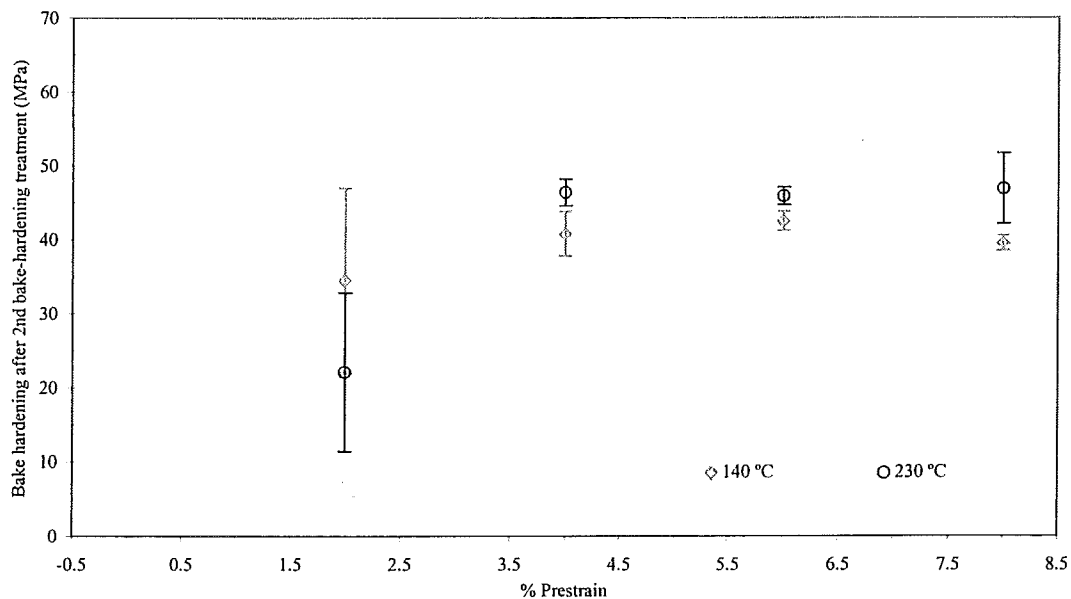


Figure 50 Dependence of bake hardening response at temperatures indicated for 20 minutes according to the level of prestrain for the second bake hardening treatment only

Upon combining the two increments of bake hardening response reached after each bake hardening treatment, a maximum bake hardening response of 96 MPa at 230 °C for 8% prestrain and 55 MPa at 140 °C for 6% prestrain is obtained. (Figure 51)

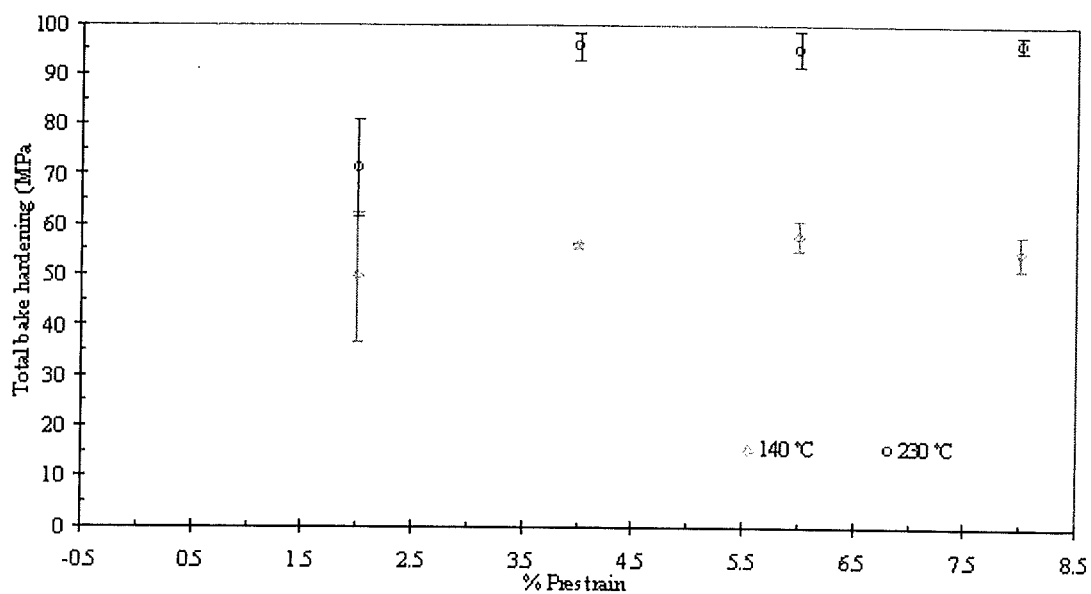


Figure 51 Total bake hardening response achieved after double bake hardening treatment at the temperatures indicated for 20 minutes as a function of the level of prestrain

#### 4.4 Compression tests

The cubical samples were subjected to prestrain levels between 2% and 8%. The bake hardening treatment was carried out before re-testing. Some typical true stress - true strain compression curves, of material in the as-received and after bake hardening treatment (170 °C, 20 minutes) condition, are given in Figure 52 and Figure 53. Figure 52 (for the as received sample) shows a continuous yielding behaviour, which shows that the material has not aged, yet. After bake hardening treatment (at 170 °C for 20 minutes) a more distinct yield stress is observed (Figure 53).

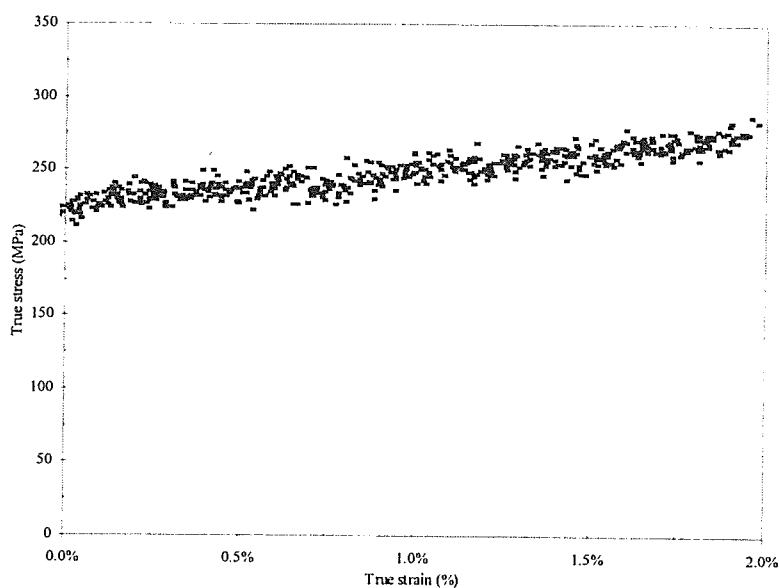


Figure 52 True stress - true strain curves for compression sample in the as-received condition

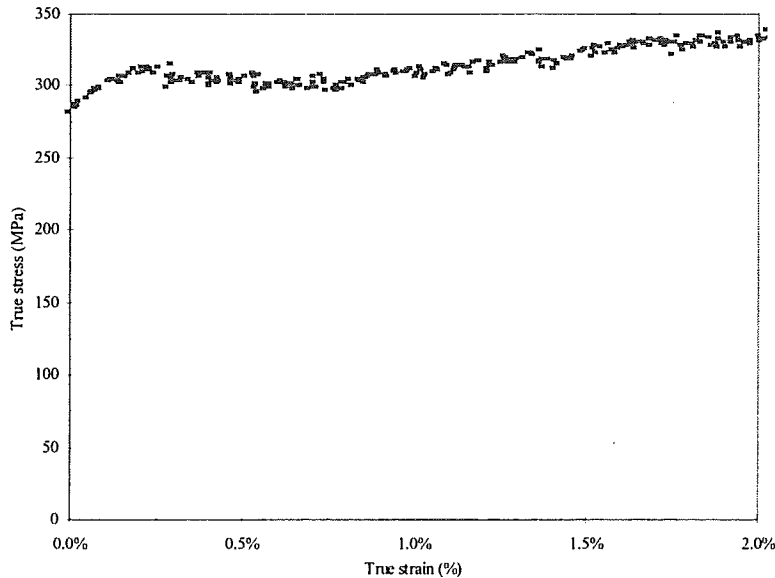


Figure 53 True stress - true strain curves for compression sample after 170 °C-20 min-2%prestrain

#### 4.4.1 Cube-samples

It was possible to determine the bake hardening response of compression samples after various prestraining, due to the distinct lower yield point that was registered after the paint baking simulation.

##### 4.4.1.1 Dependence on prestrain and temperature

Figure 54 presents the bake hardening response calculated for the different prestrain levels and various ageing conditions (different temperatures for 20 minutes). As has been observed with the tensile samples, the bake hardening response is strongly influenced by the level of prestrain. The large data scatter is attributable to the insensitivity of the load-cell of the Gleeble-3500. As a consequence it is not possible to distinguish any trends for the effect of ageing after 140°C, 170°C and/or 230°C. Generally it is observed that the bake hardening response is constant at 30 MPa for prestrain levels up to 4%. For  $\epsilon_t > 4\%$  there is an increase of the bake hardening response until approximately 50 MPa at 8% prestrain.

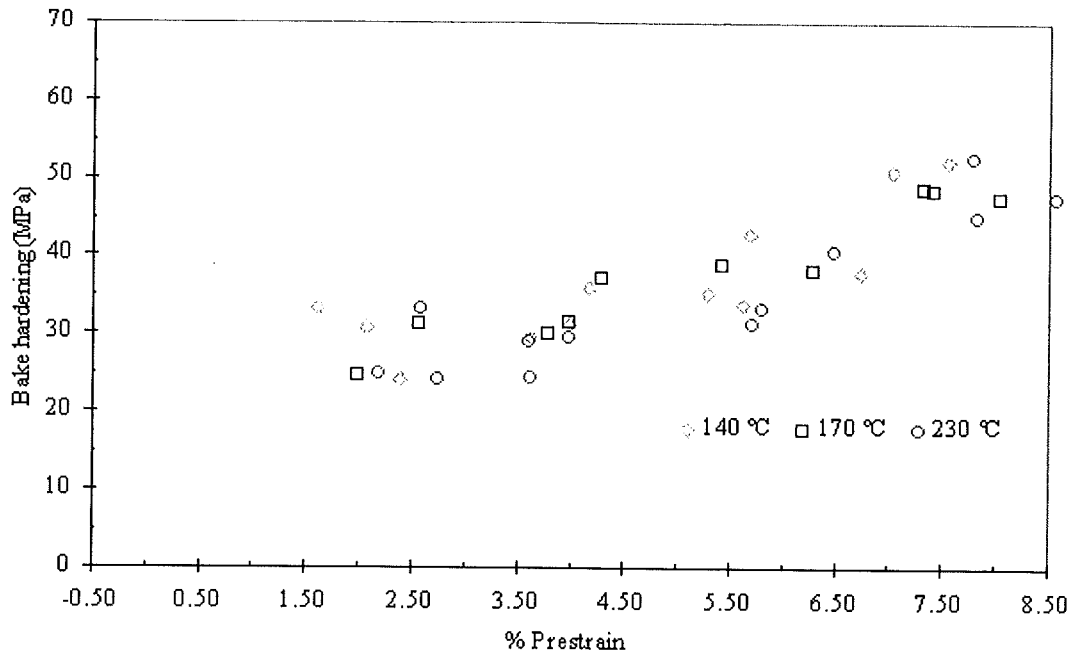


Figure 54 Dependence of bake hardening response at various temperatures for 20 minutes and prestrain levels

#### 4.5 Transmission electron microscopy (TEM)

The TEM micrographs of samples aged at 230 °C for 20 minutes at 0% prestrain and at 2% prestrain are shown in Figure 55 and in Figure 56. It is observed in Figure 55 that the sample without prestrain reveals a cellular dislocation structure and that the sample prestrained for 2% (Figure 56) has a banded dislocation structure.

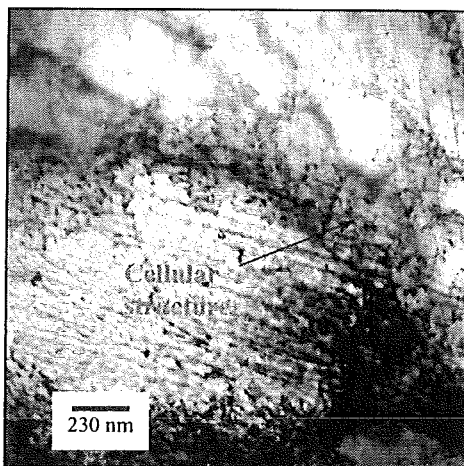


Figure 55 TEM-photograph of X sample after 230 °C - 20 min - 0% prestrain

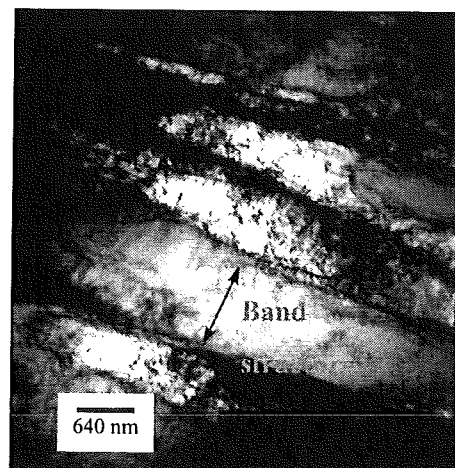


Figure 56 TEM-photograph of X sample after 230 °C - 20 min - 2% prestrain

In Figure 57 and Figure 58 carbides of rod-like morphology can be seen. These carbide-precipitates are more uniform in distribution and larger in size in samples at 0% prestrain than at 2% prestrain. In order to identify the crystal structure of carbides, electron diffraction patterns were recorded. The co-ordinates of the diffracting spots is related to the Miller indices of the crystal. In this research, the diffraction patterns shown in Figure 59 and Figure 60 resemble the hexagonal crystal structure of epsilon

carbide. The orientation of the carbide with respect to the ferrite matrix is given by  $[100]_{\alpha_{Fe}} / [\bar{1}2\bar{1}0]_{\epsilon}$ .

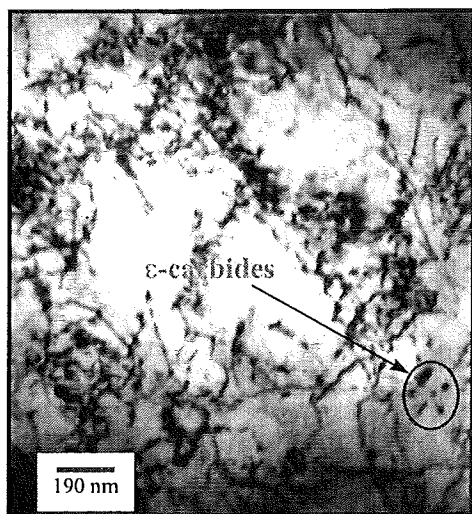


Figure 57 TEM-photograph of X sample after 230 °C - 20min - 0% prestrain

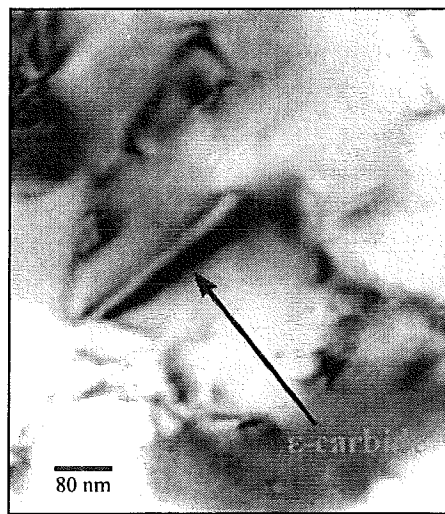


Figure 58 TEM-photograph of X sample after 230 °C - 20min - 0% prestrain

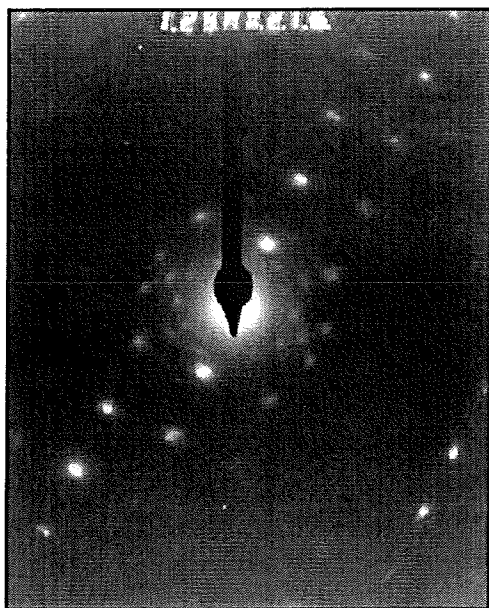


Figure 59 X sample after 230 °C - 20 min - 2% prestrain - diffraction pattern of epsilon-carbide precipitate

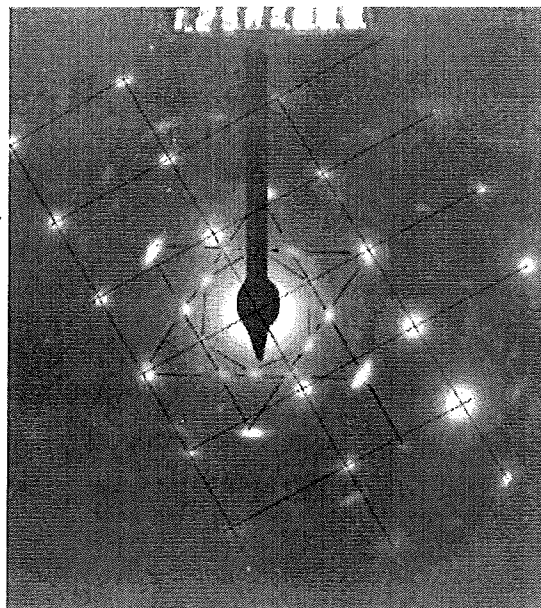


Figure 60 X sample after 230 °C - 20 min - 2% prestrain - diffraction pattern of epsilon-carbide precipitate

## **Chapter 5: Discussion of results**

### **5.1 Introduction**

As was shown in Chapter 4, the bake hardening response is influenced by the sample orientation, the deformation mode (i.e. compression and tensile testing), the level of prestraining and the bake hardening treatment used. The results will be discussed according to the following structure;

- Influence of deformation type in §5.2
- Influence of sample orientation in §5.3
- Influence of prestrain in §5.4
- Influence of baking temperature and time in §5.5

### **5.2 Influence of deformation type**

For both test types (i.e. tension and compression) a bake-hardening response was measured, although compression tests generally gave more conservative bake-hardening values. After the standard bake-hardening treatment (170 °C - 20 minutes - 2% prestrain), the bake-hardening response is 35 MPa for tensile testing (Figure 46) and 30 MPa for compression testing (Figure 48). Theoretically it was shown that the compression test simulates a biaxial stretching mode, which is closely related to the deformation mode applied by the automotive industry to form exposed panels. This could imply that more reliable values for bake hardening (for the in-service performance) can be obtained via compression testing. However, difficulties to control the level of prestrain, the inadequate sensitivity of the load-cell of the Gleeble, tedious sample preparation and specimen alignment make these measurements much more complicated compared to conventional tensile testing. These difficulties prohibited a thorough study of the influence of deformation mode. Even though conventional tensile testing does not involve the same deformation mode as applied by industry, it is relatively cost effective and reasonably accurate and therefore most suitable for daily bake hardening testing. The measured bake hardening response will tend to be optimistic.

### **5.3 Influence of sample orientation**

As demonstrated in Figure 46 and Figure 48, the bake hardening response varies according to sample orientation relative to the rolling direction. This behaviour has also been observed by other researchers and has been attributed to the influence of the rolling and deformation direction on the dislocation structure of the material.

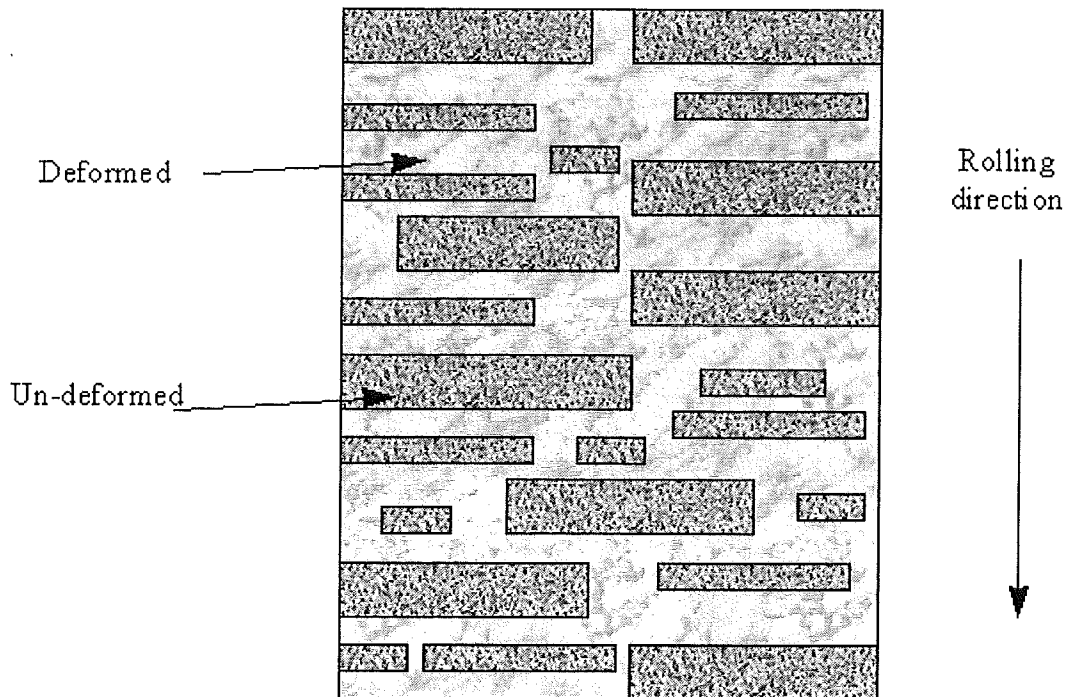


Figure 61 Schematic presentation of herringbone structure after temper rolling (strip width)

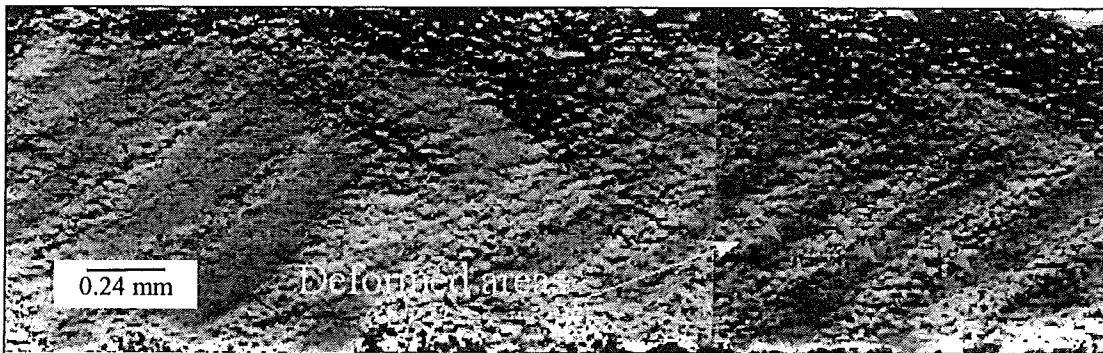


Figure 62 Through thickness microstructure of low carbon steel after 1.7% temper rolling<sup>(42)</sup>

The “herringbone” structure developed in the steel during temper rolling contains regions of deformed and non-deformed material, which tend to be orientated across the strip width (Figure 61) and are highly heterogeneous throughout the strip thickness (Figure 62). This heterogeneous dislocation structure depends strongly on the temper rolling reduction as well as the rolling conditions (tension/compression ratio, lubrication, diameter of the rolls, sheet thickness, etc.). When a bake hardening test after 0% prestrain is conducted, the dislocations available for pinning during baking are those generated during temper rolling.

Although these dislocations will be pinned to the same extent in all samples, only those lying in the active slip plane will contribute to the strength increase during subsequent tensile testing. Hence, the bake hardening response will vary according to density of dislocations that lie on the active slip plane, resulting in a variation in bake hardening response according to sample orientation as shown in Table 15.

Table 15 Bake-hardening response after different temperatures and sample orientation for 0% prestrain

Temperature (°C)	$\Delta\sigma_{BH}$ (MPa) for <i>X</i> sample	$\Delta\sigma_{BH}$ (MPa) for <i>Y</i> sample
140	22	4
170	46	28
200	55	41
230	60	44

For the material under review (*H180BD*), the maximum bake hardening was observed for the *X* samples, which are perpendicular ( $\alpha = 90^\circ$ ) to the rolling direction, thus presumably the direction with the highest dislocation density. This is in agreement with Hundy's theory, which states that dislocations preferentially form in the transverse direction during temper rolling. For both sample orientations, the bake hardening is particularly sensitive to temperature.

Increasing the temperature for a constant baking time of 20 minutes from 170 °C to 230 °C increases the bake hardening response for samples with no prestraining. This corresponds to a low dislocation density level with pinning (Cottrell atmosphere) and precipitation (further explanation in next section).

#### 5.4 Influence of prestrain

During tensile prestraining, it is expected that the dislocation structure will be more homogeneous through the sheet thickness and will be orientated according to the specific deformation path. During plastic prestraining dislocations will also be generated, thereby increasing the density of dislocations available for pinning during the baking stage, which results in a higher bake hardening response. It is possible to theoretically calculate the dislocation density in the material after different levels of prestrain by applying the Bergström model for static strain ageing on *H180BD* <sup>(43)</sup>(Table 16). The model only considers a density  $\rho$  of prestrain-induced dislocations, which is determined by the level of prestrain. The error made by neglecting the dislocation density before prestraining is insignificant, since the calculations agree fairly well with published data <sup>(11, 18, 20, 23)</sup>.

Table 16 Dislocation density based on tensile test curve (Figure 42) of *H180BD* using Bergström model for static strain ageing

Prestrain $\epsilon_i$ (%)	$\rho$ (m <sup>-2</sup> )
2	$12 \times 10^{12}$
4	$23 \times 10^{12}$
6	$32 \times 10^{12}$
8	$41 \times 10^{12}$

When the load direction after bake hardening is similar to that used during prestraining, the pinning would be more effective as most of the immobile dislocations lie in the active slip plane. This effect was clearly illustrated by the different bake hardening response recorded for *X* and *Y* samples, (Table 15) which had the same paint baking conditions.

Many researchers have investigated the influence of prestrain and the results of some of these studies will be compared to the results of this investigation. Van Snick et al. <sup>(44)</sup> proposed a three-stage behaviour, in which the bake hardening response after standard baking increased as the prestrain increased. According to Snick these stages were attributed to changes in the effectiveness of carbon in pinning dislocations as the dislocation density increased. However, Christen et al. <sup>(45)</sup> showed a decrease in bake hardening as prestrain increases. Christen suggested that it was due to carbon pinning dislocations that are already immobilised by entanglements.

From the literature overview, it was suggested that the Cottrell mechanism would precede precipitation for any level of prestrain. This would imply that the bake hardening response obtained for the samples with a high level of prestrain (high dislocation density) should have mainly been attributable to the Cottrell mechanism.

#### 5.4.1 Precipitation

It is known that ternary cementite in pure  $\alpha$ -iron precipitates as an almost globular coherent particle <sup>(46)</sup>. Some experiments with steels containing additional alloying elements such as *Al*, *Mn*, *P*, *Si* or *Ni* show that between around 300 °C and room temperature discontinuities in the precipitation behaviour appear. Certain ageing experiments for the determination of *TTP* diagrams of carbides in ferrite containing 0.045 weight % *C* with different alloying elements have been calculated and compared with experimental points from Abe <sup>(47, 48)</sup> (Figure 63). Two types of precipitates (having different structures) were distinguished, namely:  $Fe_{2.4-3.0}C$  (epsilon carbides) that precipitate in the temperature region 90 °C to 250 °C and  $Fe_{32}C_4$  (low temperature carbides) that precipitate at temperatures below 90 °C. Both these precipitates appear to have different nucleation and growth behaviour compared to cementite. The type of steel used for this research has 15 times less total carbon than that showed in Figure 63, however, it is still thermodynamically possible to form precipitates in this *H180BD* grade. The calculated *TTP* diagram show that at 230 °C for 20 minutes ( $> 1 \times 10^3$  s), precipitates are already formed.

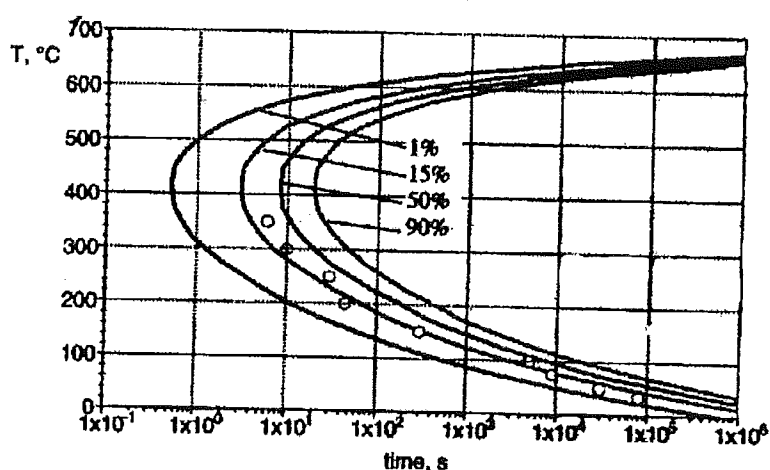


Figure 63 Calculated *TTP*-diagram for cementite precipitation in ferrite with mass content of 0.045% *C*; experimental points from Abe for 15% carbides precipitated in a steel with additional mass contents of 0.02% *P* and 0.35% *Mn*

From Figure 64, it is shown schematically that for a fixed amount of soluble carbon, more carbon will be consumed in Cottrell atmospheres when the level of prestrain

(dislocation density) is increased. As a consequence less carbon will be available to form precipitates at the high levels of prestrain, hence the contribution of precipitation strengthening (at temperatures  $\geq 200$  °C) to the bake hardening response is less for these prestrain levels (near 0 for  $\varepsilon_i > 6\%$ ). The hypothesis given above is in agreement with results obtained here for different levels of prestrain at 170, 200 and 230 °C for *X* samples.

This is also in agreement with research by Kozeschnik and Buchmayr<sup>(47)</sup> who established that at low dislocation densities mainly carbide precipitation takes place. Additionally, they found that at prestrains higher than 5%, the soluble carbon atoms in the bulk are depleted (or mostly consumed) by Cottrell atmospheres rendering less precipitation. They also found that at higher ageing temperatures; the formation of Cottrell atmospheres precedes particle precipitation to a greater degree.

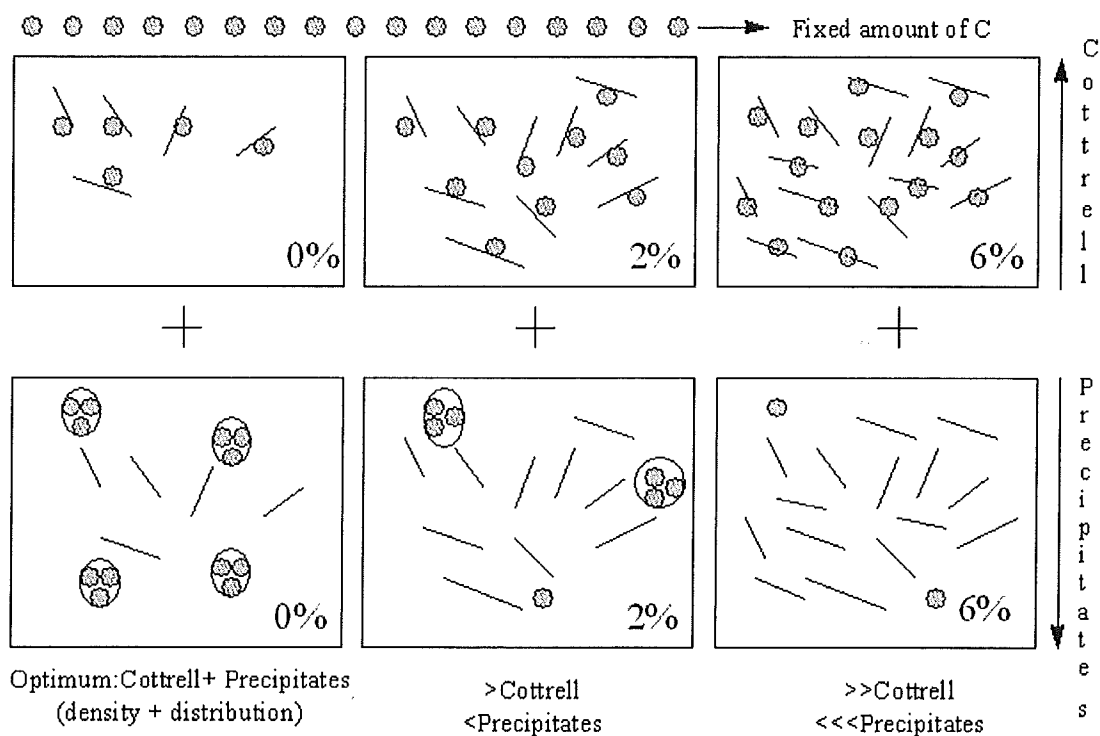


Figure 64 Hypothetical precipitation, dislocation and soluble carbon interaction of *X*-samples after bake hardening at temperatures  $>200$ °C

It was as well documented in the literature that for an initial dislocation density of approximately  $10^{12} \text{ m}^{-2}$  for an annealed<sup>(21)</sup> bake-hardenable steel, 1-ppm. carbon in solution could be enough to pin all dislocations. From Table 16, it can be deduced that for every addition 2% prestrain, about 10 ppm *C* in solution will be required to pin all dislocations. Thus, at 2% prestrain, 12 ppm. *C* and at 4% prestrain, 23 ppm. *C*. The bake hardenable steel used in this investigation has between 25 to 50 ppm. carbon in solution so it can be inferred that at 4% prestrain most of the interstitials will be present in Cottrell atmospheres at dislocations. If one assumes a conservative value of carbon in solution for the steel under investigation, no more carbon would be available to pin additional dislocations that are produced by a higher prestrain level. Hence, a further increase in the dislocation density does not increase the bake hardening value.

In order to gain more insight on the mechanism of bake hardening and to quantify the potential benefits of increasing the bake hardening response by precipitation, a double paint baking treatment was applied to tensile samples ( $X$  sample,  $\alpha = 90^\circ$  to the rolling direction). In the previous hypothesis it was assumed that the Cottrell mechanism precedes precipitation, hence the fraction of precipitation depends on the volume of Cottrell atmospheres formed, which in turn depends on the prestrain level (dislocation density). By performing a paint baking treatment (at temperatures higher than  $200^\circ\text{C}$ ) on the as received material (without prestrain) we anticipate promotion of carbide precipitation, since a very low dislocation density should be present. Subsequently the material is prestrained (creating more dislocations as the prestrain increases) followed by a second paint baking treatment. A further strength increase would then be attributable to work hardening and the forming of Cottrell atmospheres (dislocation pinning) and if there is still enough free carbon further precipitation or precipitation coarsening.

The results presented in Figure 51 (compared with Figure 46) shows that the double bake hardening tests renders significant higher total bake hardening response compared to the single bake hardening tests at various level of prestrain. A bake hardening of around 90 MPa for a prestrain of 8% at  $230^\circ\text{C}$  for 20 minutes in a double bake hardening treatment compared to  $\sim 45$  MPa for the same prestrain and baking conditions in a single bake hardening was achieved. If we neglect the total bake hardening time difference then the bake hardening response can be explained as follows. For the double bake hardening tests precipitation strengthening was promoted during the first bake hardening treatment (as detailed in the previous paragraph) and during the second bake hardening treatment dislocations were pinned by the formation of Cottrell atmospheres. For the single bake hardening tests the strengthening mechanisms followed that of conventional bake hardening (sequential order of Snoek, Cottrell, Precipitation). Note that when precipitation has started additional Cottrell atmospheres could still form. However, in the hypothesis stated earlier we stated that at high prestrain ( $> 4\%$ ) the volume of precipitation is insignificant therefore the bake hardening response obtained was mainly due to Cottrell atmospheres pinning dislocations. This would explain the low bake hardening response recorded at prestrain levels greater than 4% for the single bake hardening tests compared to that of the double bake hardening tests.

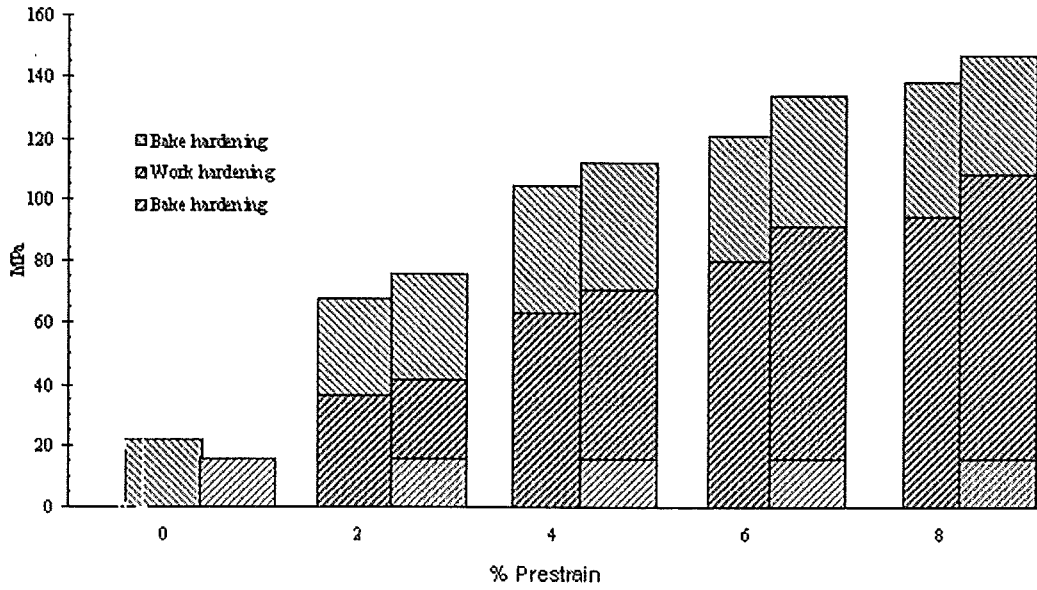


Figure 65 Work hardening and bake hardening for single (bar at the left) and double (bar at the right) heat treatment (140 °C – 20 minutes) at different levels of prestrain

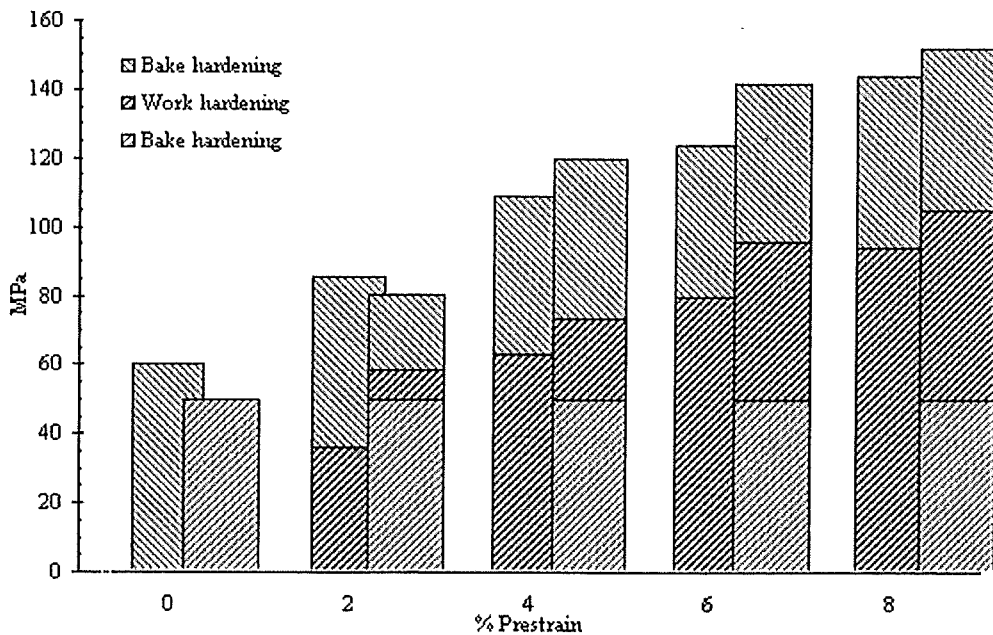


Figure 66 Work hardening and bake hardening for single (bar at the left) and double (bar at the right) heat treatment (230 °C – 20 minutes) at different levels of prestrain

Note that for the double bake hardening test at 0% prestrain only the first paint baking treatment was performed.

It is remarkable that the work hardening achieved for different levels of prestrain during the double paint baking tests (at 140 °C or 230 °C for 20 minutes) is much less than that obtained during the single paint baking tests (Figure 65 and Figure 66). Knowing that the work hardening is dependent on the movement and creation of dislocations, the lower work hardening for the double paint baking tests can be

explained by the lower dislocation movement due to more obstacles in the dislocations' paths<sup>(49)</sup>. An increase in obstacles that impede movement of dislocations after they have been created or freed from their pinned position (it is more difficult for dislocations to travel through the lattice after baking due to strain ageing), lowers the work hardening total. This provides further evidence of the formation of solute clusters and  $\epsilon$ -carbide particles during bake hardening. For any level of prestrain, at a baking temperature of 230 °C there was less work hardening (as calculated by Equation 11) than at 140 °C.

The results also revealed that the sum of work hardening and bake hardening for both the single and double bake-hardening tests for a given prestrain level is practically the same ( $\pm 10$  MPa standard deviation). The slight increase in double tests could be attributed to longer ageing times. It is deduced that even though carbide precipitation enhances the bake hardening response, it also prevents a high work hardening degree (movement and creation rate of dislocations decreases due to precipitates) and less carbon will be available to pin mobile dislocations after the second bake hardening treatment. As a consequence, the total bake hardening and work hardening response for single and double paint baking tests at a particular level of prestrain is fixed.

### **5.5 Influence of baking temperature and time**

A baking treatment of 170 °C for 20 minutes is currently used to simulate the paint curing cycle during automotive production. Significant variations in the paint baking process can occur during ageing, depending on the equipment used. In this research an oil bath provided an efficient and fast heat transfer to the material, thereby allowing simulation of various paint curing cycles. Variations in heat treatment are likely to result in differences in the bake hardening response, as the mechanisms responsible for the strength increase are diffusion controlled.

The results given in Figure 47 and Figure 49 show that there is hardly any time dependence of the bake hardening response, for the range between 10 and 25 minutes measured after baking at temperatures between 140 °C and 170 °C. The bake hardening response was approximately 35 MPa (*X* sample) and 15 MPa (*Y* sample), and independent of both baking temperature (140°C or 170°C) and baking time. Studies (similar experiments as for *X* samples) conducted by other researchers demonstrated that the maximum bake hardening response that can be attributed to the Cottrell mechanism, is around 35 MPa. The lower value obtained for the *Y* samples is due to sample orientation (see discussion section: Sample orientation). This would then imply that for all the testing times, we had complete migration of carbon to the dislocations, hence the same bake hardening response.

Increasing the baking temperature from 140 °C to 170 °C had little influence on bake hardening response and it is believed that the end of Cottrell locking mechanism prevails at these temperatures; however, a marked increase of the bake hardening response was observed after baking at 200 °C. This additional increase is assumed to be due to the formation of fine clusters of precipitates on the saturated dislocation atmospheres. *TEM* studies here revealed very fine precipitates in samples at 230 °C (at 0% and 2% prestrain, 20 minutes baking time) and there is strong evidence that they are epsilon carbides (Figure 58 and Figure 60).

For a 2% level of prestrain, the effect of precipitation strengthening on the bake hardening response is a function of temperature and sample orientation. By applying a high enough baking temperature (200°C or 230°C) the bake hardening response obtained after 20 minutes is the same for *X* and *Y* samples. This would therefore imply that the amount of precipitation strengthening for *Y* samples must have been significantly higher. Apparently the dislocation structure (at 2% prestrain) does not have a significant influence on the bake hardening response obtained after high (>200°C) baking temperatures. However, at higher levels of prestrain this is not the case.

It is assumed that temperatures higher than 200 °C are sufficient for precipitates ( $\epsilon$ -carbides) to form, which renders a further strength increase. Although it is possible that precipitates form at temperatures as low as 140 °C, it is suspected that these precipitates would be too small and sparsely distributed to influence the mechanical properties, unless additional ageing is conducted at temperatures above 170 °C.

The results indicate that variations in baking time during a heat treatment at 170 °C are unlikely to dramatically alter the bake hardening response. However, variations in temperature may have an impact on the bake hardening response. Hundy's equation, used to determine time and temperature equivalents for different baking cycles, is therefore not valid for the time and temperature range used in this research (See also Chapter 4). Nevertheless, further research is necessary to establish whether a time dependence for the bake hardening exists for times shorter than 10 minutes.

Although a heat treatment of 170 °C for 20 minutes has been adopted as the standard in many bake-hardening tests it is unlikely that it accurately reflects the baking cycles encountered during automotive production.

It can be concluded from this study that for bake hardenable steels in which strain ageing is controlled by carbon the strength increase observed, after baking at 140 °C, is predominantly a result of Cottrell locking of dislocations. There is, however, an opportunity to increase the bake hardening response by using temperatures higher than that applied by car manufacturers. This is due to formation of carbon clusters and the precipitation of epsilon carbides.

## **Chapter 6: Conclusions & references**

### **6.1 Conclusions**

1. The mechanism of bake hardening (increase of the lower yield strength after baking), as investigated in the bake hardenable steel *H180BD* can be treated as a continuous process formed by three stages: Snoek effect, Cottrell atmosphere and  $\epsilon$ -carbide precipitation
2. The increase in strength is due to diffusion of dissolved interstitial atoms (in bake-hardenable steels this is limited to *C*) to dislocations and grain boundaries and/or  $\epsilon$ -carbide precipitation
3. The bake hardening response can also be measured by means of compression testing, however sample preparation and testing procedures are more complicated compared to tensile testing. The bake hardening response measured by tensile testing gives optimistic values
4. The tensile samples should be taken from the uniform prestrained region of the strips
5. The bake hardening response is dependent on the sample orientation, which is higher when the tensile samples are taken perpendicular ( $90^\circ$ ) to the rolling direction of the strip. The dislocations generated during temper rolling are mainly in the transverse slip planes therefore a higher strength is recorded after bake hardening
6. The bake hardening response is dependent on the level of prestrain and temperature for a baking time of 20 minutes
  - For  $140\text{ }^\circ\text{C} \leq T \leq 230\text{ }^\circ\text{C}$  for a given level of prestrain, there is a higher bake hardening response at higher baking temperatures (increasing diffusion rate)
  - At different levels of prestrain and
    - For  $T \leq 170\text{ }^\circ\text{C}$ , the bake hardening increases as prestrain increase. This is due to the Cottrell mechanism, which prevails for any level of prestrain (higher dislocation density would result in a higher bake hardening response assuming there is enough carbon for pinning all dislocations)
    - For  $T > 170\text{ }^\circ\text{C}$ , the bake hardening decreases as prestrain increases. Up to 2% prestrain, there is a contribution of precipitation strengthening but for prestrain larger than 2% the soluble carbon atoms in the bulk are mostly consumed in Cottrell atmospheres, which render less precipitation strengthening
7. The bake hardening response for low levels of prestrain ( $\leq 2\%$ ) exhibits no time dependence for baking times between 10 and 25 minutes and the temperature dependence is as follows
  - For  $140\text{ }^\circ\text{C} \leq T \leq 170\text{ }^\circ\text{C}$ , the increase in bake hardening is due to Cottrell atmospheres pinning dislocations
  - For  $170\text{ }^\circ\text{C} < T \leq 230\text{ }^\circ\text{C}$ , the increase in bake hardening is due to Cottrell atmospheres pinning dislocations and  $\epsilon$ -carbide precipitation
8. Hundy's equation is not valid for the time and temperature range used in this research
9. *TEM* analysis confirmed that the precipitates, which contributed to the bake hardening response at  $T > 170\text{ }^\circ\text{C}$  and low levels of prestrain, were indeed epsilon carbides

## 6.2 References

- 1 Satoshi Hanai, Nagayasu Takemoto, Yoshikuni Tokunaga and Yaichiro Mizuyama, "Effect of grain size and solid solution strengthening elements on the bake hardenability of low carbon aluminium-killed steel", Transactions ISIJ, vol. 24, pp. 17-23, 1984
- 2 Wolfgang Bleck, "Cold-Rolled, High-Strength sheet steels for auto applications", JOM, pp. 26-30, July 1996
- 3 Wilson, "Bake-hardenable sheet steels-old and new", Sheet Metal Industries, pp. 50-52, January 1984
- 4 Patrick Elsen and Hans Paul Hougardy, "On the mechanism of bake hardening", Steel research 64, No. 8/9, pp. 431-436, 1993
- 5 Pradhan, Bethlehem Steel corporation, "Continuous annealing of steel", ASM International, vol. 4, pp. 56-66, 2000
- 6 Llewellyn and R.C. Hudd, "Steels: Metallurgy and Applications", third edition 1998
- 7 Wolfgang Bleck, Rolf Bode, and Wolfgang Muschenborn, "Electrogalvanized and hot dip Galvanized strip with bake hardening properties for automotive use", International Congress and Exposition, Detroit, Michigan March 1-5, 1993
- 8 Japanese Industrial Standard G3135, Cold Rolled High Strength Steel Sheets with Improved Formability for Automobile Structural Uses, 1986
- 9 International Standard 14590, Cold-reduced Steel Sheet of High Tensile Strength and Low Yield Point with Improved Formability, 1999
- 10 Steel-Iron material Information Sheet (SEW) of the Verein Deutscher Eisenhüttenleute 094, Cold Rolled Coil and Sheet with Higher Yield Points for Cold Forming from Phosphorised Steels and from Steels with Additional Hardening after Heat Treatment (Bake Hardening), 1987
- 11 Atsuki Okamoto, Kouichi Takeuchi, and Michio Takagi, "A mechanism of paint bake hardening", The Sumitomo Search No. 39, pp. 183-194, September 1989
- 12 Schoeck and A. Seeger, "The flow stress of iron and its dependence on impurities", Acta Metallurgica, Vol. 7, pp. 469-477, July 1959
- 13 Rosinger, "Snoek Rearrangement and long-range diffusion during strain-ageing in iron", Metal Science, Vol. 9, pp. 1-7, 1975
- 14 Wilson and B. Russell, J.D. Eshelby, "Stress induced ordering and strain-ageing in low carbon steels", Acta Metallurgica, Vol. 7, pp. 628-631, September 1959

- 15 L. Snoek, "Effect of small quantities of carbon and nitrogen on the elastic and plastic properties of iron", *Physica* VIII, no. 7, pp. 711-733, January 17<sup>th</sup> 1941
- 16 Nakada and A. S. Keh, "Kinetics of Snoek ordering and Cottrell atmosphere formation in Fe-N Single Crystals", *Acta Metallurgica*, Vol. 15, pp. 879-883, May 1967
- 17 Harper, S.: *Physical Review* 83, pp. 709-712, 1951
- 18 Zhao, A.K. De, B.C. De Cooman, "Kinetics of Cottrell atmosphere formation during strain aging of ultra-low carbon steels", *Materials Letters*, pp. 374-378, July 2000
- 19 De, K. De Blauwe, S. Vandeputte, B.C. De Cooman, "Effect of dislocation density on the low temperature ageing behaviour of an ultra low carbon bake hardening steel", *Journal of Alloys and Compounds*, 310, pp. 405-410, 2000
- 20 Zhao, A.K. De and B.C. De Cooman, "A model for the Cottrell Atmosphere Formation during ageing of Ultra low Carbon Bake Hardening Steels", *ISIJ International*, Vol. 40, No. 7, pp. 725-730, 2000
- 21 Cottrell and B.A. Bilby, *Proc. Phys. Soc.*, vol. 62, ser. A, pp. 49-62, 1949
- 22 A.H. Cottrell, "Theory of Crystal dislocations", 1964 by Gordon and Breach Science Publishers, Inc.
- 23 De, S. Vandeputte, and B.C. De Cooman, "Static Strain Aging Behaviour of ultra low carbon bake hardening steel", *Scripta Materialia*, Vol. 41, No. 8, pp. 831-937, 1999
- 24 A.K.De, S.Vandeputte and B.C. De Cooman, "Kinetics of low temperature precipitation in a ULC-Bake hardening steel", *Scripta Materialia*, 44, pp. 695-700, 2001.
- 25 Rubianes, P. Zimmer, "The bake-hardenable steels", *La Revue de Metallurgie-CIT*, pp. 100-109, January 1996
- 26 Bailey, R.P. Foley and D.K. Matlock, "Processing and prestrain in path effects on the strain-ageing behaviour of a batch annealed bake-hardenable sheet steel", *high Strength Steels for Automotive Symposium Proceedings*, pp. 119-133, 1994
- 27 George E. Dieter, "Mechanical Metallurgy", SI Metric Edition, 2001
- 28 A. Kelly and R.N. Nicholson, "Precipitation Hardening", in B. Chalmers (ed.), *Progr. Mater. Sci.*, 10:379 (1963)
- 29 Kohsaku Ushioda, Naoki Yoshinaga, Kazuo Koyama and Osamu Akisue, "Application of ultra low carbon steels to the development of superformable sheet steels, solution-hardened high strength sheet steels and bake-hardenable sheet

- steels”, International Forum “Physical Metallurgy of IF steels”, Tokyo, May 10-11, 1994
- 30 Hoggan and G. Mu Sung, “Cold Rolled Batch Annealed Bake Hardening Steel for the Automotive Industry”, Iron and Steel Society/AIME, 39<sup>th</sup> Mechanical Working and Steel Processing Conference Proceedings, Volume XXXV (USA) pp. 17-29, 1998
  - 31 Stephenson, Trans. Met. Soc. A.I.M.E. 233, 1183, 1965
  - 32 Mizui, A. Okamoto and T. Taniouky, Steel in Motor Vehicle Manufacture, Dusseldorf, p. 85, 1990
  - 33 Foley, M.E. Fine and S.K. Bhat “Bake hardening steels: toward improved formability and strength”, 39<sup>th</sup> mechanical working and steel processing, ISS, Vol. XXXV, pp. 653-666, 1998
  - 34 Pierre Messien and Vincent Leroy, “Scavenging additions of boron in low C- low Al steels”, Steel Research 60, No. 7, pp. 320-328, 1989
  - 35 Woo Chang Jeong, “Effect of prestrain on aging and bake hardening of cold-rolled, continuously annealed steel sheets”, Metallurgical and Materials transactions A, Volume 29A, February 1998
  - 36 Rubianes and P. Zimmer, “Development of bake-hardenable steels for automotive applications at Sollac”, High-Strength steels for automotive symposium proceedings, 1994
  - 37 Katsumi Tanikawa, Yoshihiro Hosoya and Takehide Koike, “Strain aging properties of extra-low carbon bake-hardenable cold rolled steel sheets”, NKK Technical Review No. 72, 1995
  - 38 Orowan, “Causes and effect of internal stresses”, Internal Stresses and Fatigue in Metals”, Elsevier Publishing Company, New York, 1959
  - 39 Robert W. Cahn and Peter Haase, “Physical Metallurgy”, Fourth, revised and enhanced edition, vol. III, 1996
  - 40 Hundy, “Accelerated Strain Ageing of Mild Steel”, Journal of the Iron and Steel Institute, September 1954
  - 41 Corus internal report code IJTC/AUT-SHT/C/R/6525/02/X
  - 42 Corus internal report No. 72793
  - 43 Y. Bergstrom, “A dislocation model for stress-strain behaviour of polycrystalline  $\alpha$ -Fe with special emphasis on the variation of the densities of mobile and immobile dislocation”, Mater. Sci. Eng., 5 pp. 193-200, 1969/70

- 44 A. Van Snick, D. Vanderschueren, S. Vandeputte, J. Dilewijns, "Influence of carbon content and coiling temperature on hot and cold rolled properties of bake hardenable Nb – ULC steels", 39<sup>TH</sup> MWSP Conf. Proc., ISS, Vol. XXXV, pp. 225-232, 1998
- 45 J.L. Christen, J.M. Rubianes, A. Col, "The Bake-hardening steels for automotive outer body panels. Correlation between the BH measurement and the dent resistance", 40<sup>TH</sup> MWSP, Conf. Proc., ISS, pp. 77-81, 1998
- 46 W.C. Leslie, R.M. Fisher and N. Sen, "Morphology and crystal structure of carbides precipitated from solid solution in alpha iron", Acta Metallurgica, Vol. 7, pp. 632-644, September 1959
- 47 Ernst Kozeschnik and Bruno Buchmayr, "A contribution to the increase in yield strength during the bake hardening process", Steel research 68, No. 5, pp. 224-230, 1997
- 48 Hideo Abe, "Carbide precipitation during ageing treatments", Scandinavian Journal of Metallurgy 13, pp. 226-239, 1984
- 49 F.R.N. Nabarro, "Dislocations in Solids", Vol. 4, North-Holland Publishing Company, 1979

